Quantum Integrable Systems and Special Functions Arising from Separation of Variables

Author:
Sean R. Dawson

Supervisor:
Holger Dullin

A Doctoral Thesis submitted in partial fulfilment
of the requirements for the degree of
Doctor of Philosophy
in Mathematics

The School of Mathematics and Statistics
at the University of Sydney

August 26, 2024

Statement of Originality

This is to certify that to the best of my knowledge, the content of this thesis is my own work. This thesis has not been submitted for any degree or other purposes. I certify that the intellectual content of this thesis is the product of my own work and that all the assistance received in preparing this thesis and sources have been acknowledged.

Sean Russell Dawson 21/05/2024

Author Attribution Statement

I certify that the intellectual content of this thesis is the product of my own work and that all the assistance received in preparing this thesis and sources have been acknowledged.

The following chapters contain unaltered manuscripts:

- Chapter 2 of this thesis is published as [DDN21]
  Section 2.4 and the results for the quantum system in sections 2.5 and 2.6 were researched and written by me. Sections 2.2, 2.3 and the classical aspects of sections 2.5 and 2.6 were researched and written by Diana Nguyen. Holger Dullin guided the research, edited the paper and wrote section 2.1.
- Chapter 3 of this thesis is published as [DDN22]
  I wrote sections 3.4 and 3.7 and produced all figures contained within. Sections 3.3 and 3.6 were researched and written by Diana Nguyen. Holger Dullin guided the research, edited the paper and wrote sections 3.1, 3.2, 3.5.
- Chapter 4 of this thesis is published as [DD24]
  This paper was researched and written by me. Holger Dullin guided the research and edited the paper.

Sean Russell Dawson 21/05/2024

As supervisor for the candidature upon which this thesis is based, I can confirm that the authorship attribution statements above are correct.

Holger Dullin 21/05/2024

Acknowledgements

First and foremost, I would like to thank my supervisor Professor Holger Dullin for his continual guidance and support over this program. This thesis would not have been possible without him.

To my parents, who have loved and cared for me over the years, I'm grateful to them for being there for me through all the highs and lows.

There have been many challenges along the road to this point. I've been fortunate to have the unwavering support of my partner, Jessie, whose inspiring words have kept me going in the face of self doubt.

For some of my toughest times, I've been blessed to have the best friends anyone could ask for in Nick, Dillon, James, Jake, Dom, Terry, Taiga, Jen and Kevin. Over the last three years at Lyra, I am grateful to have had the mentorship of Tim and Kelly, both of whom have taught me many valuable life lessons.

Contents

List of Figures

Quantum Integrable Systems and Special Functions Arising from Separation of Variables

Abstract

In this thesis, we study three families of quantum integrable systems and the corresponding special functions that arise from separation of variables. By analysing the respective classical systems, we are able to elucidate connections between the classical and quantum systems, their symmetries and the latter's associated special functions.

In Chapter 2 we study both the classical and quantum integrable systems arising from separating the free particle on $\mathbb{R}^3$ in prolate spheroidal coordinates. In doing so, we obtain the spheroidal wave equation as a separated linear ODE whose solutions are the well known spheroidal wave functions. By reducing to T^*S^2 we show that the joint spectrum of these eigenfunctions on $L_2(S^2)$ has a defect, i.e. quantum monodromy, meaning a global assignment of quantum numbers is impossible. Considering the semi-classical limit of the quantum operators, we construct a semi-toric integrable system with a non-degenerate focus-focus point, thereby proving the existence of monodromy.

In Chapter 3 we study what we call the Harmonic Lagrange Top, the well-known Lagrange top with an added quadratic potential. Our key result is that the non-trivial ODE obtained by separating the Schrödinger equation for this system yields the most general confluent Heun equation. In the physics literature, this is known as Teukolsky's master equation. The reduced system is semi-toric without the harmonic potential, but more complicated in general, while retaining a global S^1 symmetry.

Finally, we investigate the families of quantum systems arising from separating the Schrödinger equation on S^3. There are 6 orthogonal separable coordinate systems on this space: ellipsoidal, prolate, oblate, Lamé, spherical and cylindrical. From this, we obtain a vast array of special functions; in particular the generalised Lamé wave functions, Heun and Gegenbauer polynomials. We show that all separated ODEs possess only regular singularities. This stands in contrast with the previous systems studied (on non compact manifolds) for which there is an irregular singularity at infinity. In this family, we find integrable systems without an S^1 symmetry, some with an S^1 symmetry (including a semi-toric case) and one toric integrable system.

Chapter 1

Introduction

1.1. Overview

This thesis investigates the relationship between classical integrable systems, their quantum counterparts and special function solutions. The theory of classical integrable systems is well known and has led to many powerful results, see e.g. [PVuN09], [Del88] and [MW74]. Similarly, quantisation and subsequent study of the resulting quantum integrable systems is flourishing; see e.g. [CPVuN13] and [PVuN12]. We show that by analysing the ordinary differential equations and special functions that arise from quantised classical systems, new insights can be found for both the classical and quantum systems. In particular, this work focuses on the study of three families of integrable systems.

The first system, detailed in Chapter 2, arises from studying the free particle in $\mathbb{R}^3$ in prolate spheroidal coordinates, one of the 11 orthogonal separable coordinates of $\mathbb{R}^3$. Separating the Schrödinger equation in these coordinates yields a family of ordinary differential equations (ODEs), the most interesting of which is the confluent Heun equation. Solving these ODEs yields what we call spheroidal harmonics - extensions of the well known spherical harmonics. Returning to the classical mechanics, we perform a reduction to T^*S^2 and also show that the corresponding (reduced) integrable system is symplectically equivalent to the C. Neumann system. We also show that the spheroidal harmonics are eigenfunctions of the two reduced quantum operators on $L_2(S^2)$. A key result is that the corresponding joint spectrum is shown to have quantum monodromy, meaning that a global labelling of joint eigenstates is impossible. This is proven by studying the semiclassics; we construct the corresponding classical system and show that it is of the semi-toric type. By proving the existence of a non degenerate focus-focus point, the key result is shown. Chapter 2 was published in its entirety as [DDN21] and also contains further results on the classical system which were found by Diana Nguyen.

The next family of integrable systems studied arises from rigid body dynamics. Motivated by the results in Chapter 2, we set out to construct a classical integrable system that, when quantised, yielded the most general form of the confluent Heun equation. Our efforts led us

to define what we term the "Harmonic Lagrange Top" - the conventional Lagrange top well known in rigid body dynamics subject to a harmonic potential. The resulting most general confluent Heun equation is also known in the literature as Teukolsky's master equation and is studied in the context of rotating black holes (i.e. the Kerr metric) [Teu73]. Our result, however, is in some sense more general since one parameter in the master equation is restricted to be the spin of a particle while in our case it can be any integer. Chapter 3 was published in its entirety as [DDN22] and was co-written with Diana Nguyen.

Finally, our attention then shifts in Chapter 4 to a much larger family of integrable systems that arise from separating the geodesic flow on S^3. From [KM86], it is known that there are six distinct orthogonal separable coordinates on the $3-$sphere, the most general of which are known as the ellipsoidal coordinates. In these coordinates, we again separate the Schrödinger equation. This time, we recover a family of ODEs, all consisting of the generalised ellipsoidal wave equation. Our analysis extends the results of [SZ07b].

The other five separable coordinate systems: prolate, oblate, Lamé, spherical and cylindrical are all obtainable from the ellipsoidal coordinates by various degenerations. For the prolate system, separation yields the well known Heun equation and Heun polynomials. Like the free particle on $\mathbb{R}^3$, the joint spectrum is shown to possess quantum monodromy and this is proved by showing the corresponding classical system is semi-toric. We then study the oblate system; separation again yields the Heun equation with Heun polynomial solutions. However, unlike the prolate system, monodromy is not observed in the joint spectrum because there are hyperbolic singularities. For the Lamé system, separation yields both the Lamé wave equation and hypergeometric equation with Lamé and Gegenbauer polynomials as respective solutions. When studying the spherical coordinates, we obtain a family of hypergeometric equations and obtain the Gegenbauer and Jacobi polynomials as solutions. Finally, for cylindrical coordinates, a single non trivial hypergeometric equation is obtained whose solution are the Jacobi polynomials. This corresponds to a classical system on $S^2 \times S^2$ that is toric. For all coordinate systems, we also investigate how the discrete symmetry class of the corresponding classical system descends to both the joint spectra and ODEs. This gives five examples illustrating the relationship between the classical and quantum dynamics. We hope that future work will extend these methodologies and allow for more connections to be drawn between special functions and the corresponding classical integrable systems.

Chapters 2, 3 and 4 are all published in their entirety as separate papers as, respectively, [DDN21], [DDN22] and [DD24]. With this in mind, this dissertation is presented as a thesis by publication. The contribution of this author to [DDN21] and [DDN22] was primarily in the quantum mechanics and the classical mechanics was the focus of Diana Nguyen and her PhD thesis. In the rest of this chapter, we focus on the necessary background required to understand this thesis.

1.2. HAMILTONIAN MECHANICS

In this section we introduce the necessary foundations of Hamiltonian mechanics for Chapters 2, 3 and 4. The study of Hamiltonian systems arose in the early 19th century as a reformulation of Lagrangian mechanics. Via its connections to symplectic and Poisson geometry, it has since gone on to serve as a way of linking classical and quantum mechanics.

The interested reader should seek out [Arn78], a thorough introduction to the field. Further texts include [CB15], [BF04] and [MR94].

Hamiltonian dynamics take place on sympletic manifolds.

Definition 1. *A sympletic manifold (M, ω) is a pair consisting of a smooth manifold M and a differential $2-$form ω that is closed $(d\omega = 0)$ and non degenerate (meaning $\omega(v, \cdot) = 0$ only if $v = 0$).*

It follows from the definition that all symplectic manifolds are orientable and of even dimension.

Darboux's theorem [Arn78] guarantees the existence of so-called Darboux coordinates.

Theorem 1.1. *Let (M, ω) be a $2n$ dimensional symplectic manifold. Then, in a neighbourhood of every point $x \in M$, there exist local coordinates $(q_1, \ldots, q_n, p_1, \ldots, p_n)$ in which the symplectic form can be written as*

$$\omega = \sum_{i=1}^{n} dq_i \wedge dp_i.$$

Due to the non degeneracy condition of the symplectic form, an isomorphism can be constructed between the tangent (TM) and cotangent bundles (T^*M) of a symplectic manifold. Let $\mathcal{X}(M)$ be the set of smooth vector fields and $\Omega^1(M)$ be the set of smooth differentiable $1-$forms on M. With $X \in \mathcal{X}(M)$ and $\alpha \in \Omega^1(M)$, it is easily shown that

$$i_X \omega = \alpha$$

is such an isomorphism where $i_X \omega = \omega(X, \cdot)$.

Given a smooth function $H : M \to \mathbb{R}$, one can define a Hamiltonian vector field.

Definition 2. *The Hamiltonian vector field $X_H \in \mathcal{X}(M)$ corresponding to Hamiltonian function H is given by*

$$i_{X_H} \omega = dH$$

where dH is the differential of H.

In the case of canonical coordinates (q, p) where $\omega = dq \wedge dp$, the Hamiltonian vector field

is given by the familiar Hamilton's equations

$$\dot{q} = \frac{\partial H}{\partial p} \quad \dot{p} = -\frac{\partial H}{\partial q}. \tag{1.1}$$

Definition 3. *Let $\Phi_t^H : M \to M$ denote the flow of the Hamiltonian vector field X_H. A function $f \in C^\infty(M)$ that is invariant under Φ_t^H for all t is said to be a first integral or constant of motion of the Hamiltonian.*

Poisson brackets are an efficient tool for checking first integrals and writing the equations of motion for a given Hamiltonian.

Definition 4. *On a symplectic manifold, the Poisson bracket $\{\cdot,\cdot\}$ of two smooth functions $f, g \in C^\infty(M)$ is given by*

$$\{f, g\} = \omega(X_f, X_g).$$

Again, consider canonical coordinates (q, p) on the cotangent bundle T^*M. Then, Hamilton's equations (1.1) can be rewritten as

$$\dot{q} = \{q, H\} \quad \dot{p} = \{p, H\}$$

and it follows that for a function f

$$\dot{f} = \{f, H\}.$$

Thus, a function f is a first integral of the Hamiltonian if and only if $\{f, H\} = 0$, i.e. f and H Poisson commute.

The idea of a Hamiltonian system can be generalised to a Poisson system where the symplectic manifold is generalised to a Poisson manifold.

Definition 5. *(Poisson Manifold) A Poisson manifold $(P, \{\cdot,\cdot\})$ is a smooth manifold P equipped with a Poisson bracket $\{\cdot,\cdot\} : C^\infty(P) \times C^\infty(P) \to C^\infty(P)$ which satisfies the following:*

1) Bi-linearity:

$$\{\alpha f + \beta g, h\} = \alpha\{f, h\} + \beta\{g, h\} \quad \forall f, g, h \in C^\infty(P) \text{ and } \alpha, \beta \in \mathbb{R},$$

2) Skew symmetry

$$\{f, g\} = -\{g, f\} \quad \forall f, g \in C^\infty(P),$$

3) Jacobi identity

$$\{f, \{g, h\}\} + \{g, \{h, f\}\} + \{h, \{f, g\}\} = 0 \quad \forall f, g, h \in C^\infty(P),$$

4) Leibniz rule

$$\{fg, h\} = \{f, h\}g + f\{g, h\} \quad \forall f, g, h \in C^\infty(P).$$

Note that conditions 1) through 3) make $C^\infty(P)$ a Lie algebra. Further, it is also clear that a symplectic manifold is always a Poisson manifold but the reverse is not true.

Consider a point on a Poisson manifold, around which local coordinates z_i are defined. Then, the Poisson bracket can be written using a $2-$tensor B called the Poisson tensor. Specifically, one may write

$$\{f, g\} = \sum_{i<j} B^{ij}(z) \frac{\partial f}{\partial z_i} \frac{\partial g}{\partial z_k}.$$

The Poisson tensor does not need to have full rank. If it does not, the degeneracy prohibits the construction of a compatible symplectic form on the manifold. However, if the tensor has full rank then this means the manifold is symplectic.

Consider a function $H : P \to \mathbb{R}$ on a Poisson manifold $(P, \{\cdot, \cdot\})$.
Definition 6. *The Hamiltonian vector field X_H of H on P is given by*

$$X_H f = \{f, H\}$$

for all smooth function $f \in C^\infty$.

We say two functions f and g are in involution if they Poisson commute, i.e. $\{f, g\} = 0$.
Definition 7. *A Casimir is a function $\mathcal{C} \in C^\infty(P)$ that is in involution with all other functions $f \in C^\infty(P)$ on the Poisson manifold, i.e. $\{\mathcal{C}, f\} = 0$ for all f.*

Liouville integrable systems are defined on symplectic manifolds and are a key concept in this thesis.
Definition 8. *Liouville Integrable System : Let (M, ω) be a $2n$ dimensional sympletic manifold and let $F_i : M \to \mathbb{R}$ where $i \in \{1, \ldots, n\}$ be first integrals. If*

1. The F_i are functionally independent, i.e. $dF_1 \wedge \cdots \wedge dF_n \neq 0$ almost everywhere on M and

2. The F_i are all in involution, i.e. $\{F_i, F_j\} = 0$ for all $i, j = 1, \ldots, n$

then we call the triple $(M, \omega, \boldsymbol{F})$ where $\boldsymbol{F} = (F_1, \ldots, F_n)$ an n dimensional Liouville integrable system.

The Hamiltonian H could be any of the F_i or a function of the F_i. We default to the convention of setting $F_1 = H$.
Definition 9. *A point $x \in M$ is called regular if the F_i are independent at x, i.e. if*

$$(dF_1 \wedge \cdots \wedge dF_n)(x) \neq 0$$

then x is regular, otherwise it is known as a critical point.

Consider the level sets of the integrals

$$M_{\boldsymbol{c}} = \{x \in M | \boldsymbol{F}(x) = \boldsymbol{c}\}$$

where $\boldsymbol{c} = (c_1, \ldots, c_n)$, i.e. $F_i(x) = c_i$. If $M_{\boldsymbol{c}}$ only contains regular points then $\boldsymbol{c}$ is known as a regular value, otherwise it is a critical point.

Definition 10. *The mapping $\boldsymbol{F} : M \to \mathbb{R}^n$ is called the momentum map of the integrable system. The image of all critical points under $\boldsymbol{F}$ is the set of critical values also known as the bifurcation diagram.*

The following was proven in [Arn78] and is a key result in the study of integrable systems since it gives a general description of the dynamics on regular level sets.

Theorem 1.2. *Consider $(M, \omega, \boldsymbol{F})$, an n dimensional integrable system and let $\boldsymbol{c}$ be a regular value of $\boldsymbol{F} : M \to \mathbb{R}^n$. Further, let $F_1 = H$ be the Hamiltonian. Then:*

1) *$M_{\boldsymbol{c}}$ is a smooth manifold invariant under the Hamiltonian flow induced by H,*

2) *If M_c is compact and connected then it is diffeomorphic to the $n-$torus T^n,*

3) *There exist local symplectic coordinates $(\theta_1, \ldots, \theta_n, I_1, \ldots, I_n)$ near $M_{\boldsymbol{c}}$ such that the I_i are constant, $\dot{\theta}_i = I_i$ and the symplectic form can locally near $M_{\boldsymbol{c}}$ be re-written as*

$$\omega_{\boldsymbol{c}} = \sum_{i=1}^{n} d\theta_i \wedge dI_i.$$

Near regular values, all integrable systems have the same trivial dynamics as described by the theorem above. Interesting invariants of integrable systems thus appear at critical values, and hence the bifurcation diagram, definition 10, is a central object in this thesis.

1.3. Quantum Mechanics

Quantisation is a deeply technical field and we only give a brief overview of the necessary concepts required for this thesis. The interested reader is encouraged to read these excellent texts on the matter, for example: [SVuN17], [OdA88], [CAM+03] and [LL77].

Quantisation is the mechanism by which one goes from a classical integrable system (with integrals defined on a symplectic manifold) to a quantum integrable system (with commuting operators on a Hilbert space). Conversely, the process by which a quantum integrable system is converted into a classical system is called taking the semi-classical limit, if possible.

Consider $\mathbb{R}^{2n}$ with standard symplectic form form ω and let $\boldsymbol{x} \coloneqq (x_1, \ldots, x_n)$ and $\boldsymbol{p} \coloneqq (p_1, \ldots, p_n)$ be Darboux coordinates. We then say that the corresponding Hilbert space $\mathcal{H}$ is the space $L^2(\mathbb{R}^n)(\boldsymbol{x})$; the space of square integrable functions of $\boldsymbol{x}$.

Definition 11. *The Dirac rule quantises functions of the local symplectic coordinates $(\boldsymbol{x}, \boldsymbol{p})$ as follows. The position variable x_j is associated with the quantum position operator which is multiplication by x_j, i.e. $x_j u$ where $u \in L^2(\mathbb{R}^n)$ though the product is not necessarily in $L^2(\mathbb{R}^n)$. In other words, x_j must be viewed as an unbounded operator. Similarly the momentum p_j is associated with the (also unbounded) quantum momentum operator $\frac{\hbar}{i}\frac{\partial}{\partial x_j}$ where $\hbar > 0$ is known as the semi-classical parameter.*

Much like the classical Poisson bracket, there exists what we call the standard commutator between quantum operators on a Hilbert space.

Definition 12. *Let $\hat{F}$ and $\hat{G}$ be quantum operators on a Hilbert space. Then the commutator between these operators is given by*

$$\left[\hat{F}, \hat{G}\right] \coloneqq \hat{F}\hat{G} - \hat{G}\hat{F}.$$

If $\left[\hat{F}, \hat{G}\right] = 0$, then we say the two are commuting operators.

The position and momentum operators do not commute under the standard commutator. Specifically, we have

$$\left[\frac{\hbar}{i}\frac{\partial}{\partial x_j}, x_j\right] = \frac{\hbar}{i}. \tag{1.2}$$

As the order of the operators matters, Dirac quantisation is not unique. Further, simply replacing position and momentum variables by their corresponding operators is not even guaranteed to give a Hermitian operator.

It can be shown that the quantum operators $\frac{\hbar}{i}\frac{\partial}{\partial x_j} \circ x_j$ and $x_j \circ \frac{\hbar}{i}\frac{\partial}{\partial x_j}$ have the same classical limit - $x_j p_j$. However, because of the non vanishing bracket (1.2), measuring position and momentum is order dependent. In other words, measuring position and then momentum yields a different result to the reverse operation. The property (1.2) is known as the uncertainty principle.

We note that, due to the non-commutativity of the position and momentum operators (1.2), the Dirac rules are insufficient for quantising general functions.

We now have all the ingredients necessary to define a quantum integrable system.

Definition 13. *Let $(\mathbb{R}^{2n}, \omega)$ be an $2n$ dimensional symplectic manifold equipped with Liouville integrable system $\boldsymbol{F} = (F_1, \ldots, F_n)$, i.e. $\{F_i, F_j\} = 0$ for all i, j where $\{\cdot, \cdot\}$ is the canonical Poisson bracket. We say that the quantum integrable system corresponding to $(M, \omega, \boldsymbol{F})$ is a collection $(\hat{F}_1, \ldots, \hat{F}_n)$ of n pairwise commuting self-adjoint operators on $\mathcal{H}$, the Hilbert space corresponding to the quantised symplectic manifold.*

While the Dirac method on $\mathbb{R}^n$ is a relatively straightforward method of quantisation and so is a good introduction to the space, it has many limitations. By contrast, there are two well know methodologies for quantising certain integrable systems. These are Weyl quantisation on a cotangent bundle $M = T^*X$ where X is a smooth n dimensional manifold and Berezin-Toeplitz quantisation on compact symplectic manifolds. For the latter, the set of admissible values of the semi-classical parameter $\hbar$ is itself quantised with $\hbar = \frac{1}{k}$ where $k \in \mathbb{N}^*$ and the Hilbert space itself is finite with its dimension dependent on $\hbar$. For more detail, see [Cha03].

Consider an n dimensional quantum integrable system $(\hat{F}_1, \dots, \hat{F}_n)$ on a Hilbert space $\mathcal{H}$.

Definition 14. *Let $\psi \in \mathcal{H}$ be a simultaneous eigenstate of all of the $\hat{F}_j$, i.e.*

$$\hat{F}_j\psi = \lambda_j\psi \quad \forall j.$$

We say that ψ is a joint eigenstate of $(\hat{F}_1, \dots, \hat{F}_n)$. The set of all $n-$tuples $(\lambda_1, \dots, \lambda_n)$ for all joint eigenstates ψ is called the joint spectrum of the quantum integrable system.

The joint spectrum of a quantum integrable system with a semiclassical limit is a function of the semi-classical parameter $\hbar$. The limit $\hbar \to 0$ is known as the semi-classical limit and one recovers the corresponding classical system. The integrals obtained from degenerating the operators in this limit are known as the principal symbols.

From [PVuN15], we have the following theorem which relates the joint spectrum in the semi-classical limit to the image of the momentum map.

Theorem 1.3. *Let $I \subset (0, 1]$ be a set with a limit point at 0. Then the limit set of the joint spectrum of a family of pairwise commuting self-adjoint semiclassical operators*

$$\hat{F}_1 \coloneqq (\hat{F}_{1,\hbar})_{\hbar\in I}, \dots, \hat{F}_n \coloneqq (\hat{F}_{n,\hbar})_{\hbar\in I}$$

is the classical spectrum $\mathcal{S} \subset \mathbb{R}^n$ of the corresponding classical integrals $(F_1, \dots, F_n)$ where F_i is the classical integral corresponding to $\hat{F}_i$. That is, the limit set of the joint spectrum is the closure of the image of the momentum map of the classical integrals $F_1, \dots, F_n$.

In particular this means that the joint spectrum is contained in the image of the momentum map, as we will see in our examples.

1.4. Differential Equations

Deeply related to our investigation of the quantum mechanics is the study of ordinary differential equations. See e.g. [SL00], [Ars64], [RA95] and [Inc56].

At the heart of this thesis's study of quantum mechanics is the Laplace Beltrami operator.

Consider a manifold with local coordinates x_i and metric tensor elements g_{ij}.

Definition 15. *The Laplace Beltrami operator of a twice differentiable function f is the divergence of the gradient, i.e.*

$$\Delta f := \nabla \cdot (\nabla f). \tag{1.3}$$

In local coordinates, one may rewrite (1.3) as

$$\Delta f = \frac{1}{\sqrt{|g|}} \partial_i \left(\sqrt{|g|} g^{ij} \partial_j f \right)$$

where $|g| := |\det(g_{ij})|$ is the absolute value of the determinant of the metric tensor, g^{ij} is the (i,j)th component of the inverse of the metric tensor and we use the Einstein summation convention.

The well known Schrödinger equation in physics for a free particle (i.e. no potential) is simply the eigenvalue equation of the Laplace Beltrami Operator

$$\Delta f = Ef \tag{1.4}$$

where E denotes the total energy of the system. One can recover the Schrödinger (and, in turn, the Laplace Beltrami operator) from (1.4) by using the Dirac rule by swapping instances of x_j with multiplication by x_j and those of p_j with multiplication by $\frac{\hbar}{i}\frac{\partial}{\partial x_j}$.

In this thesis, we focus on solving the Schrödinger equation by using the method of separation of variables. For more details, see the works of [KKM18] and [KWMW76]. In particular, we focus on $\mathbb{R}^3$ and S^3. For the former, there exist 11 orthogonal separable coordinates and for the latter, there exist 6 such coordinate systems.

As all systems studied in this thesis arise from separation of variables, we know that all resulting systems are Stäckel systems [Eis34]. Thus, we know that classically the Hamiltonian, along with integrals obtained via separation, will be quadratic in the momenta.

From the quantum perspective, it is known that the Schrödinger equation is separable in a given orthogonal coordinate system if the corresponding Hamilton-Jacobi equation is separable and if the Robertson condition is satisfied [Rob27, BCR02]. Further, from [Eis34, BCR02] we know that the latter is satisfied if and only if the Ricci tensor is diagonal. Since all the systems we study in $\mathbb{R}^3$ and S^3 have diagonal Ricci tensor, we are guaranteed separable solutions to the Schrödinger equation if the classical system separates. All ODEs arising from separation studied in this thesis are of second order.

Consider a second order linear ODE given by

$$v''(z) + a(z)v'(z) + b(z)v(z) = 0 \tag{1.5}$$

where $a(z)$ and $b(z)$ are analytic functions. The following is well known in the fields of special functions and ODEs. For more detail, see [Kri10, SL00].

Definition 16. *Let $z = z_0$ be a singular point of (1.5). We say that z_0 is a regular singular point if we can rewrite $a(z) = \frac{A(z)}{z-z_0}$ and $b(z) = \frac{B(z)}{(z-z_0)^2}$ where $A(z)$ and $B(z)$ are analytic functions in some neighbourhood of z_0. If this is not the case, then we say z_0 is an irregular singular point.*

Since $A(z)$ and $B(z)$ are analytic, they can be expressed locally as power series about $z = z_0$, i.e. $A(z) = \sum_{i=0}^{\infty} a_i(z - z_0)^i$ and $B(z) = \sum_{i=0}^{\infty} b_i(z - z_0)^i$. Thus, around regular singular points, one can use the Frobenius ansatz $v(z) = \sum_{i=0}^{\infty} v_i(z - z_0)^{\alpha+i}$ where $v_0 = 1$. Substituting this expression for $v(z)$ into (1.5) gives a three term recurrence relation which begins with

$$\alpha^2 + (a_0 - 1)\alpha + b_0 = 0. \tag{1.6}$$

Definition 17. *Equation (1.6) is called the indicial equation for (1.5). The roots (α_1, α_2) to the indicial equation are known as the exponents for the root z_0.*

A special family of linear ODEs encountered in this thesis are known as Fuchsian equations.

Definition 18. *A second order differential equation with rational coefficients and $N+1$ singularities is called Fuchsian if all singularities are regular.*

A Fuchsian equation can be written in the following form [Inc56]

$$w'' + \left(\sum_{j=1}^{N} \frac{\gamma_j}{z - e_j}\right) w' + \left(\sum_{j=1}^{N} \frac{q_j}{z - e_j}\right) w = 0 \tag{1.7}$$

where $\sum_{j=1}^{N} q_j = 0$, the exponents at the e_j are $(0, 1 - \gamma_j)$, those at ∞ are denoted by (α, β) such that

$$\alpha + \beta + 1 = \sum_{j=1}^{N} \gamma_j \quad \alpha\beta = \sum_{j=1}^{N} e_j q_j. \tag{1.8}$$

The q_j in (1.7) are called the accessory parameters. For a Fuchsian equation with N finite singularities, there are $N - 2$ free accessory parameters. The Heun and Hypergeometric equations are Fuchsian equations with $N = 3$ and $N = 2$ respectively. In this thesis we also study the collision of singular points. This is known as confluence and the resulting ODE can remain Fuchsian (e.g. going from Heun to Hypergeometric) or an irregular singularity can appear (e.g. Heun to confluent Heun equation).

It is well known, see [KM86] and [KKM06], that separation in orthogonal coordinate systems yields special functions like Heun, ellipsoidal, Jacobi functions and so forth. These functions, their symmetries and their relationships to their corresponding classical systems will be a central focus of this thesis.

As we discover via the examples studied in this thesis, the separated ODEs that arise from the compact manifold S^3 are all Fuchsian type equations. Separation on $\mathbb{R}^n$ (with or without potential) results in confluent ODEs. In particular, in the first two examples, the confluent Heun equation occurs when the singularity at infinity is irregular.

The ODEs obtained by separation, along with their boundary conditions, allow us to compute the joint spectrum. For most systems with at most $N = 3$ finite singularities, this is a relatively straightforward affair. On compact manifolds, equations such as those arising (after substitution) from (1.5) will truncate as a result of a quantisation condition. This leads to a finite three term recurrence relation from which spectral parameters can be found; see Chapter 4. For non compact manifolds (see Chapters 2 and 3) no such truncation occurs, but a numerically accurate approximation for the spectra can be computed from an infinite tri-diagonal matrix.

There is one system we study for which there are $N = 4$ finite singularities; these arise from separating the Schrödinger equation in ellipsoidal coordinates on S^3. In this case, we employ the method of Heine-Stieltjes polynomials as described in [Ala79] and [ARZ85].

Chapter 2

Monodromy in Prolate Spheroidal Harmonics

Abstract

We show that spheroidal wave functions viewed as the essential part of the joint eigenfunction of two commuting operators of $L_2(S^2)$ has a defect in their joint spectrum that makes a global labelling of the joint eigenfunctions by quantum numbers impossible. To our knowledge this is the first explicit demonstration that quantum monodromy exists in a class of classically known special functions. Using an analogue of the Laplace-Runge-Lenz vector we show that the corresponding classical Liouville integrable system is symplectically equivalent to the C. Neumann system. To prove the existence of this defect we construct a classical integrable system that is the semi-classical limit of the quantum integrable system of commuting operators. We show that this is a generalised semi-toric system with a non-degenerate focus-focus point, such that there is monodromy in the classical and the quantum system.

2.1. INTRODUCTION

Prolate spheroidal wave functions are important and well known special functions that appear when separating variables in problems that have the symmetry of prolate ellipsoids. Classical references on spheroidal wave functions are [WW65, MS54, Fla57, SMC+59, Ars64]. One inspiration for our work is the general theory of separation of variables developed in [MJ77, BKM76, KKM18]. There spheroidal harmonics appear as the joint eigenfunctions of two commuting operators on the Hilbert space $L_2(S^2)$. The two operators are constructed from separation of variables in spheroidal coordinates. In the spherical limit the spheroidal harmonics reduce to the well known spherical harmonics. In this paper we study the joint spectrum of these two commuting operators and show that the lattice of joint eigenvalues has a global defect. Even though prolate spheroidal wave functions are very well studied special functions this observation about the joint spectrum seems to be new.

Another inspiration for our work is the study of quantum and Hamiltonian monodromy in integrable systems, specifically so-called semi-toric integrable systems. The global study of Liouville integrable systems was initiated by Duistermaat in [Dui80]. In a subsequent paper with Cushman [CD88] it was shown that classically and quantum mechanically the spherical pendulum has Hamiltonian and quantum monodromy, respectively. It was realised that classically [Mat96, Zun97] and quantum mechanically [VuN99] monodromy is caused by a so-called focus-focus equilibrium point of the classical system. More recently a global classification of semi-toric integrable systems has been achieved [PVuN09]. By definition [VuN07], semi-toric systems have two degrees of freedom and one proper global integral which induces an S^1 action. Furthermore, no critical points can be of hyperbolic or degenerate type. The condition of properness is rather restrictive, such that, e.g., the spherical pendulum and the integrable system studied in this paper are not semi-toric system in this strict sense. They are, however, *generalised* semi-toric systems [PR$^+$17], for which only the combined moment map needs to be proper. In general integrable systems that come from separation of variables of the free particle in $\mathbb{R}^3$ do not possess a global S^1 action. If we restrict to those coordinate systems that have rotational symmetry we do have a global S^1-action: rotation about the symmetry axis. As we will show, separation in spheroidal coordinates provides an example of a generalised semi-toric system.

In two recent papers [DW18] and [CDEW19] we have used separation in spheroidal coordinates for the Kepler problem in space and the harmonic oscillator in space, respectively, and shown that both problems – when considered in prolate spheroidal variables – have Hamiltonian and quantum monodromy. The present paper grew out of the realisation that an even simpler problem, namely the free particle, can be studied in a similar way, and leads to similar results, namely monodromy in the joint spectrum. As in the two previous works it is crucial for this approach that the system under consideration is superintegrable. In the Kepler problem and the harmonic oscillator superintegrability implies that the flow of the Hamiltonian is periodic with constant period, and hence it is possible to consider symplectic reduction with respect to this flow, viewed as an action of the group S^1. The reduced system inherits two constants of motion which are the separation constants from the separation of variables. In the present example of the free particle the orbits of the Hamiltonian are not periodic orbits, but instead straight lines. Thus we need to consider reduction not with respect to a compact group S^1 but with respect to the non-compact group $\mathbb{R}^1$. Even though there are no general theorems about reduction in this case it turns out that the reduction can be performed nicely and elegantly using the invariants of the Hamiltonian flow. This leads to the classical analogue of the commuting operators described by Kalnins and Miller [BKM76], and we then show using singular reduction with respect to the global S^1 action (the angular momentum about the z-axis) that the system is generalised semi-toric and has a non-degenerate focus-focus point and hence monodromy.

The fact that the free particle when treated in this way has monodromy was first observed in [MDEW19, Mar18] as a special limit of Euler's two-centre problem in which the masses of both centres vanish. The main point of [MDEW19, Mar18] was the investigation of scattering monodromy, and in [Mar18] it was shown that after reduction by the free flow the degenerate C. Neumann system aka the quadratic spherical pendulum is obtained. The presence of monodromy in the quadratic spherical pendulum is well known [BZ93, Efs05], and the interpretation as a degeneration of the C. Neumann system was elucidated in [DH12]. The reduction using invariants we perform in this paper leads to the classical analogue of the work of Kalnins and Miller [KKM18], and gives rise to a generalised semi-toric system with Lie-Poisson structure $e^*(3)$, see Theorem 1. From [Mar18] we know that this system must be equivalent to the degenerate C. Neumann system on T^*S^2, and in Theorem 5 we give the explicit symplectomorphism that establishes this equivalence. Thus Theorem 6 is already known indirectly, because using Theorem 5 the monodromy in the degenerate C. Neumann system applies. Nevertheless, we give a direct proof of monodromy in Theorem 6, and illustrate it following an idea from [CIAD14].

The third inspiration for our work is to connect the two threads described above: separation of variables including the corresponding special functions on the one hand and the global theory of integrable systems on the other hand. Special functions related to (confluent) Fuchsian equation beyond the (confluent) hypergeometric equation are for example discussed in [Ars64, SL00]. The spheroidal wave equation is a particular case of the confluent Heun equation, see [RA95] and the references therein. In our setting spheroidal harmonics are joint eigenfunctions of two commuting operators, and we show that a defect in the joint spectrum of these operators can be understood from the analysis of the corresponding Liouville integrable system. This is more than a WKB analysis of the solutions, since it takes into account global information about the action variables of the integrable system. Nevertheless, we remark that the essence of the defect could have been observed by analysing well known asymptotic expansions [AS92] for the eigenvalues of the spheroidal wave equation; but to our knowledge such an analysis has not been presented before.

The solutions of the Helmholtz equation inside the prolate ellipsoid (aka the quantum billiard in the prolate ellipsoid) have been studied in [WD02], and monodromy was found in the joint spectrum. Since this is a system with three commuting operators (as opposed to two in the current paper) the radial equation has to be included and this leads to two coupled boundary value problems that were numerically solved in [WD02]. In the present problem we only study the angular wave equation and find monodromy also in this simpler setting.

The plan of the paper is as follows. In section 2 we describe a reduction of the free particle in $\mathbb{R}^3$ that leads to a reduced system with a Lie-Poisson structure of the algebra $e^*(3)$ of

the Eulidean group of translations and rotations $E(3)$. To obtain an integrable system on the reduced space separation of variables in prolate spheroidal coordinates is employed in the next section. The centrepiece of the paper is the description of monodromy in the corresponding quantum system, which is obtained from separation of variables of the Helmholtz equation in $\mathbb{R}^3$. We show that the joint spectrum of the two commuting operators has quantum monodromy. In particular this can be seen from the analysis of the classical asymptotic series for the eigenvalues in two distinct limits. Then we show that the spheroidal harmonics integrable system is in fact symplectically equivalent to the integrable C. Neumann system of a particle constrained to move on a sphere with an added harmonic potential, which in this case has rotational symmetry. The analysis of monodromy using well known asymptotic formulas is somewhat heuristic, and to prove monodromy we show that the underlying classically integrable spheroidal harmonics system is generalised semi-toric with a non-degenerate focus-focus point corresponding to a doubly pinched torus.

2.2. THE FREE PARTICLE

The free particle in $\mathbb{R}^3$ lives on the phase space $T^*\mathbb{R}^3 \cong \mathbb{R}^6$ with global coordinates $\boldsymbol{Q} \coloneqq (x, y, z)^T$ and $\boldsymbol{P} \coloneqq (p_x, p_y, p_z)^T$. The Hamiltonian is simply $H = \frac{1}{2}\left(p_x^2 + p_y^2 + p_z^2\right)$ and the equations of motion are $\dot{\boldsymbol{Q}} = \boldsymbol{P}$ and $\dot{\boldsymbol{P}} = \boldsymbol{0}$. The trajectories or geodesics are

$$\boldsymbol{Q} = \boldsymbol{P}t + \boldsymbol{Q}_0, \quad \boldsymbol{P} = \boldsymbol{P}_0$$

where $\boldsymbol{Q}_0, \boldsymbol{P}_0$ are the intitial position and momentum vectors, respectively, and t is time. In position space, the geodesics are oriented lines through $\boldsymbol{Q}_0$ in the direction of $\boldsymbol{P} = \boldsymbol{P}_0$. We can perform a symplectic reduction that identifies the oriented straight lines of the flow of H to points and so lowers the dimensionality of the phase space from 6 to 4. We will see that this reduction also produces a compact configuration space, which is the space of oriented lines through the origin, which is a sphere. The conserved quantities are the linear momenta $\boldsymbol{P} = (p_x, p_y, p_z)$ and the angular momenta $\boldsymbol{L} \coloneqq \boldsymbol{Q} \times \boldsymbol{P} = (l_x, l_y, l_z)^T$, since

$$\boldsymbol{L}(t) = (\boldsymbol{Q}_0 + t\boldsymbol{P}_0) \times \boldsymbol{P}_0 = \boldsymbol{Q}_0 \times \boldsymbol{P}_0 = \text{constant}.$$

By construction we have $\boldsymbol{P} \cdot \boldsymbol{L} = \boldsymbol{0}$.

The six invariants $\boldsymbol{P}$, $\boldsymbol{L}$ are closed under the standard Poisson bracket in $T^*\mathbb{R}^3$. For example $\{p_x, l_y\} = p_z$, and $\{l_x, l_y\} = l_z$, etc. Assembling all such identities into a 6×6 matrix B

gives[1]

$$B = -\begin{pmatrix} \mathbf{0} & \hat{\boldsymbol{P}} \\ \hat{\boldsymbol{P}} & \hat{\boldsymbol{L}} \end{pmatrix} . \tag{2.1}$$

The matrix B is the matrix of a Lie-Poisson structure on $\mathbb{R}^6$ with coordinates $\boldsymbol{P}$ and $\boldsymbol{L}$. This Lie-Poisson structure is the algebra $e^*(3)$ corresponding to the Euclidean group $E(3)$, the group of isometries of Euclidean space $\mathbb{R}^3$. In particular the components of $\boldsymbol{P}$ are generators of translations, while the components of $\boldsymbol{L}$ are generators of rotations. Given a Hamiltonian G the time evolution of any function $f(\boldsymbol{P}, \boldsymbol{L})$ is given by $\dot{f} = \{f, G\} = \nabla f^t B \nabla G$ and thus

$$\dot{\boldsymbol{P}} = -\boldsymbol{P} \times \nabla_L G, \quad \dot{\boldsymbol{L}} = -\boldsymbol{P} \times \nabla_P G - \boldsymbol{L} \times \nabla_L G \,. \tag{2.2}$$

The Poisson structure B has rank 4 with two Casimirs $C_1 = \boldsymbol{P} \cdot \boldsymbol{P} = 2E$ and $C_2 = \boldsymbol{P} \cdot \boldsymbol{L} = 0$, such that $B\nabla C_i = 0$. The first Casimir $C_1 = 2E$ is often set to 1 by normalisation of the speed of the particle, whereas the second Casimir C_2 is an identity that states that $\boldsymbol{L}$ is orthogonal to $\boldsymbol{P}$. In addition to these 6 basic invariants an analogue of the Laplac-Runge-Lenz (LRL) vector can be defined and we will discuss this in more detail in section 2.5.

Fixing the two Casimirs defines the reduced phase space of T^*S^2 as a subset of $\mathbb{R}^6$ with coordinates $\boldsymbol{P}$ and $\boldsymbol{L}$. Here the sphere is defined in momentum space, and reflects the constancy of the kinetic energy of the particle, while the tangent space to the sphere is the set of planes with normal vectors $\boldsymbol{P}$ in $\boldsymbol{L}$ space, hence $C_2 = 0$. Every point on T^*S^2 represents a line (geodesic) in the original $T^*\mathbb{R}^3$ with direction $\boldsymbol{P}$ (the point on the sphere) and angular momentum $\boldsymbol{L}$ (the vector in the tangent space of the sphere). Note that $\boldsymbol{L}$ is a normal vector to the plane that contains the geodesic and the origin, and the length of $\boldsymbol{L}$ is the distance of the geodesic to the origin divided by the value of C_1. There are four oriented lines with direction $\pm\boldsymbol{P}$ in a given plane with normal vector $\pm\boldsymbol{L}$. Changing the orientation of the geodesic amounts to changing the sign of $\boldsymbol{P}$ and $\boldsymbol{L}$. Changing the sign of $\boldsymbol{L}$ but not of $\boldsymbol{P}$ represents a parallel line with the same orientation in the same plane that is passing on the other side of the origin. Lastly, changing the sign of $\boldsymbol{P}$ but not of $\boldsymbol{L}$ represents a parallel line with the opposite orientation that is passing on the other side of the origin. Later we will identify any two such geodesics, which will lead to $T^*\mathbb{RP}^2$ instead of T^*S^2.

Since we have reduced by the dynamics of H there are no dynamics defined on T^*S^2 at the moment. In the next section we are going to define an integrable system on T^*S^2 by separating the free particle in spheroidal coordinates. The separation constant and the angular momentum will induce an integrable system on T^*S^2.

[1] For a vector $\boldsymbol{v} \in \mathbb{R}^3$ the corresponding antisymmetric hat matrix $\hat{\boldsymbol{v}}$ is defined by

$$\hat{\boldsymbol{v}}\boldsymbol{u} = \boldsymbol{v} \times \boldsymbol{u} \quad \forall \boldsymbol{u} \in \mathbb{R}^3.$$

Later we also use hat to denote the quantum operator corresponding to a classical observable; from the context it should be clear which one is meant.

2.3. THE SPHEROIDAL HARMONICS INTEGRABLE SYSTEM

Prolate ellipsoids are formed by rotating an ellipse around its focal axis. Let the foci of the resulting ellipsoid be located at $(0, 0, \pm a)$. Prolate spheroidal coordinates are then defined by

$$\begin{aligned} x &= a\sqrt{(\xi^2-1)\,(1-\eta^2)}\cos(\phi), \\ y &= a\sqrt{(\xi^2-1)\,(1-\eta^2)}\sin(\phi), \\ z &= a\xi\eta\,, \end{aligned} \tag{2.3}$$

where $\eta \in [-1, 1]$, $\xi \in [1, \infty)$ and $\phi \in [0, 2\pi) = S^1$. Each point of $\mathbb{R}^3$ is associated with the intersection of the ellipsoid described by (2.3), a confocal hyperboloid and a plane. These surfaces correspond to fixed ξ, η and ϕ respectively. The Hamiltonian of the free particle in prolate spheroidal coordinates is

$$H = \frac{1}{2a^2}\left(\frac{(1-\eta^2)p_\eta^2 + (\xi^2-1)p_\xi^2}{(\xi^2-\eta^2)} + \frac{p_\phi^2}{(1-\eta^2)\,(\xi^2-1)}\right) \tag{2.4}$$

where p_η, p_ξ and p_ϕ are the momenta conjugate to η, ξ, ϕ, respectively. Clearly p_ϕ is a constant angular momentum, since H is independent of ϕ. To separate the variables observe that

$$0 = (H-E)2a^2(\xi^2-\eta^2) = G(\eta, p_\eta) - G(\xi, p_\xi),$$

where

$$G(q,p) = (1-q^2)(p^2 - 2a^2E) + \frac{p_\phi^2}{1-q^2} \tag{2.5}$$

such that $G(\xi, p_\xi) = g = G(\eta, p_\eta)$ where g is the separation constant. Substituting $E = H$ into G gives

$$G = \frac{p_\eta^2 - p_\xi^2}{\xi^2-\eta^2}(1-\eta^2)(\xi^2-1) + p_\phi^2\frac{\xi^2-\eta^2}{(\xi^2-1)(1-\eta^2)}\,.$$

To convert this to the original variables observe that

$$|\boldsymbol{L}|^2 = \frac{(\xi^2-1)(1-\eta^2)}{(\xi^2-\eta^2)^2}(p_\xi\eta - p_\eta\xi)^2 + p_\phi^2\left(\frac{1+\xi^2-\eta^2}{(\xi^2-1)(1-\eta^2)}\right)$$

and

$$a^2(p_x^2+p_y^2) = \frac{(\xi^2-1)(1-\eta^2)}{(\xi^2-\eta^2)^2}(p_\xi\xi - p_\eta\eta)^2 + p_\phi^2\frac{1}{(\xi^2-1)(1-\eta^2)}$$

such that

$$G = |\boldsymbol{L}|^2 - a^2(p_x^2+p_y^2)\,. \tag{2.6}$$

This is a smooth function on T^*S^2, as is $p_\phi = L_z$, and it is easy to check that they have vanishing Poisson bracket. This can be computed in the original variables $(\boldsymbol{Q}, \boldsymbol{P})$ with respect to the canonical bracket on $T^*\mathbb{R}^3$, or in the variables $(\boldsymbol{P}, \boldsymbol{L})$ after reduction to T^*S^2

with respect to the induced bracket with Poisson tensor B. In both cases $\{|\boldsymbol{L}|^2, L_z\} = 0$ and also $\{p_x^2 + p_y^2, L_z\} = 0$ and hence $\{G, L_z\} = 0$. We write L_z for the function that maps a point $(\boldsymbol{P}, \boldsymbol{L})$ to the coordinate l_z. Thus we arrive at the main classical object of this paper:

Theorem 2.1 (Spheroidal harmonics integrable system)**.** *Consider $\mathbb{R}^6$ with coordinates $(\boldsymbol{P}, \boldsymbol{L})$ and Lie-Poisson structure of $e^*(3)$ with Poisson tensor B given by (2.1) and Casimirs $\boldsymbol{P} \cdot \boldsymbol{P} = 2E$ and $\boldsymbol{P} \cdot \boldsymbol{L} = 0$. The functions $(L_z, G) = (l_z, l_x^2 + l_y^2 + l_z^2 - a^2(p_x^2 + p_y^2))$ define a Liouville integrable system on T^*S^2.*

The values of (L_z, G) will be denoted by (m, g). We call this integrable system the (prolate) *spheroidal harmonics integrable system*, since it arises from separation of variables in spheroidal coordinates. It is the classical analogue of the compact part of the spheroidal wave equation, whose solutions are known as spheroidal harmonics.[2] In this work we are only interested in the prolate spheroidal harmonics. Formally the oblate case can be found by flipping the sign of a^2, and this system is also Liouville integrable. However, the dynamics in the oblate case are quite different and in particular does not exhibit monodromy, so we do not consider this case in the present work. Repeating this procedure for any of the 11 separating coordinate systems on $\mathbb{R}^3$ gives rise to an integrable system on $e^*(3)$. The list of the resulting smooth commuting integrals is given in [MPW81]. For example, for Euclidean coordinates the integrals are the components of $\boldsymbol{P}$, and the dynamics produces straight lines in $\boldsymbol{L}$. This is an integrable system, but all the dynamics is unbounded. Separation in ellipsoidal coordinates leads to an integrable system on $e^*(3)$ with two quadratic commuting functions and with two parameters. Under the mapping described in Theorem 5 this integrable system is equivalent to the (non-degenerate) C. Neumann system. It is an interesting research project to study these integrable Hamiltonian systems alongside the corresponding special functions. In this paper we restrict our attention to spheroidal coordinates, because, as we will show, it leads to a generalised semi-toric system that exhibits Hamiltonian monodromy. The related quantum system has quantum monodromy. In other words, the eigenvalues of the spheroidal wave equation exhibit monodromy. Before we describe the spheroidal wave equation and its quantum monodromy in the next section, here we are going to describe some aspects of the dynamics of the spheroidal harmonics integrable system. A detailed analysis including the proof that it is a generalised semi-toric system with Hamiltonian monodromy is postponed to a later section.

The vector field that is generated by the Hamiltonian L_z is given by $B\nabla L_z$ which

[2]The term spheroidal harmonics is used in different ways in the literature. The strict use of "harmonics" refers to solutions of the Laplace equation. When considering the Laplacian in $\mathbb{R}^3$ separated in spheroidal coordinates the eigenfunctions are products of associated Legendre functions, however, one of them is evaluated outside the usual range $|z| < 1$, and is thus sometimes referred to as a spheroidal harmonic [DLMF, 14.3]. Our use of the term spheroidal harmonic is different and serves as a "reminder of the kinship with the spherical harmonics" [PFTV88, 17.4].

gives

$$\dot{\boldsymbol{P}} = -\boldsymbol{P} \times \boldsymbol{e}_z, \quad \dot{\boldsymbol{L}} = -\boldsymbol{L} \times \boldsymbol{e}_z \,. \tag{2.7}$$

The solution is a rotation of the first two components of $\boldsymbol{P}$ and $\boldsymbol{L}$ by the same amount; the third components are unchanged. Thus the point $\boldsymbol{P}$ on S^2 is rotated about the p_z-axis, while $\boldsymbol{L}$ in the tangent space is rotated in the same way. The north- and the south-poles of S^2 are fixed by this rotation, but then $\boldsymbol{L} = (l_x, l_y, 0)^T$ is not fixed, unless it vanishes. A vector $\boldsymbol{L} = (0, 0, l_z)^T$ that is in the tangent space of a point $\boldsymbol{P} = (\cos\phi, \sin\phi, 0)$ on the equator of the sphere is fixed by this rotation, but the corresponding $\boldsymbol{P}$ is not. This shows that the only fixed points of this S^1 action are $\boldsymbol{P} = (0, 0, \pm 1)^T$, $\boldsymbol{L} = (0, 0, 0)^T$. They correspond to geodesics along the z-axis, i.e., lines through the two foci of the ellipsoid of the spheroidal coordinates.

The vector field that is generated by the Hamiltonian G is

$$\dot{\boldsymbol{P}} = -2\boldsymbol{P} \times \boldsymbol{L}, \quad \dot{\boldsymbol{L}} = a^2 \boldsymbol{P} \times (\boldsymbol{P} - \boldsymbol{e}_z p_z) = -a^2 p_z \boldsymbol{P} \times \boldsymbol{e}_z \,. \tag{2.8}$$

Clearly $\boldsymbol{L} = \boldsymbol{0}$ and $\boldsymbol{P} = \boldsymbol{e}_z p_z$ is an equilibrium point. Moreover, for $\boldsymbol{P} = (p_x, p_y, 0)^T$ and $\boldsymbol{L} = (0, 0, l_z)^T$ we have $\boldsymbol{L} = const$, $p_z = 0 = const$ and $\dot{p}_x = -2l_z p_y$ and $\dot{p}_y = 2l_z p_x$, a periodic solution along the equator with orientation depending on the sign of l_z. For $l_z = 0$ the equator is a circle of non-isolated equilibrium points of the flow of G.

In the limiting case $a \to 0$ the integral G becomes the angular momentum squared. In this limit the equations of motion can be solved explicitly in terms of trigonometric functions. Since $\dot{\boldsymbol{L}} = 0$ the equation for $\dot{\boldsymbol{P}}$ is that of a rotation about the fixed axis $\boldsymbol{L}$. The period of these rotation is given by $\sqrt{|\boldsymbol{L}|}$. If instead of $G = |\boldsymbol{L}|^2$ we consider $|\boldsymbol{L}|$ as a Hamiltonian then the period is 2π, and hence $|\boldsymbol{L}|$ is an action variable. To see this just integrate $\dot{\boldsymbol{P}} = -\boldsymbol{P} \times \boldsymbol{L}/|\boldsymbol{L}|$ for constant non-zero $\boldsymbol{L}$. The solution is a rotation of $\boldsymbol{P}$ about the fixed normal vector in the direction of $\boldsymbol{L}$. The only problem with the flow of $|\boldsymbol{L}|$ is that the vector field is not defined when $\boldsymbol{L} = \boldsymbol{0}$ and hence the flow does not define a global S^1 action. When instead the flow of $G = |\boldsymbol{L}|^2$ (for $a = 0$) is considered the vector field simply vanishes when $\boldsymbol{L} = \boldsymbol{0}$, and so the whole sphere $|\boldsymbol{P}| = 2E$ is a sphere of fixed points.

The spheroidal harmonics integrable system has a number of discrete symmetries. We restrict our attention to discrete symmetries that are canonical transformations.

Proposition 1 (Discrete symmetries)**.** *The group of linear discrete canonical symmetries of the spherical harmonics integrable system is* $\mathbb{Z}_2 \times \mathbb{Z}_2$. *For* $s_i = \pm 1$, $i = 1, 2, 3$ *define* $S = \mathrm{diag}(s_1, s_2, s_3)$ *and* $\tilde{S} = \mathrm{diag}(s_2 s_3, s_1 s_3, s_1 s_2)$ *so that a linear map of* $(\boldsymbol{P}, \boldsymbol{L})$ *is given by* $(S\boldsymbol{P}, \tilde{S}\boldsymbol{L})$. *The non-trivial elements of* $\mathbb{Z}_2 \times \mathbb{Z}_2$ *are obtained from* $S_1 = \mathrm{diag}(+, +, -)$, $S_2 = \mathrm{diag}(-, -, -)$ *and* $S_3 = \mathrm{diag}(-, -, +)$.

Proof. Since $S^{-1} = S^t$ the map $\boldsymbol{Q} \mapsto S\boldsymbol{Q}$ extends to a symplectic map as $(\boldsymbol{Q}, \boldsymbol{P}) \mapsto$

$(S\boldsymbol{Q}, S\boldsymbol{P})$. The induced sign flip on the angular momentum is $\boldsymbol{L} \mapsto \tilde{S}\boldsymbol{L}$ where $\hat{S} = \mathrm{diag}(s_2s_3, s_1s_3, s_1s_2)$ is found by computing the cross product $\boldsymbol{Q} \times \boldsymbol{P}$. The integral G is invariant under all such sign flips, since it is quadratic in components of $\boldsymbol{P}$ and $\boldsymbol{L}$. In addition $L_z = xp_y - yp_x$ should be invariant under the discrete symmetry which requires $s_1s_2 = +1$. Thus the discrete symmetries of the spheroidal harmonics system are $S_1 = \mathrm{diag}(++-)$, $S_2 = \mathrm{diag}(---)$ and $S_3 = \mathrm{diag}(--+)$ together with the corresponding induced map $\tilde{S}_i$ on $\boldsymbol{L}$. Together with the identity they form the group $\mathbb{Z}^2 \times \mathbb{Z}^2$.

■

In prolate spheroidal coordinates (2.3) the symmetry operations are realised as follows. Changing the sign of η changes the sign of z but leaves x and y unchanged, so that $\eta \mapsto -\eta$ corresponds to the symmetry S_1. Adding π to ϕ changes the signs of x and y while z is unchanged, so that $\phi \mapsto \phi + \pi$ corresponds to the symmetry S_3. The composition of both gives S_2.

2.4. QUANTUM MONODROMY IN PROLATE SPHEROIDAL HARMONICS

Separation of variables of the Laplace equation or the Helmholtz equation in $\mathbb{R}^3$ in spheroidal coordinates leads to spheroidal harmonics. The classical references on spheroidal harmonics are [SMC+59, MS54, Fla57], and a few more modern ones are [PFTV88, FAW03, Vol03, DLMF, Zha17]. We would like to mention that prolate spheroidal wave functions have found applications as band-limited functions [Sle83], also see [XRY01, Boy04] and the references therein. Here we will derive the spheroidal wave equation in the traditional way from the Schrödinger equation of the free particle separated in spheroidal coordinates. This will allow us to connect to the spheroidal harmonics integrable system by way of semi-classical quantisation, a connection we need later to prove the existence of quantum monodromy.

The stationary Schrödinger equation for the free particle is $-\frac{1}{2}\hbar^2\Delta\Psi = E\Psi$, or we can think of it as Helmholtz's wave equation $\Delta\Psi + k^2\psi = 0$. Writing the Laplacian Δ in spheroidal coordinates (2.3) gives

$$\frac{1}{(\xi^2-\eta^2)}\left(\frac{\partial}{\partial\xi}\left((\xi^2-1)\frac{\partial\Psi}{\partial\xi}\right)+\frac{\partial}{\partial\eta}\left((1-\eta^2)\frac{\partial\Psi}{\partial\eta}\right)\right)+\frac{1}{(1-\eta^2)(\xi^2-1)}\frac{\partial^2\Psi}{\partial\phi^2}=-\frac{2Ea^2}{\hbar^2}\Psi\,. \tag{2.9}$$

Separation into product form $\Psi(\eta,\xi,\phi) = \psi_\eta(\eta)\psi_\xi(\xi)\psi_\phi(\phi)$ yields the simple equation

$$\hat{L}_z^2\psi_\phi + m^2\psi_\phi = 0, \quad \hat{L}_z^2 = \frac{\partial^2\psi_\phi}{\partial\phi^2} \tag{2.10}$$

and the (prolate angular) spheroidal wave equation

$$\hat{G}\psi_\eta = g\psi_\eta, \quad \hat{G} = -\frac{d}{d\eta}\left((1-\eta^2)\frac{d}{d\eta}\right) + \frac{m^2}{1-\eta^2} - \gamma^2(1-\eta^2), \quad \gamma^2 = \frac{2Ea^2}{\hbar^2} \tag{2.11}$$

with separation constants m and g. The third separated equation is found by replacing η by ξ. The difference is in the domain $\eta \in [-1, 1]$ while $\xi \geq 1$.

For general values of γ the equation (2.11) is a singular Sturm-Liouville equation. It can be transformed into an equation with periodic (but still singular) coefficients, see, e.g. [Ars64]. Viewed as a polynomial differential equation in the complex plane it can be transformed into the confluent Heun equation [RA95]. The general Heun equation is the second order ordinary differential equation of Fuchsian type with four regular singular points. Letting two of the regular singular points coalesce leads to an irregular singular point. The result is the confluent Heun equation.

The quantum integrable system (QIS) on the reduced space consists of two self-adjoint operators $\hat{L}_z$ and $\hat{G}$ acting on functions on the sphere S^2. The eigenvalues g_l^m of $\hat{G}$ are those values of g in (2.11) for which the solution of the spheroidal wave equation for η leads to a smooth function $\psi_\eta\psi_\phi$ on the sphere. This is because, as we shall see below, said eigenvalues will be obtained from an infinite series of smooth Legendre polynomials. These coefficients will be set so as to give a final bounded and smooth wavefunction. In our treatment we ignore the equation for ξ.

The solution ψ_ϕ to the angular equation is equal to linear combinations of $e^{\pm im\phi}$ and 2π-periodicity in ϕ implies $e^{\pm im2\pi} = 1$, and hence m must be an integer. This integer m is the quantum number for the z-component of the angular momentum $l_z = m\hbar$.

When g is an eigenvalue g_l^m of the singular Sturm-Liouville problem (2.11) the corresponding eigenfunction bounded on $(-1, 1)$ is called the (prolate angular) spheroidal wave function of the first kind, which we denote by $S_l^m(\gamma, \eta)$.[3] In the limit $\gamma \to 0$ these solutions degenerate to the associated Legendre polynomials of the first kind $P_l^m(\eta)$. For $\gamma \neq 0$ the spheroidal wave functions can be written as a (generally infinite) series of associated Legendre polynomials

$$S_l^m(\gamma, \eta) = \sum_{k=0,1}^{\infty}{}' \, d_k^{lm}(\gamma) P_{m+k}^m(\eta) \tag{2.12}$$

where d_k^{lm} are the expansion coefficients and the prime on the summation indicates to sum over odd k if $l - m$ is odd and over even k if $l - m$ is even. Expressions for the resulting three term recursion relation that determines d_k^{lm} can be found, e.g., in [AS92, 21.7.3].

[3] The notation for the angular spheroidal wave function varies, see [AS92] for a table comparing various common notations. Our notation loosely follows [AS92], but we prefer to write l instead of n as in [SMC+59, MF53], and we write the indices ${}_l^m$ as in the associated Legendre polynomials.

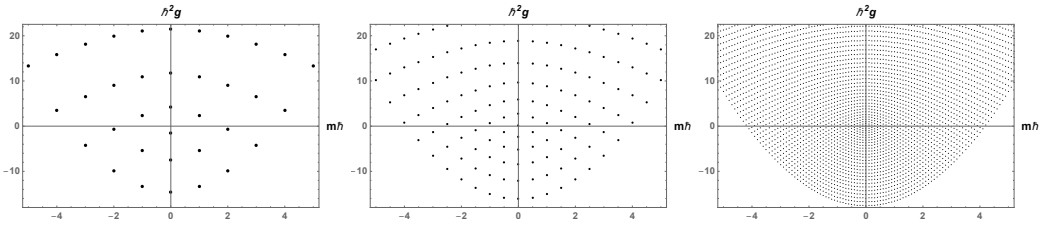

Figure 2.1: Joint spectrum $(\hbar m, \hbar^2 g_l^m)$ of the spheroidal harmonics with $2Ea^2 = 18$ for $\hbar = 1.0, 0.5, 0.1$ illustrating the semi-classical limit $\hbar \to 0$.

The product of the eigenfunctions of (2.10) and (2.11) gives the spheroidal harmonics

$$Z_l^m(\gamma, \eta, \phi) := \frac{1}{\sqrt{2\pi}} S_l^m(\gamma, \eta) e^{im\phi} = \sum_k d_k^{lm} Y_{m+k}^m(\eta, \phi) \tag{2.13}$$

expressed as a series of spherical harmonics Y_l^m. In the limit $\gamma \to 0$ we have $Z_l^m = Y_l^m$. Normalisation on the sphere requires

$$\int_0^{2\pi} \int_0^{\pi} Z_l^m \, (Z_l^m)^* \sin\theta d\theta d\phi = 1.$$

and the d_k^{lm} are chosen such that this holds, see, e.g., [AS92]. An example of the spheroidal wave function $S_l^m(\gamma, \eta)$ is shown in Fig. 2.7 and a comparision of $Z_l^m(\theta, \phi)$ with the corresponding spherical harmonic $Y_l^m(\theta, \phi)$ is presented in Fig. 2.8.

We now consider the joint spectrum of the QIS $(\hat{L}_z, \hat{G})$. The joint spectrum of a QIS $(\hat{H}_1, \ldots, \hat{H}_n)$ is the set of $(\lambda_1, \ldots \lambda_n) \in \mathbb{R}^n$ where $\hat{H}_i \psi = \lambda_i \psi$ for $i = 1, \ldots, n$ and ψ is a joint eigenfunction. For periodicity in ϕ we need to require that the eigenvalue of $\hat{L}_z$ is $\hbar$ times an integer m. The eigenvalues g_l^m of $\hat{G}$ can in general only be computed numerically. The Mathematica [rWR19] function `SpheroidalEigenvalue[`l, m, γ`]` gives the spheroidal eigenvalue g_l^m of (2.11). From general results in microlocal analysis, see, e.g., [PPVuN14], we know that in the semiclassical limit $\hbar \to 0$ the joint spectrum $(\hbar m, \hbar^2 g_l^m)$ is locally a lattice $\hbar\mathbb{Z}^2$. For a fixed spheroidal coordinate system, i.e., a fixed value of a decreasing $\hbar$ makes this local lattice finer and finer, see Fig. 2.1.

In the following we prefer to absorb $\hbar$ in the definition of the single parameter $\gamma = 2Ea^2/\hbar^2$ and present the scaled joint spectrum (m, g_l^m). When changing γ the values and the distribution of the joint eigenvalues changes. We are going to explain the structure of the joint spectrum and its dependence on γ in the course of the paper. Two examples of the joint spectrum are shown in Fig. 2.2 for $\gamma = 8, 32$. Note that this lattice is bounded below by a parabola (given by the critical values of the energy-momentum map, see below) but unbounded from above. We can observe that, locally the lattice is isomorphic to $\mathbb{Z}^2$ thus allowing local assignments of quantum numbers. However, there is a lattice defect at the origin, and thus we do not have a global $\mathbb{Z}^2$ lattice, indicating the presence of quantum

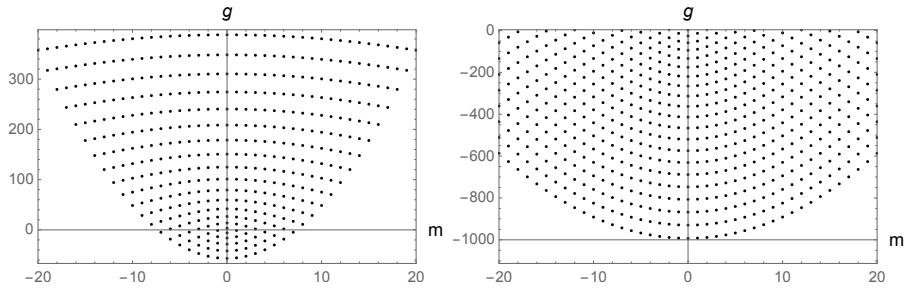

Figure 2.2: Joint spectrum (m, g_l^m) of the spheroidal harmonics for $\gamma = 8, 32$. The asymptotic expansion for g_l^m (2.14) is valid in the top part of the left figure, while (2.15) is valid in the bottom part of the right figure.

monodromy.

The spectrum of the spheroidal wave equation is well understood, and asymptotic expansions for the eigenvalues g_l^m are well known [MS54, AS92, DLMF, Ars64]. Here we are going to use these formulas to describe the quantum monodromy in the joint spectrum.

When $a \to 0$ the constant $\gamma \to 0$ and the operator $\hat{G} \to |\boldsymbol{L}|^2$ becomes that of the associated Legendre equation with spectrum $g_l^m = l(l+1)$ and corresponding eigenfunction the associated Legendre polynomial $P_l^m(\eta)$ for $-l \leq m \leq l$. The spectrum is degenerate since g_l^m is independent of m. The labelling of eigenvalues in the spheroidal wave equation is continued from this limit for non-zero a. This means that in the Sturm-Liouville problem of the operator $\hat{G}$ for given fixed integer m the eigenvalue g_l^m of the ground state is labelled by $l = |m|$. The degeneracy is split for non-zero γ and

$$\hat{g}_l^m = l(l+1) - \frac{1}{2}\left(1 + \frac{(2m-1)(2m+1)}{(2l-1)(2l+3)}\right)\gamma^2 + O(\gamma^4/l^2), \tag{2.14}$$

see, e.g., [MS54, AS92, DLMF, Ars64]. This expansion converges when $\gamma^2 < \rho_l^m$ where $\rho_l^m > 4l + 6$ for $l - |m| = 0, 1$ and $\rho_l^m > 4l - 2$ for $l - |m| \geq 2$, see [MS54, 3.22]. This means that for fixed γ one can always choose l large enough so that the series converges. For fixed γ this approximation can be understood as a semi-classical limit with fixed a but large quantum number l or correspondingly large values of the eigenvalue g_l^m.

When $\gamma \to \infty$ the spectrum also becomes simpler, but in this limit we are only aware of an asymptotic series expansion for the eigenvalues. The leading order of the operator $\hat{G}$ is $-a^2(\hat{p}_x^2 + \hat{p}_y^2)$. The eigenvalues satisfy

$$\check{g}_l^m = -\gamma^2 + (2(l - |m|) + 1)\gamma - \tfrac{3}{4} + m^2 - \tfrac{1}{2}(l - |m|)(l - |m| + 1) + O(1/\gamma), \tag{2.15}$$

see [MS54, AS92, DLMF, Ars64, Mül63]. Thus eigenvalues with the same value of $l - |m|$

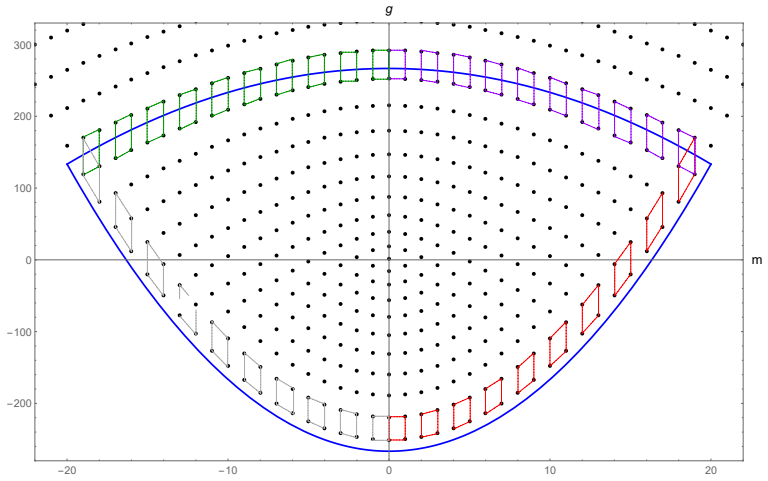

Figure 2.3: Joint spectrum (m, g_l^m) of the spheroidal harmonics for $\gamma = 16$. A lattice unit cell is transported around the origin. The lower blue parabola is $g = -\gamma^2 + m^2$ and the upper blue parabola is $2g = 2l^2 - \gamma^2 - m^2(\gamma/l)^2$ for $l = l^*$. The red and purple cells are transports of the bottom cell B_l^m and the top cell T_l^m, respectively, for positive m. The grey and green cells are those for negative m.

and small $|m|$ are degenerate at leading order. The limit of large γ can be understood as the semiclassical limit where $\hbar \to 0$ for fixed value of a for quantum numbers l close to the ground state with $l = |m|$.

Fig. 2.3 illustrates the monodromy about the origin. A unit cell is parallel transported along a path that encloses the origin. As the basis vectors (say v_1 is the vertical vector and v_2 is the horizontal one) are fully transported around the loop, we observe that v_1 stays constant whilst v_2 becomes $v_2 + 2v_1$. This implies that we have a basis transformation according to

$$\begin{pmatrix} v_1' \\ v_2' \end{pmatrix} = \begin{pmatrix} 1 & 0 \\ k & 1 \end{pmatrix} \begin{pmatrix} v_1 \\ v_2 \end{pmatrix} \tag{2.16}$$

where $k = 2$. This integer is called the monodromy index. In the figure the full loop is broken up into two symmetric half-loops. At each of the two points where the two half-loops meet a basis transformation with $k = 1$ occurs, and their product gives the monodromy with $k = 2$. In the next section we will prove monodromy by showing that in the classical phase space there are isolated critical points of focus-focus type and the pre-image of the corresponding critical value is a doubly pinched torus. Here we give a direct quantum mechanical interpretation of monodromy that is based on discrete symmetries and the well known asymptotic formulas (2.14) and (2.15). We should emphasise that the following discussion is a heuristic analysis of monodromy. While (2.14) can be extended to a convergent series, we are not aware of a a convergent extension of the asymptotic formula (2.15). Because of this it is not easy to make the following argument rigorous.

The monodromy along a loop in the joint spectrum around the origin can be analysed by

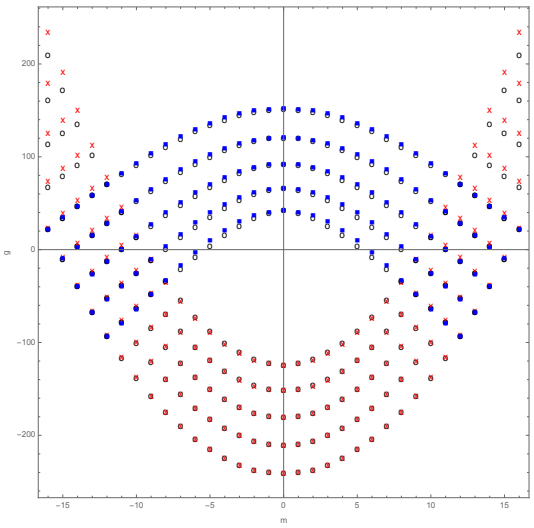

Figure 2.4: Joint spectrum (m, g_l^m) (black dots) compared to the asymptotic formulas $(m, \hat{g}_l^m)$ (blue dots) and $(m, \check{g}_l^m)$ (red dots) for $\gamma = 16$. The two asymptotic formulas approximately agree near the lattice point $l = |m| = l^* = 12$.

transporting a unit cell, see Fig. 2.3. Transporting a unit cell only makes sense where there are at least two negative eigenvalues in the sequence g_l^0, $l = 0, 1, \ldots$. The ground state g_0^0 is always non-positive. For $\gamma = \pi$ we have $g_1^0 < 0 < g_2^0$ and hence we require $\gamma \geq \pi$. The transport is done along the lower parabola where $l^2 - m^2 = 0$ in the joint spectrum and near a particular "upper" parabola where $l = l^* = \lceil \kappa\gamma \rceil$ is constant in the joint spectrum. The factor κ needs to satisfy $\kappa > 1/\sqrt{2}$ so that $g_{l^*}^0(\gamma) > 0$. In Fig. 2.3 we choose $\kappa = \sqrt{2/3}$ and in Fig. 2.4 we choose $\kappa = 3/4$. To see that these are indeed parabolas in (m, g)-space a truncation of (2.14) gives $g = -\gamma^2 + m^2$ and a truncation of (2.15) gives $g = (l^*)^2 - \gamma^2/2 - \frac{1}{2}m^2(\gamma/l^*)^2$. Note that it is neither required nor necessary that these parabolas go through points in the spectrum. They merely serve as an approximate guide to where the lattice structure of the joint spectrum is going to be analysed.

A unit cell in the joint spectrum is defined at $l = m = 0$ and moved along the lower parabola. Another unit cell in the joint spectrum is defined at $l = l^*, m = 0$ and transported along the upper parabola. The two parabolas meet where $m = l^*$. A unit cell near the bottom parabola is defined by its four corners as $B_l^m = (g_l^m, g_{l+1}^{m+1}, g_{l+2}^{m+1}, g_{l+1}^m)$ moving counterclockwise around the unit cell. A unit cell near the top parabola is defined by its four corners as $T_l^m = (g_l^m, g_l^{m+1}, g_{l+1}^{m+1}, g_{l+1}^m)$ moving counterclockwise around the unit cell. For negative m cells are obtained by reflection about $m = 0$. The cell at the top has a natural labelling, which is inherited from the spherical harmonics limit. Now the cells are moved together to the point where the parabolas meet. There $B_{l^*-1}^{l^*-1}$ is compared with $T_{l^*}^{l^*-1}$. The 2nd and 3rd state in the two unit cells agree, and the last of B with the first of T. Thus a basis transformation will add 1 unit to l. A mirror symmetric situation occurs for negative m, and hence the total monodromy around the loop is 2.

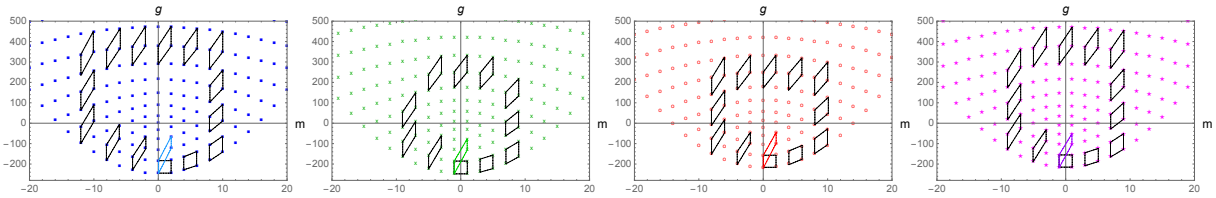

Figure 2.5: a) and b) Joint spectrum where $l - m$ is even and m is even/odd respectively. c) and d) where $l - m$ is odd and m is even/odd respectively. a) is invariant under the whole discrete symmetry group, b), c), d) are invariant under S_1, S_3, S_2, respectively.

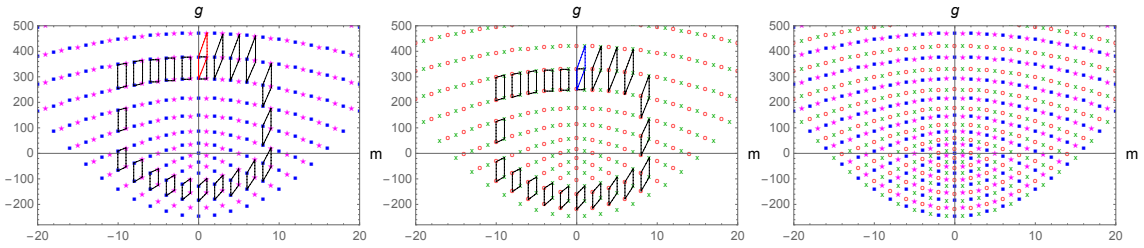

Figure 2.6: Parts of the joint spectrum whose eigenfunctions are a) even under S_2, b) odd under S_2 and c) the complete joint spectrum. The spectra shown in a) and b) both have monodromy index 1.

When repeating this process with the asymptotic formulae (2.14) and (2.15) instead of with the (numerically computed) exact spectrum, the cell B_l^m is defined using $\check{g}_l^m$ in (2.14) and T_l^m is defined using $\hat{g}_l^m$ in (2.15). Approximate eigenvalues in these cells will only approximately agree near $l = l^* = |m|$. In Fig. 2.4 the exact eigenvalues are shown as black dots, approximations from (2.14) (using $\check{g}_l^m$ up to including terms of order γ^4) are shown as blue dots for $l - l^* = 0, \ldots, 4$, $\pm m = 0, \ldots, l$ and approximations from (2.15) (using $\hat{g}_l^m$ up to including terms of order γ^{-2}) are shown as red dots for $l - |m| = 0, \ldots, 4$, $\pm m = 0, 1, \ldots, l^* + 4$. The blue dots sit nearly on top of the black dots for larger l, while the red dots sit nearly on top of the black dots for small $l - |m|$. The choice of κ and hence l^* is selecting the region near $(l, m) = (l^*, l^*)$ where both formulas work. To make this quantitative we introduce a measure for the quality of the asymptotic formulas as the relative error

$$e(l, m) = \frac{\hat{g}_l^m - \check{g}_l^m}{\hat{g}_{l+1}^m - \hat{g}_l^m}$$

evaluated at lattice points (l, m) where both hold approximately. Evaluated with $\kappa = 3/4$ this gives $|e(l^*, l^*)| < 0.07$, $|e(l^* + 1, l^* + 1)| < 0.07$ for the two lower states near (l^*, l^*) and $|e(l^* + 1, l^*)| < 0.19$, $|e(l^*, l^* - 1)| < 0.19$ for the two higher states. These estimates hold for any $\gamma > \pi$. This implies that even though there is a considerable error, it is still possible to identify the unit cells, since the error is less than 20% for all four corners relative to the size of the cell. Thus it is possible to define quantum monodromy using the asymptotic formulas alone.

The joint spectrum can be divided into symmetry classes. Since (2.11) is even in η the eigenfunctions S_l^m are even or odd. They inherit the symmetry of P_l^m so that S_l^m is even when $l-m$ is even and odd when $l-m$ is odd. Accordingly $S_l^m \circ S_1 = (-1)^{l-m} S_l^m$. Similarly for $\psi_\phi = e^{im\phi}$ it holds that $\psi_\phi \circ S_3 = (-1)^m \psi_\phi$. Thus every point in the joint spectrum can be classified according to the parity of $l-m$ and m. This is illustrated in Fig. 2.5 a) through d), where each subfigure contains one quarter of the number of points the full spectrum possesses. Despite this, the unit cell is still deformed in the same way as in Fig. 2.3 and the monodromy index is 2.

It is interesting to note that when selecting states according to their symmetry under $S_2 = S_1 \circ S_3$ the monodromy index changes to 1. The (semi-)classical explanation for this is that after discrete symmetry reduction by S_2, the reduced phase space is $T^*(\mathbb{RP}^2)$. See Lemma 10 for more detail. Further related to this, as we will see, such a reduction will give a system with the same action variables, but different Maslov indices. Since Z_l^m is the product of ψ_ϕ and S_l^m it is invariant under S_2 if $l-m$ and m are either both even or both odd. The corresponding joint eigenvalues are shown in Fig. 2.6 left and middle, and for this selection of joint eigenstates the monodromy is 1.

The most striking effect of the monodromy is a change in what the symmetry of horizontally neighbouring states near the line $m = 0$ is. Consider Fig. 2.6 left and middle. When $g \ll 0$ the horizontally neighbouring states have the same symmetry type, while for $g \gg 0$ the symmetry type changes. Not only does the symmetry type change, but also the location of states comparing $m = 0$ and $m = 1$. For $g \gg 0$ horizontally neighbouring states with $m = 0$ and $m = 1$ have nearly the same eigenvalue. By contrast, for $g \ll 0$ consider a state with $m = 0$. Now there is no horizontally neighbouring state with $m = 1$. Instead the eigenvalue for a state with $m = 1$ is approximately half way between the nearby states with $m = 0$.

We are now going to make these observations precise using (2.14) and (2.15). Consider states invariant under S_2, hence with even $l-m$ and even m, see Fig. 2.6, left. Observe the upper end of the figure where $g \gg 0$ with $m = 0$ and $l \gg 0$. These states are described by (2.15), the asymptotics for large γ or small $\hbar$. Horizontally neighbouring states with $m = 0$ and $m = 1$ have nearly the same eigenvalue. Using (2.15) we find

$$g_{l+1}^1 - g_l^0 = 1 + O(1/\gamma), \quad \text{for } g_l^0 \gg 0.$$

The same analysis holds for Fig. 2.6, where l in the above formula is odd, while in the left figure it is even. Note that the separation of states in the vertical direction $g_{l+2}^0 - g_l^0 = 4\gamma + (2l+3) + O(1/\gamma)$ is of order γ, and hence we perceive the neighbour in the horizontal direction as nearly the same. If we were to present eigenvalues with dimensions then the difference in eigenvalue of two horizontally neighbouring states would be of order $\hbar^2$, while those of two vertically neighbouring states would be $\hbar$.

Now compare this to the situation with $g \ll 0$ and hence small l near the line $m = 0$. There the state with $m = 1$ is approximately equal to the average of neighbouring states with $m = 0$. Using (2.14) we find

$$\frac{g_l^0 + g_{l+2}^0}{2} - g_{l+1}^1 = 1 + O(\gamma^2), \quad \text{for } g_l^0 \ll 0$$

in the horizontal direction, while in the vertical direction the separation is $g_{l+1}^1 - g_l^0 = 2(l+1) + O(\gamma^2)$. A comment similar to the previous case about the scaling with $\hbar$ applies here.

The previous discussing of neighbouring states was done separately for states that are either invariant under S_2 or not. The reason is that for these subsets the monodromy index is 1. When considering all states the monodromy index is 2, and its manifestation on the symmetry and labelling of states is different. In the set of all states in both limits, large positive and large negative g_l^0, there is always a horizontally neighbouring state with almost the same eigenvalue, see Fig. 2.6, right. A direct consequence of monodromy is the following observation: for large l such that $g_l^0 \gg 0$ for horizontally neighbouring states $g_l^0 - g_l^1 = O(\gamma^2)$. For small l such that $g_l^0 \ll 0$ however this difference is not small, $g_l^0 - g_l^1 = 2\gamma + O(1)$. This means that states with the same l are not horizontal neighbours, instead the index l needs to be increased by 1 when going to the right, then $g_l^0 - g_{l+1}^1 = 1 + O(1/\gamma)$ is small. This means that when comparing the labelling of states along the line $m = 0$ with the line $m = 1$ there is a mismatch that occurs for small l (negative g), while for large l (positive g) states are labelled in the natural way. As already mentioned the fact that this labelling is "natural" in the latter case is a choice that was made in order to have continuity with the labelling in the spherical harmonics limit $a \to 0$. One could redefine the labelling to be "natural" with respect to the Sturm-Liouville problems for fixed m, then each ground state for fixed m would have the same quantum number. Then the mismatch in the labelling of horizontal neighbours would appear for states with large eigenvalues g_l^m. The fact that this mismatch cannot be avoided is an expression of the quantum monodromy in the system.

The discussion of monodromy using the asymptotic expansions (2.14) and (2.15) is enlightning, but it is somewhat heuristic, since we don't know about the convergence of (2.15). If we stay near the line $m = 0$ and observe the change in lattice for small and large g (as we did in the discussion of neighbours above) we cannot complete a loop around the focus-focus point, because neither formula is valid there. If we do complete the loop along the parabolas as indicated in Fig. 2.3 we are stretching the asymptotic expansions to the limit of their validity. For this reason we are going to prove existence of monodromy in the semi-classical limit by a detailed analysis of the corresponding classically integrable system in section 2.6, and by appealing to the general theory of quantum monodromy [VuN99]. It is interesting to note that the general theory only makes sense in the semi-classical limit;

when explicit approximate formulas for the quantum eigenvalues like (2.14) and (2.15) are known, quantum monodromy makes sense as long as there are at least a few eigenvalues $g_l^0 < 0$, so down to say $\gamma = \pi$.

2.5. LAPLACE-RUNGE-LENZ AND C. NEUMANN

In this section we will show that the spheroidal harmonics system is symplectomorphic to the degenerate C. Neumann system. The C. Neumann system is a famous integrable system that was studied by Jacobi's student Carl Neumann [Neu59], as a prime example of separation of variables. It consists of a particle constrained to move on the unit sphere (in any dimension) under influence of an additional harmonic potential [Mos80a, Mos80b, Ves80, Raţ81]. The degenerate case has been studied in [Vuk08, DH12], and the action variables in the general case were analysed in [DRVW01], also see [DVuN07]. For the quantisation of the C. Neumann system (in the non-degenerate case) see [BT92, Tot93, Gur95].

The invariants $\boldsymbol{P}$ and $\boldsymbol{L} = \boldsymbol{Q} \times \boldsymbol{P}$ of the free particle are of degree 1 and 2 in the original phase space variables. Invariant degree 3 polynomials can be formed from them using an analogue of the Laplace-Runge-Lenz vector $\boldsymbol{A} = \boldsymbol{P} \times \boldsymbol{L}$. As in the Kepler problem it is useful to scale with the energy: $\boldsymbol{K} = \boldsymbol{A}|\boldsymbol{P}|^{-\alpha}$. The Poisson tensor in $\mathbb{R}^9$ with coordinates $(\boldsymbol{P}, \boldsymbol{L}, \boldsymbol{K})$ then is

$$B_\alpha = \begin{pmatrix} \mathbf{0} & -\hat{\boldsymbol{P}} & \hat{\boldsymbol{P}}^2|\boldsymbol{P}|^{-\alpha} \\ -\hat{\boldsymbol{P}} & -\hat{\boldsymbol{L}} & -\hat{\boldsymbol{K}} \\ -\hat{\boldsymbol{P}}^2|\boldsymbol{P}|^{-\alpha} & -\hat{\boldsymbol{K}} & \hat{\boldsymbol{L}}|\boldsymbol{P}|^{2(1-\alpha)} \end{pmatrix}. \tag{2.17}$$

In the Kepler problem the idea is to have the bracket between $\boldsymbol{L}$ and $\boldsymbol{K}$ close, so there the choice is $\alpha = 1$ so that $|\boldsymbol{P}|$ drops out in the lower right corner and the algebra is $so(4)$. In our case the choice $\alpha = 1$ leads to a realisation of the spheroidal harmonic system on $so(3,1)$, but the Hamiltonian G is not smooth when written in terms of $\boldsymbol{L}$ and $\boldsymbol{K}$, so we do not investigate this further. Instead we are interested to make the bracket between $\boldsymbol{P}$ and $\boldsymbol{K}$ close. To achieve this we need to eliminate $\boldsymbol{L}$. Using standard cross product identities we find $\boldsymbol{P} \times \boldsymbol{A} = -|\boldsymbol{P}|^2\boldsymbol{L} + \boldsymbol{P}(\boldsymbol{P} \cdot \boldsymbol{L})$. Choosing $\alpha = 2$ thus gives $\boldsymbol{P} \times \boldsymbol{K} = -\boldsymbol{L} + \boldsymbol{P}(\boldsymbol{P} \cdot \boldsymbol{L})|\boldsymbol{P}|^{-2}$. Now fixing the Casimir $\boldsymbol{P} \cdot \boldsymbol{L} = b$ of B_α allows us to eliminate $\boldsymbol{L}$ and the resulting Poisson structure on $\mathbb{R}^6$ with coordinates $(\boldsymbol{P}, \boldsymbol{K})$ is

$$B_{P,K} = |\boldsymbol{P}|^{-2} \begin{pmatrix} \mathbf{0} & \hat{\boldsymbol{P}}^2 \\ -\hat{\boldsymbol{P}}^2 & -\hat{\boldsymbol{U}} \end{pmatrix}, \quad \text{where} \quad \boldsymbol{U} = \boldsymbol{P} \times \boldsymbol{K} - b\boldsymbol{P}|\boldsymbol{P}|^{-2} \tag{2.18}$$

with Casimirs $\boldsymbol{P} \cdot \boldsymbol{P}$ and $\boldsymbol{P} \cdot \boldsymbol{K}$. Setting the magnetic term $b = 0$ and using the identity $\boldsymbol{P}\boldsymbol{P}^t - \hat{\boldsymbol{P}}^2 = id\boldsymbol{P} \cdot \boldsymbol{P}$ we see that this is the Dirac structure of T^*S^2 embedded in $\mathbb{R}^6$ as, e.g., derived in [DH12]. When considering the Dirac structure of T^*S^2 in $\mathbb{R}^6$ we use coordinates $\boldsymbol{x} = (x_1, x_2, x_3)^t \in S^2$ and momenta $\boldsymbol{y} = (y_1, y_2, y_3)^t$ in the tangent space of the sphere so

that $\boldsymbol{x} \cdot \boldsymbol{y} = 0$. Thus define the Dirac structure B_D of T^*S^2 in $\mathbb{R}^6$ as

$$B_D = \begin{pmatrix} \mathbf{0} & -id + \boldsymbol{x}\boldsymbol{x}^t|\boldsymbol{x}|^{-2} \\ id - \boldsymbol{x}\boldsymbol{x}^t|\boldsymbol{x}|^{-2} & -\widehat{\boldsymbol{x} \times \boldsymbol{y}}|\boldsymbol{x}|^{-2} \end{pmatrix} \tag{2.19}$$

with Casimirs $\boldsymbol{x} \cdot \boldsymbol{x}$ and $\boldsymbol{x} \cdot \boldsymbol{y} = 0$. Note that the lower left block is the projector to the subspace orthogonal to $\boldsymbol{x}$.

Lemma 2. *Consider the manifold* $M_r = \{(\boldsymbol{x}, \boldsymbol{y}) \in \mathbb{R}^6 \mid \boldsymbol{x} \cdot \boldsymbol{x} = r^2, \boldsymbol{x} \cdot \boldsymbol{y} = 0\}$ *for* $r > 0$. *The map* $\mu : M_r \to M_r$, $(\boldsymbol{x}, \boldsymbol{y}) \mapsto (\boldsymbol{x}, -\boldsymbol{x} \times \boldsymbol{y})$ *is a diffeomorphism with inverse* $(\boldsymbol{x}, \boldsymbol{y}) \mapsto (\boldsymbol{x}, \boldsymbol{x} \times \boldsymbol{y}/r^2)$.

Proof. Composing μ with μ^{-1} and using the vector triple product expansion formula gives $-\boldsymbol{x} \times (\boldsymbol{x} \times \boldsymbol{y})/r^2 = \boldsymbol{y}(\boldsymbol{x} \cdot \boldsymbol{x})/r^2 - \boldsymbol{x}(\boldsymbol{x} \cdot \boldsymbol{y})/r^2 = \boldsymbol{y}$.

■

Note that for $r = 1$ the map μ of M_1 has order 3. If we think of a curve $\boldsymbol{x}(t)$ on the sphere such that $\boldsymbol{y}$ is the tangent vector to the curve then μ maps the tangent vector to the normal vector. When applied a second time μ maps the normal vector to the binormal vector. When applied a third time μ maps the binormal vector back to the tangent vector.

Proposition 3. *The map* $(\boldsymbol{P}, \boldsymbol{L}) \mapsto (\boldsymbol{x}, \boldsymbol{y}) = (\boldsymbol{P}, \boldsymbol{P} \times \boldsymbol{L}|\boldsymbol{P}|^{-2})$ *is a symplectomorphism between the co-adjoint orbit of the Lie-Poisson structure of* $e^*(3)$ *in* $\mathbb{R}^6$ *with variables* $\boldsymbol{P}, \boldsymbol{L}$ *given by* (2.1) *to* T^*S^2 *embedded in* $\mathbb{R}^6$ *with variables* $\boldsymbol{x}, \boldsymbol{y}$ *with Dirac structure given by* (2.19).

Proof. The Jacobian of the mapping is

$$M = \begin{pmatrix} id & 0 \\ -\hat{\boldsymbol{L}}|\boldsymbol{P}|^{-2} - 2(\boldsymbol{P} \times \boldsymbol{L})\boldsymbol{P}^t|\boldsymbol{P}|^{-4} & \hat{\boldsymbol{P}}|\boldsymbol{P}|^{-2} \end{pmatrix}.$$

Computing MBM^t gives all blocks but the lower right block of $B_{P,K}$ immediately. For this block notice the identity $\hat{\boldsymbol{L}}\hat{\boldsymbol{P}}^2 + \hat{\boldsymbol{P}}^2\hat{\boldsymbol{L}} - \hat{\boldsymbol{P}}\hat{\boldsymbol{L}}\hat{\boldsymbol{P}} = -\hat{\boldsymbol{L}}|\boldsymbol{P}|^2$ (or in cross-product terms $\boldsymbol{L} \times (\boldsymbol{P} \times (\boldsymbol{P} \times \boldsymbol{v})) + \boldsymbol{P} \times (\boldsymbol{P} \times (\boldsymbol{L} \times \boldsymbol{v})) - \boldsymbol{P} \times (\boldsymbol{L} \times (\boldsymbol{P} \times \boldsymbol{v})) = \boldsymbol{L} \times \boldsymbol{v}|\boldsymbol{P}|^2$ for all $\boldsymbol{v} \in \mathbb{R}^3$) while all other terms vanish because $\boldsymbol{P}$ is in the kernel of $\hat{\boldsymbol{P}}$. Now using the map μ from the Lemma we see that $\boldsymbol{P} = \boldsymbol{x}$ and $\boldsymbol{L} = -\boldsymbol{x} \times \boldsymbol{y}$ and this gives the result.

■

Having established the equivalence of the Lie-Poisson structure of $e^*(3)$ of the spheroidal harmonics system with the Dirac structure of T^*S^2 the question is what the Hamiltonian G becomes when interpreted in these terms.

Theorem 2.2. *The integrable spheroidal harmonics system of Theorem 2.1 with energy* $|\boldsymbol{P}| = \sqrt{2E}$ *is symplectomorphic to the integrable C. Neumann system of a particle constrained to move on the*

unit sphere $|\boldsymbol{x}| = 1$ *with a harmonic potential. In the coordinates* $(\boldsymbol{x}, \boldsymbol{y})$ *on* $T^*S^2 \in \mathbb{R}^6$ *with the Dirac structure* (2.19) *the Hamiltonian of the Neumann system is*

$$G_N = \frac{1}{2}(y_1^2 + y_2^2 + y_3^2) - Ea^2(x_1^2 + x_2^2)$$

with second integral $L_N = -x_1y_2 + x_2y_1$.

Proof. We start with an $\boldsymbol{x}$ that is not yet restricted to the unit sphere. The map from Proposition 3 gives $|\boldsymbol{L}| = |\boldsymbol{x}||\boldsymbol{y}|$, so that the the term $|\boldsymbol{L}|^2$ in G becomes $|\boldsymbol{x}|^2|\boldsymbol{y}|^2$. Finally we do a symplectic scaling to the unit sphere, namely $\boldsymbol{x} = c\tilde{\boldsymbol{x}}$ and $\boldsymbol{y} = \tilde{\boldsymbol{y}}/c$ where $c = \sqrt{2E}$. Dropping the tildes and dividing by 2 gives G_N.

■

Theorem 2.2 has been proved in [Mar18] in the context of scattering problems. Here we prove the result by explicitly constructing the symplectomorphism. In its usual form the C. Neumann system has a positive attractive potential. This can be adjusted by shifting the potential by the constant term $Ea^2|\boldsymbol{x}|^2$, such that the shifted potential is $Ea^2x_3^2$. To keep the analogy with the spheroidal harmonics integrable system we choose not to do this shift.

Note that while in the spheroidal harmonics system L_z is a coordinate after reduction, and this coordinate is a constant of motion, in the Neumann system the corresponding integral is again the angular momentum $x_1y_2 - x_2y_1$ about the third axis but here this is a function of the coordinates $\boldsymbol{x}$ and $\boldsymbol{y}$. Even when interpreting L_z as a function of the original coordinates $\boldsymbol{Q}$ and $\boldsymbol{P}$ before reduction the difference is that then $\boldsymbol{P}$ was the momentum, while now after renaming $\boldsymbol{P}$ as $\boldsymbol{x}$ this is the coordinate in configuration space. When considering the units of the quantities defined we see, however, that $\boldsymbol{x} = \boldsymbol{P}$ does have units of momentum while $\boldsymbol{y} = \boldsymbol{P} \times (\boldsymbol{Q} \times \boldsymbol{P})|\boldsymbol{P}|^{-2}$ has units of length, so that $\boldsymbol{x} \times \boldsymbol{y}$ does have units of angular momentum, except it has the opposite sign: $\boldsymbol{x} \times \boldsymbol{y} = \boldsymbol{P} \times (\boldsymbol{P} \times (\boldsymbol{Q} \times \boldsymbol{P})|\boldsymbol{P}|^{-2} = -\boldsymbol{Q} \times \boldsymbol{P}$.

We can introduce spherical coordinates on the unit sphere by

$$x_1 = \sin\theta\cos\phi, \quad x_2 = \sin\theta\sin\phi, \quad x_3 = \cos\theta$$

which transforms the Hamiltonian G_N to

$$G_N(\theta, \phi, p_\theta, p_\phi) = \frac{1}{2}\left(p_\theta^2 + \frac{p_\phi^2}{\sin^2\theta}\right) - Ea^2\sin^2\theta \tag{2.20}$$

where $p_\theta^2 = \frac{y_3^2}{\sqrt{1-x_3^2}}$ and $p_\phi = x_1y_2 - x_2y_1$ are canonically conjugate momenta to θ and ϕ, respectively.

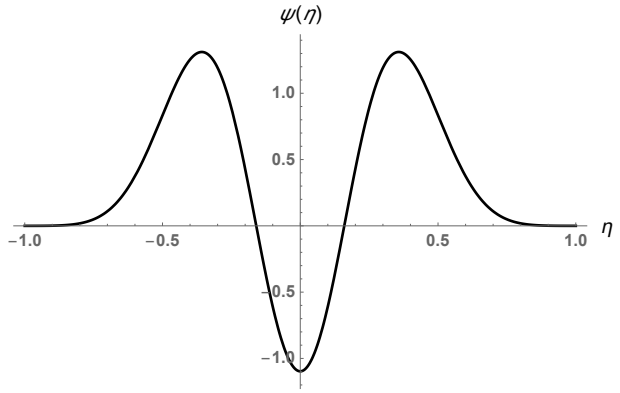

Figure 2.7: Spheroidal wave function with $(n, m, \gamma) = (4, 2, 20)$.

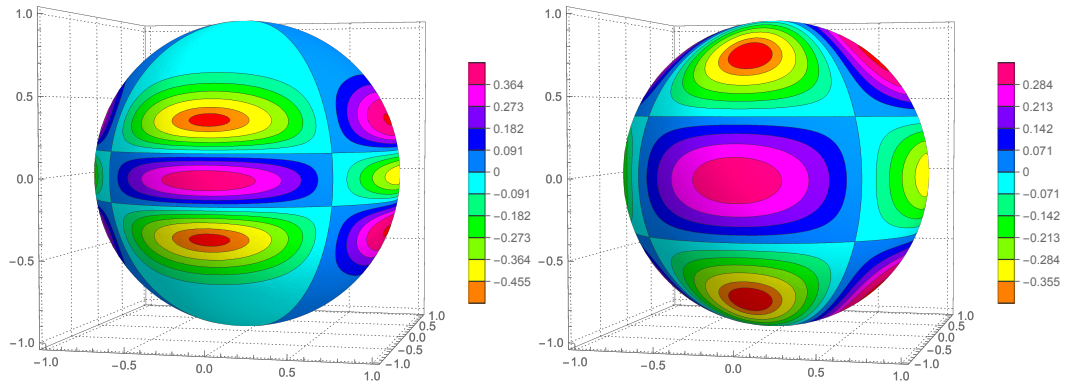

Figure 2.8: a) The spheroidal harmonic $Z_4^2(\theta, \phi)$ with $\gamma = 20$. b) The spherical harmonic $Y_4^2(\theta, \phi)$ for comparison.

Thus we see that separation of the (rotationally symmetric) Neumann system in spherical coordinates leads to the same Hamiltonian as the prolate spheroidal harmonics system obtained from separation in $\mathbb{R}^3$ in prolate spheroidal coordinates. A corresponding statement holds for the quantum systems. Since the phase space T^*S^2 is a cotangent bundle, we quantise by mapping the coordinate variables (x_i, y_i) to the operators $(x_i, \frac{\hbar}{i}\frac{\partial}{\partial x_i})$. The operator corresponding to the Hamiltonian G_N is

$$2\hat{G}_N = -\hbar^2 \nabla_{S^2} - 2Ea^2 \sin^2\theta$$

which for $\hbar = 1$ can be seen to be the same as (2.11) by making the substitution $\eta = \cos\theta$. We close this section by showing the graph of a spheroidal wave function for $m = 2, l = 4$ and a contour plot of the real part of the corresponding spheroidal harmonic Z_l^m on the sphere, along with the spherical harmonic Y_l^m for comparison. Since the potential has its maximum at the poles (and its minimum along the equator) the wave function is "repelled" from the poles.

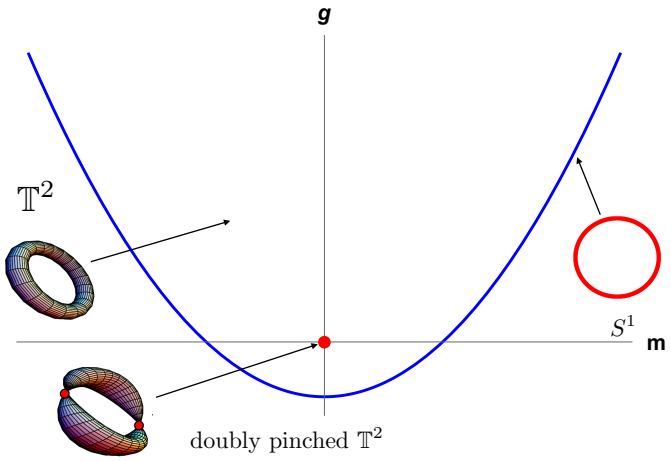

Figure 2.9: Bifurcation diagram of the spheroidal harmonics integrable system.

2.6. MOMENTUM MAP OF THE SPHEROIDAL HARMONICS SYSTEMS

We are now going to analyse the global geometry of the singular Liouville foliation of the integrable spheroidal harmonics system. In a number of steps we will prove

Theorem 2.3. *The spheroidal harmonics integrable system is a generalised semi-toric system with global S^1 action L_z. The momentum map $F = (L_z, G) : T^*S^2 \to \mathbb{R}^2$ has two isolated co-rank 2 critical points $\boldsymbol{P} = \pm \boldsymbol{e}_z\sqrt{2E}$, $\boldsymbol{L} = \boldsymbol{0}$ and a family of co-rank 1 critical points $\boldsymbol{P} = \sqrt{2E}(\cos\phi, \sin\phi, 0)^t$, $\boldsymbol{L} = \boldsymbol{e}_z m$, $\phi \in S^1$, $m \in \mathbb{R}$. The image of the co-rank 2 critical points is the critical value $(0,0)$, which is a non-degenerate focus-focus value and $F^{-1}(0,0)$ is a doubly pinched torus. The image of the co-rank 1 critical points is the parabola $(m, m^2 - 2Ea^2)$, points on which are of elliptic-transversal type and $F^{-1}(m, m^2 - 2Ea^2)$ is a periodic orbit consisting of co-rank 1 critical points parametrised by ϕ. The pre-image of each regular value of F is a single torus $\mathbb{T}^2$.*

As already mentioned in the introduction, the results of Theorem 2.3 have been established in [BZ93, Efs05, CVuN02] in the context of the quadratic spherical pendulum on T^*S^2. Using the equivalence given by Theorem 2.2 these results also hold for the spheroidal harmonics integrable system on $e^*(3)$. Here we prove these results directly on $e^*(3)$ so that the connection to the spheroidal wave functions is more transparent. The system will be analysed using singular reduction (using invariants), regular reduction (using global but singular canonical coordinates) and reconstruction to understand the fibres of the momentum map. In particular we will show that the focus-focus critical value is non-degenerate and hence there is Hamiltonian monodromy in the classical system invoking [Mat96, Zun97]. In particular this also implies the existence of quantum monodromy in the semiclassical limit as shown in general by San Vũ Ngọc in [VuN99].

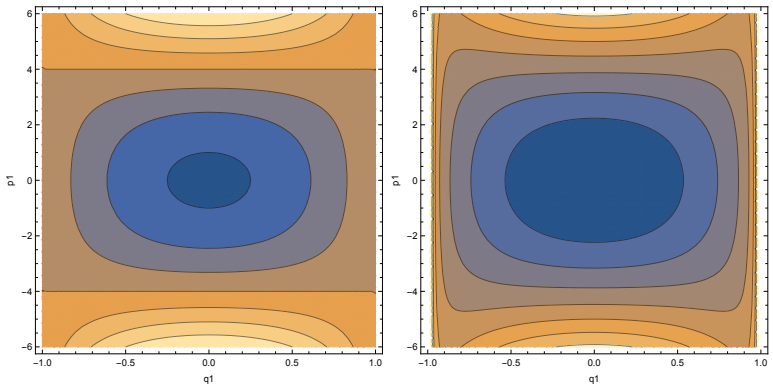

Figure 2.10: Level lines of $G(q,p)$ for $m=0$ (left) and $m=1$ (right), $\gamma=4$.

We already know a symmetry reduced description (2.5) from separation of variables, albeit in singular coordinates. Eqn. (2.5) is connected to the Neumann system (2.20) via the transformation $\eta=\cos\theta$. Setting $\hbar=1$ we have $l_z=m$ and arrive at the one degree of freedom Hamiltonian

$$G(q,p)=(1-q^2)(p^2-\gamma^2)+\frac{m^2}{1-q^2}\,. \tag{2.21}$$

There is a coordinate singularity at $|q|=1$. The phase portrait of this reduced Hamiltonian is shown in Fig. 2.10. Away from the singularity there is an equilibrium at the origin with critical value $G(0,0)=m^2-\gamma^2$. This gives the line of critical values $g=m^2-\gamma^2$ in the bifurcation diagram Fig. 2.9. The corresponding motion in the original system in Euclidean coordinates is a periodic orbit along the equator of the sphere, as already discussed in section 2.3. The parabola of critical values $g=m^2-\gamma^2$ is also the lower boundary of the joint spectrum and is hence shown in Fig. 2.3.

Since the coordinate system from the separation of variables is singular along the z-axis we now use singular reduction starting from the global Euclidean description in $(\boldsymbol{P},\boldsymbol{L})\in\mathbb{R}^6$ to understand the global dynamics.

Lemma 4. *Reduction of the spheroidal harmonics system of Theorem 2.1 by the global S^1 symmetry leads to a Poisson structure in $\mathbb{R}^3$ with coordinates (b_1,b_2,b_3). The reduction map $T^*S^2\to\mathbb{R}^3$ for $|\boldsymbol{P}|=\sqrt{2E}$ is given by*

$$b_1=\frac{p_z}{\sqrt{2E}},\qquad b_2=l_x^2+l_y^2,\qquad b_3=\frac{l_xp_y-l_yp_x}{\sqrt{2E}}\,.$$

with syzygy

$$C_3(b_1,b_2,b_3)=(1-b_1^2)b_2-b_1^2m^2-b_3^2=0\,.$$

The Poisson tensor is $\widehat{\nabla C_3}$.

Proof. The global S^1 action L_z as a Hamiltonian with respect to the Poisson structure B generates a rotation in the first two components of $\boldsymbol{P}$ and $\boldsymbol{L}$ and fixes the third component,

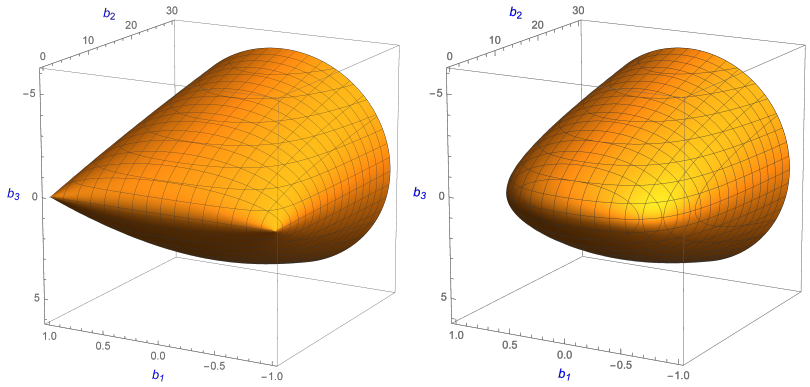

Figure 2.11: a) The singular reduced phase space $P_{m=0}$ with two singular points at $(b_1, b_2, b_3) = (\pm 1, 0, 0)$; b) A regular reduced phase space $P_{m=2}$ with non zero m.

see (2.7). Thus p_z and l_z are invariant under this symmetry. Introducing $p_w = p_x + ip_y$ and $l_w = l_x + il_y$ the S^1 action is multiplication of p_w and l_w by $e^{i\phi}$. Any polynomial of p_z and l_z is also invariant. Additional quadratic polynomial invariants are $|p_w|^2$, $|l_w|^2$ and the real and imaginary part of $p_w\bar{l}_w$. All other polynomial invariants are functions of these 6 invariants, 2 linear and 4 quadratic. The Casimirs of the Poisson structure B expressed in these invariants read $|p_w|^2 + p_z^2 = 2E$ and $\Re(p_w\bar{l}_w) + p_z l_z = 0$ and can be used to eliminate $|p_w|^2$ and $\Re(p_w\bar{l}_w)$ wherever they appear. As before we set $l_z = m$ where m is now considered as a parameter. In addition we scale the momentum with $\sqrt{2E}$ as for the transformation to the Neumann system. The remaining invariants are denoted by b_i where $b_2 = |l_w|^2$ and $b_3 = \frac{\Im(p_w\bar{l}_w)}{\sqrt{2E}}$. This gives the stated reduction map. The invariants satisfy $|b_1| \leq 1$ and $b_2 \geq 0$ by construction. The identity $\Re(p_w\bar{l}_w)^2 + \Im(p_w\bar{l}_w)^2 = |p_w\bar{l}_w|^2 = |p_w|^2|l_w|^2$ rewritten in terms of the invariants gives $C_3 = 0$. A fundamental property of invariants is that their Poisson bracket is again an invariant. By using the original Poisson structure B in the original variables $(\boldsymbol{P}, \boldsymbol{L})$ one can verify that

$$\{b_1, b_2\} = 2b_3, \quad \{b_1, b_3\} = 1 - b_1^2, \quad \{b_2, b_3\} = 2b_1 m^2 + 2b_1 b_2\,.$$

The right hand sides are given by the derivatives $\partial C_3/\partial b_i$, such that the reduced Poisson structure is $\widehat{\nabla C_3}$ as claimed. By construction then C_3 is a Casimir of the reduced Poisson structure. Since this encodes an identity between invariants (a so-called syzygy) the value of C_3 must be zero.

■

The invariants can of course also be written in the coordinates $(\boldsymbol{x}, \boldsymbol{y})$ of the Neumann system on the unit sphere where they look more natural as

$$b_1 = x_3, \qquad b_2 = y_1^2 + y_2^2, \qquad b_3 = y_1 x_2 - y_2 x_1\,.$$

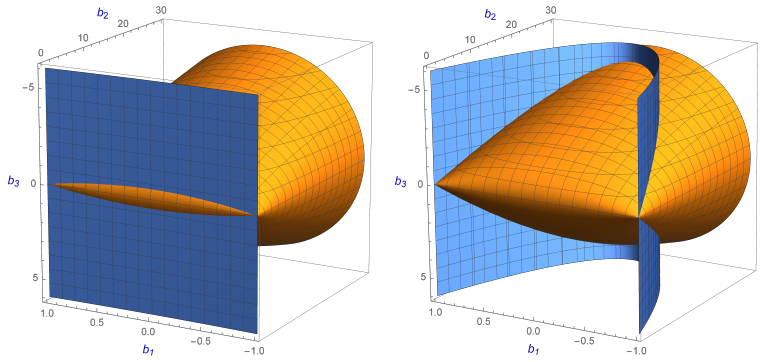

Figure 2.12: Separatrix connecting the singular points. It is given by the intersection of the singular reduced phase space P_0 (yellow) with the energy surface $\{G = 0\}$ (blue) for $\gamma = 0.5$ (left) and $\gamma = 5$ (right).

The points $\boldsymbol{P} = (0, 0, \pm\sqrt{2E})$ and $\boldsymbol{L} = (0, 0, 0)$ are fixed under rotations about the third axis. Hence the global S^1 action has fixed points and the symmetry reduced phase space is not in general a smooth manifold. This is the reason that we are using singular reduction. This fixed point occurs for $l_z = m = 0$ and its image under the reduction map is $(\pm 1, 0, 0)$. We now verify that these are exactly the singular points of the reduced phase space.

Lemma 5. *The reduced phase space* $P_m = \{(b_1, b_2, b_3) \mid C_3 = 0, b_2 \geq 0, b_1^2 \leq 1\}$ *is a smooth surface for* $m \neq 0$ *and a singular semi-algebraic variety with two conical singularities at* $(b_1, b_2, b_3) = (\pm 1, 0, 0)$ *for* $m = 0$.

Proof. The reduced phase space is the subset of $\mathbb{R}^3$ with coordinates b_1, b_2, b_3 for which the syzygy Casimir is satisfied, $C_3 = 0$, and in addition the inequalities $b_2 \geq 0$ and $b_1^2 \leq 1$ hold. Singular points occur when $\partial C_3/\partial b_i = 0$ which implies $b_3 = 0$, $b_1 = \pm 1$ and $b_2 = -m^2$, which is only possible for $m = b_2 = 0$. Thus for $m = 0$ the variety $\{C_3 = 0\}$ is not a smooth manifold, but has two singular points at $(\pm 1, 0, 0)$, see Fig. 2.11. For $m \neq 0$ it is a smooth manifold. The inequalities select one connected component.

■

The next step is the analysis of the dynamics of the reduced system. We write the Hamiltonian G of (2.6) in terms of invariants as

$$G(b_1, b_2, b_3) = b_2 + m^2 - \gamma^2(1 - b_1^2) \tag{2.22}$$

using $l_z = m$ and $\gamma = 2Ea^2$ with $\hbar = 1$. The trajectories of the reduced system are given by the intersection of the reduced "energy surface" $\{G = g\}$ with reduced phase space P_m. This leads to the description of the image of the momentum map (L_z, G), see Fig. 2.9.

Lemma 6. *The set of critical values of the energy-momentum map* (L_z, G) *consists of an isolated point at the origin* $(0, 0)$ *and the parabola* $g = m^2 - \gamma^2$. *The corresponding critical points are*

$(\pm 1, 0, 0)$ *and* $(0, 0, 0)$*, respectively. The sepatratrices connecting* $(\pm 1, 0, 0)$ *are the parabolic arcs* $(b_1, b_2, b_3) = \big(b_1, \gamma^2(1 - b_1^2), \pm\gamma(1 - b_1^2)\big)$.

Proof. In general a tangency between the reduced phase space P_m and the parabolic cylinder $\{G = g\}$ occurs when their gradients are parallel, which implies $b_3 = 0$ and either $b_1 = 0$ or $b_2 = -m^2 - \gamma^2(1 - b_1^2)$. Since $b_2 \geq 0$ the latter implies $b_1 = \pm 1$ and $m = 0$. These are two isolated critical points at $(\pm 1, 0, 0)$ both with isolated critical value $(m, g) = (0, 0)$. The preimage of this critical value in the reduced system is given by the intersection of the singular reduced phase space P_0 with the reduced energy surface $\{G(b_1, b_2, b_3) = 0\}$. Solving $G = 0$ with $m = 0$ gives the equation for b_2. Inserting into $C_3 = 0$ and extracting a square root gives the equation for b_3. See Fig. 2.12

In the other case of parallel gradients with $b_1 = 0$ the Casimir $C_3 = 0$ implies $b_2 = 0$ as well, so that the critical point is $(0, 0, 0)$ with corresponding family of critical values $(m, g) = (m, m^2 - \gamma^2)$. All points in the (m, g) plane above the parabola $g = m^2 - \gamma^2$ with the exception of the origin are regular values. For each regular value the intersection of P_m and $\{G = 0\}$ is a single curve diffeomorphic to S^1. These intersections can also be seen as the level lines of $G(q, p)$ as shown in Fig. 2.10 (right).

■

The final step in the analysis of the classical dynamics is the reconstruction, which leads to a description of the invariant sets of the dynamics in the original coordinates $(\boldsymbol{P}, \boldsymbol{L})$. The reduction map of Lemma 4 is a projection from the 4-dimensional space $T^*S^2 \subset \mathbb{R}^6$ to $\mathbb{R}^3$.

Lemma 7. *For given* b_1, b_2, b_3 *points in the preimage of the reduction map are given by*

$$\boldsymbol{P} = \sqrt{2E}\left(\sqrt{1 - b_1^2}\cos u, \sqrt{1 - b_1^2}\sin u, b_1\right), \quad \boldsymbol{L} = \left(\sqrt{b_2}\cos v, \sqrt{b_2}\sin v, m\right)$$

where $u - v = \arg(-b_1 m + i b_3)$*. The* S^1 *action increases both* u *and* v *by* ϕ *and leaves the difference* $u - v$ *invariant.*

Proof. In Lemma 4 we already noted that the S^1 action is most easily described by multiplication with $e^{i\phi}$ after introducing the complex variables $p_w = p_x + ip_y$ and $l_w = l_x + il_y$. By definition b_2 is the modulus squared of l_w and b_1 is the normalised size of p_z, such that $|p_w|^2 = 2E - p_z^2 = 2E(1 - b_1^2)$. Thus there are angles u and v such $e^{i\phi}p_w = \sqrt{2E(1 - b_1^2)}e^{iu}$ and $e^{i\phi}l_w = \sqrt{b_2}e^{iv}$. For given b_1, b_2, b_3 the arguments u and v are related. On the one hand from Lemma 4 we have $\Re(p_w\bar{l}_w) = -p_z l_z$ and $\Im(p_w\bar{l}_w) = \sqrt{2E}b_3$, such that $p_w\bar{l}_w = \sqrt{2E}(b_1 m + b_3)$. On the other hand $p_w\bar{l}_w = \sqrt{2E}\sqrt{1 - b_1^2}\sqrt{b_2}e^{i(u-v)}$, and hence the result. At the singular point $(\pm 1, 0, 0)$ the angles u and v are undefined, but this is

the fixed point of the S^1 action, so the preimage of each of these points is just a single point each, instead of a circle each.

■

It is interesting to note that these formulas can be directly expressed in terms of the original separating variables. In particular both, p_w and l_w when expressed in terms of $(\xi, \eta, \phi, p_\xi, p_\eta, p_\phi)$ after cotangent lift of the definition (2.3) of spheroidal coordinates can be written as $p_w = e^{i\phi} p_{w0}$ and $l_w = e^{i\phi} l_{w0}$ where p_{w0} and l_{w0} are independent of ϕ. This leads to formulas for b_1, b_2, b_3 in terms of the separating variables. One subtlety here is that in such formulae the value of E is not fixed, but is determined by the values of ξ, η, p_ξ, p_η, while $l_z = p_\phi = m$, as always. The difference in the reconstruction formula is that there ξ and p_ξ have been eliminated.

Symplectic coordinates on the reduced phase space can be introduced by

$$(q, p) = \left(b_1, \frac{b_3}{1 - b_1^2} \right) .$$

It is easy to check that these functions satisfy $\{q, p\} = 1$, and that they reduce the Poisson structure $\widehat{\nabla C_3}$ in $\mathbb{R}^3$ to the standard symplectic structure in $\mathbb{R}^2$. Using the Casimir to express b_2 as a function of (q, p) the Hamiltonian G in (2.22) can be turned into the form (2.21). Of course reintroducing symplectic coordinates also reintroduces the coordinate singularity.

However, notice that through the chain of transformations we have arrived again at the separated Hamiltonian function G albeit evaluated in different coordinates. Originally the separation gave a function $G(q, p)$ where either $(q, p) = (\eta, p_\eta)$ or $(q, p) = (\xi, p_\xi)$. The variables (q, p) just introduced as a function of b_i however set $q = p_z/\sqrt{2E}$ and $p = \sqrt{2E}(\boldsymbol{P} \times \boldsymbol{L})_z/(p_x^2 + p_y^2)$.

In order to classify the critical point corresponding to the critical values the dynamics needs to be analysed in full phase space. First we show that the preimage of the isolated critical value $(0, 0)$ of the momentum map (L_z, G) is a doubly pinched torus, and then we will show that it is a non-degenerate focus-focus critical value.

Lemma 8. *The preimage of the critical value $(0, 0)$ of the prolate spheroidal harmonics system is a doubly pinched torus with $l_z = 0$ in the phase space T^*S^2 parametrised by p_z and ϕ as*

$$\begin{pmatrix} p_x \\ p_y \\ l_x \\ l_y \end{pmatrix} = \sqrt{2E - p_z^2} \begin{pmatrix} 1 & 0 \\ 0 & 1 \\ 0 & \pm a \\ \mp a & 0 \end{pmatrix} \begin{pmatrix} \cos\phi \\ \sin\phi \end{pmatrix} .$$

Proof. Combining the parabolic arcs from Lemma 6 with the reconstruction formula Lemma 7 for the case $g = m = 0$ gives the result. We have $\Re(p_w \bar{l}_w) = 0$ since $m = 0$ and hence $u - v = \pm\pi/2$ where the plus sign correspond to the upper parabolic arc with $b_3 \geq 0$ and the minus sign to the lower arc with $b_3 \leq 0$.

■

This Lemma gives a parametrisation of the doubly pinched torus in phase space. For the spheroidal harmonics system it is even possible to describe the dynamics on this doubly pinched torus in terms of simple formulas. Consider the local symplectic coordinates $G(q, p)$. When $m = 0$ then $G = 0$ implies either $q = \pm 1$ or $p = \pm\gamma$. We choose the second condition to stay away from the critical point. Hamilton's equations then say that $p = \pm\gamma$ is constant, as can be seen in Fig. 2.10. The remaining ODE for q can be solved to give $q(t) = \tanh(\pm 2t\gamma - c)$, which is the connection from the north-pole to the south-pole of the sphere, or vice versa, depending on the sign of $p = \pm\gamma$. The dynamics of ϕ is trivial, since $\dot{\phi} = -\partial G(q, p)/\partial m = 0$ for $m = 0$.

Lemma 9. *The critical value $(0, 0)$ of the momentum map $(L_z, G) : T^*S^2 \to \mathbb{R}^2$ is a non-degenerate focus-focus value. The critical values $(m, m^2 - \gamma^2)$ are non-degenerate values of elliptic-transversal type.*

Proof. At a critical point of the map (L_z, G) the flows (in the original coordinates) generated by G and L_z are parallel:

$$\alpha B\nabla G + \beta B\nabla L_z = \mathbf{0}, \quad \beta \in \mathbb{R}\backslash\{0\}\,. \tag{2.23}$$

The vector fields are given by (2.8) and (2.7), and since the the former is non-vanishing for $E > 0$ we can set $\alpha = 1$.

Critical points of the form $\boldsymbol{P} = (0, 0, p_z)$ and $\boldsymbol{L} = (0, 0, 0)$ with β arbitrary have the critical values $(0, 0)$. Critical points of the form $\boldsymbol{P} = (p_x, p_y, 0)$ and $\boldsymbol{L} = (0, 0, m)$ with $\beta = m$ have the critical value $(m, m^2 - \gamma^2)$.

The essential object for the classification of critical values and non-degeneracy are the eigenvalues of the Jacobian $\partial_{\boldsymbol{P},\boldsymbol{L}}\,(B\nabla G + \beta B\nabla L_z)$ at these critical points. Two of the six eigenvalues are always zero; corresponding to the two Casimirs of the Poisson structure B.

At the north and south poles of the $\boldsymbol{P}$ sphere the eigenvalues are $\lambda = \pm a p_z \pm i\beta$ where $\beta \in \mathbb{R}\backslash\{0\}$ is an arbitrary parameter and $p_z = \pm\sqrt{2E}$. This implies that the poles of the $\boldsymbol{P}$-sphere are non-degenerate focus-focus points, with corresponding non-degenerate focus-focus value $(0, 0)$.

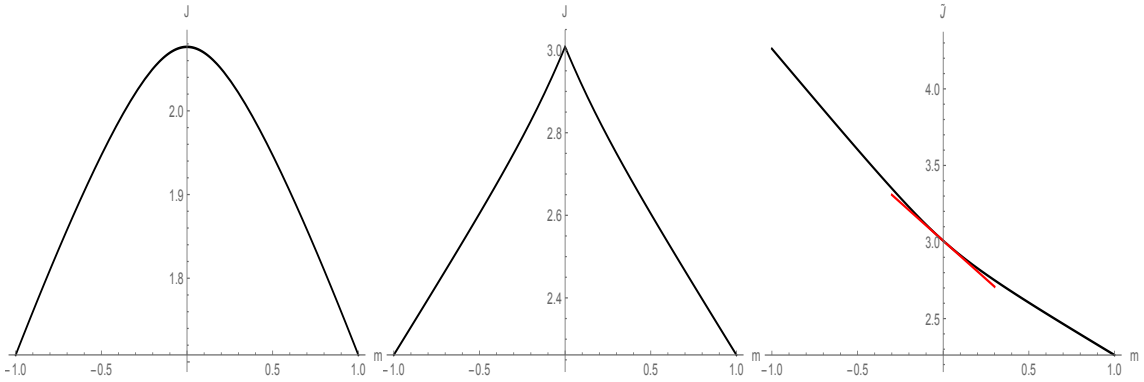

Figure 2.13: Plot of J versus m for a) $g < 0$ and b) $g > 0$. c) Plot of $J + 2\,|m|$ versus m when $g > 0$.

At the equator of the $\boldsymbol{P}$ sphere the eigenvalues are $\lambda = 0, 0, \pm i\sqrt{m^2 + \gamma^2}$. Thus, all points on the equator of the $\boldsymbol{P}$ sphere are elliptic-transversal critical points.

■

See [CVuN02] for similar results for the example of the quadratic spherical pendulum.

Note that for the elliptic-transversal points the vector field of G is $\dot{\boldsymbol{P}} = 2m\,(-p_y, p_x, 0)$ and $\dot{\boldsymbol{L}} = \boldsymbol{0}$. Thus for $m \neq 0$ the set of critical points in the preimage of $(m, m^2 - \gamma^2)$ is a periodic orbit along the equator of the $\boldsymbol{P}$-sphere. For $m = 0$ this periodic orbit degenerates into a circle of fixed points, but from the point of view of the momentum map (L_z, G) they are still non-degenerate.

The classical monodromy of the spheroidal harmonics system can also be understood from the non-trivial action variable J. Recall that L_z is already an action variable. The second action is given by $J = \frac{1}{2\pi} \oint_\beta p\, dq$ where p is obtained from solving (2.5). The β-cycle encloses the interval $[-r_1, r_1]$ where $\pm r_1$ are the two middle roots of $p^2 = 0$ and $|r_1| \leq 1$. In Fig. 2.13 we show J as a function of m for positive (a) and negative (b) values of g. Observe that J is a symmetric but non-smooth function of m for $g > 0$ at $m = 0$. The action J is a smooth function of (m, g) on the image of the momentum map with the slit $m = 0$, $g \geq 0$ removed. However, $m = 0$, $g > 0$ is not a critical value of the momentum map. Thus, there is an alternate definition of action $\tilde{J}$ that is the smooth continuation of J across the slit. This is shown in (c) and defined by $\tilde{J} = J$ for $m \geq 0$ and by $\tilde{J} = J + 2|m|$ for $m < 0$. The alternate action $\tilde{J}$ defines a smooth action function on the image of the momentum map with the slit $m = 0$, $g < 0$ removed. The action $\tilde{J}$ is a function of the values (m, g). Considering $m = L_z$ and $g = G$ as functions on phase space the action $\tilde{J}$ becomes a function on phase space, and

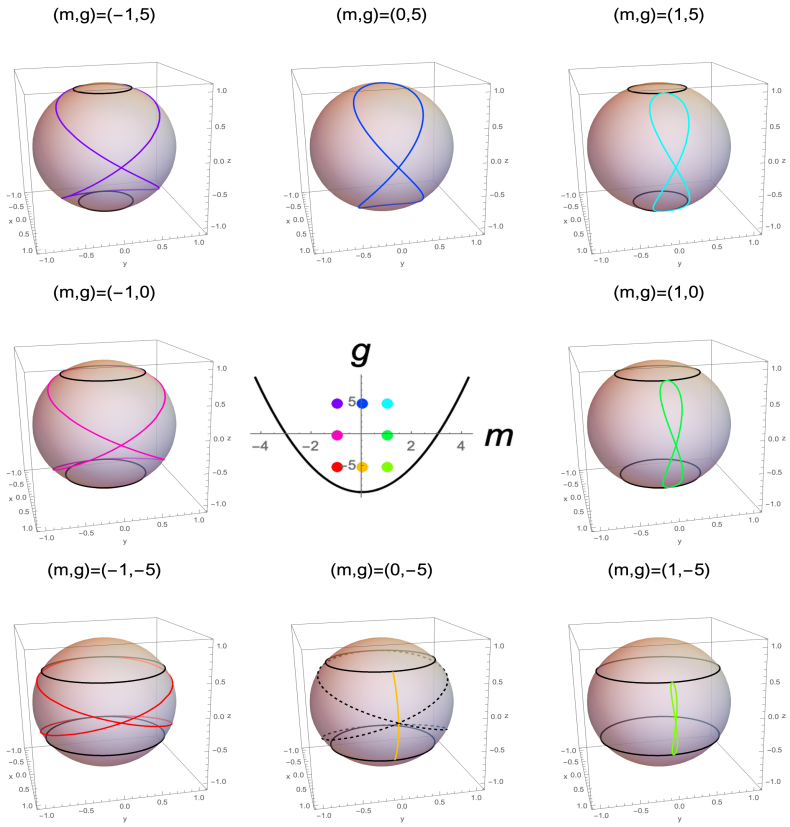

Figure 2.14: Evolution of an angle-variable on the projected torus when a loop around the focus-focus point is completed. The initial loop (orange) and the final loop (dashed) differ by 2 rotations (monodromy index 2).

hence has a Hamiltonian vector field $X_{\tilde{J}}$. From the chain rule we obtain

$$X_{\tilde{J}} = \frac{\partial \tilde{J}}{\partial g} X_G + \frac{\partial \tilde{J}}{\partial m} X_{L_z} .$$

Note that $\frac{\partial \tilde{J}}{\partial g}$ is the reduced period and $\frac{\partial \tilde{J}}{\partial m}$ is the rotation number. They constitute part of the so-called period lattice, see, e.g., [Dui80]. By definition the flow of an action is 2π-periodic, so that integrating $X_{\tilde{J}}$ gives a closed curve. The two vector fields $X_{\tilde{J}}$ and X_{L_z} can be used to generate the coordinate lines of the angle coordinates on a torus. This grid of coordinate lines has been computed in [CIAD14] in order to better understand classical monodromy, and we have done the same here for the spheroidal harmonics system. Instead of showing a whole grid we simply show a single curve, see Fig. 2.14. The reason for that is that in our case all other curves of the grid are obtained by rotation about the z-axis. The angle coordinate lines corresponding to the global action L_z are simply lines of constant latitude, and we only show the two extremal such curves which mark the caustic of the torus. We begin the loop at $m = 0$ and $g < 0$ (orange). Moving in a counter-clockwise direction around the focus-focus point we see the caustics shrink to the poles when $m = 0$, $g > 0$ (blue loop). Moving into the region where $m < 0$ we see the loop flip to the other side of the sphere. Finally, as we arrive back at the initial point on the bifurcation diagram, we see that the original loop has two cycles in the ϕ direction added, and so the monodromy index is 2.

The spheroidal harmonics system has a discrete symmetry that can be reduced such that the doubly pinched torus becomes a reduced singly pinched torus. In particular the two focus-focus critical points are identified with each other. When reducing by the full symmetry group the quotient is not a smooth manifold. Consequently, we quotient by symmetry S_2 that flips $\boldsymbol{P}$ to $-\boldsymbol{P}$ only.

Lemma 10. *After discrete symmetry reduction by S_2, the reduced phase space is $T^*\left(\mathbb{RP}^2\right)$.*

Proof. The reduced $\boldsymbol{P}$-space is $\mathbb{RP}^2$ because discrete symmetry S_2 identifies antipodal points of the sphere S^2. A possible fundamental region is the northern hemisphere with $p_z \geq 0$. Since S_2 does not act on $\boldsymbol{L}$, the reduced phase space is therefore $T^*\left(\mathbb{RP}^2\right)$. There is only one focus-focus point in the reduced phase space since S_2 maps the north-pole and the south-pole of the sphere S^2 into each other.

■

Note that the S_2 reduced system (L_z, G) on $T^*\left(\mathbb{RP}^2\right)$ has an S^1 action that is not effective. The reason is that the equator is halved by the symmetry reduction, so that the action is not free for all values (m, g) on the parabola in Fig. 2.9. Hence the symmetry reduced system is not even generalised semi-toric in the sense of [PR+17].

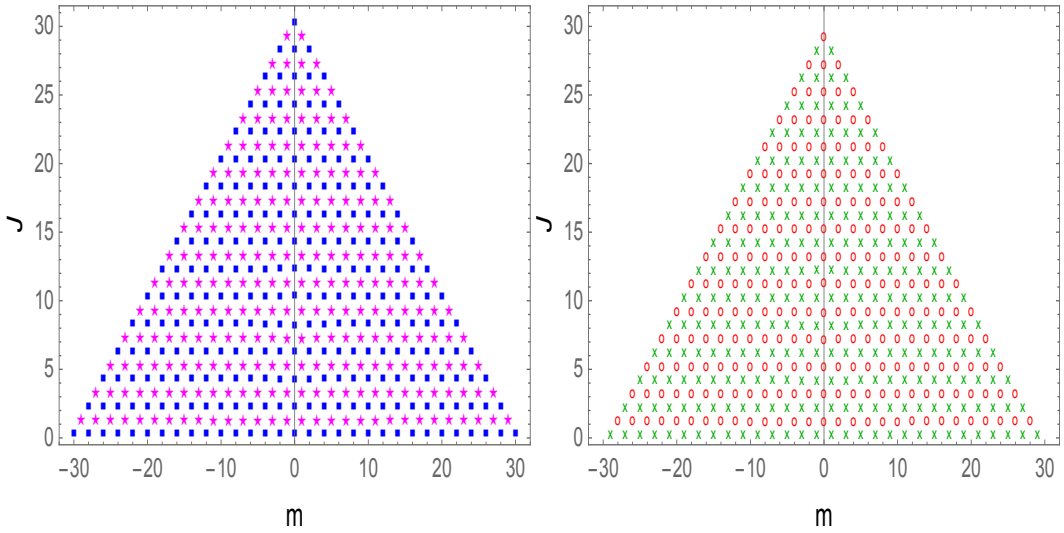

Figure 2.15: Action lattice $(m, J(m, g_l^m))$ for points in the joint spectrum that are a) invariant under S_2 b) flip sign under S_2. Note that these lattices show the interior of the semi-toric polytope. As the system is not strictly semi-toric nor is the phase space compact, the polytope itself is not compact.

The even/odd spectra in Fig. 2.6 correspond to the same classical integrable system (L_z, G) on $T^*(\mathbb{RP}^2)$ obtained in the previous Lemma. Quantum mechanically the two spectra correspond to different systems since they have different boundary conditions. Thus the semi-classical quantisation of these system will quantise the same action variables, but with different Maslov indices. This is illustrated in Fig. 2.15 which shows the action lattice $(m, J(m, g_l^m))$ for states invariant under S_2 (left) or odd under S_2 (right). Shifting all points in the right figure up by 1 unit will make them coincide (in the semi-classical approximation) with the points in the left figure, except for the line of ground states.

An interesting observation that can be made from Fig. 2.10 (left) for $m = 0$ is that because $p = const$ on the critical level the action of the critical level is simply equal to the area of the rectangle with side lengths 2γ and 2 divided by 2π, so that $I_\eta(0, 0) = 2\gamma/\pi$. By Weyl's law this tells us that in the semiclassical limit (i.e. for large γ) the number of negative eigenvalues g_l^0 is to leading order $2\gamma/\pi$, which for $\gamma = 16$ gives approximately 10, which can be observed in Fig. 2.3.

Chapter 3

The Harmonic Lagrange Top and the Confluent Heun Equation

Abstract

The harmonic Lagrange top is the Lagrange top plus a quadratic (harmonic) potential term. We describe the top in the space fixed frame using a global description with a Poisson structure on T^*S^3. This global description naturally leads to a rational parametrisation of the set of critical values of the energy-momentum map. We show that there are 4 different topological types for generic parameter values. The quantum mechanics of the harmonic Lagrange top is described by the most general confluent Heun equation (also known as the generalised spheroidal wave equation). We derive formulas for an infinite pentadiagonal symmetric matrix representing the Hamiltonian from which the spectrum is computed.

3.1. INTRODUCTION

The Lagrange top is a prime example of classical mechanics. Over centuries, it has been studied starting with Euler and Lagrange, and interest in its various features is blossoming again and again. Almost every modern development in mechanics has lead to new insights about the Lagrange top. Before we attempt to describe the place of the Lagrange top in mechanics in the remainder of this introduction, let us formulate our main observation: the quantum mechanics of the harmonic Lagrange top is described by the most general confluent Heun equation (also known as the generalised spheroidal wave equation). By harmonic Lagrange top we mean the Lagrange top with an added harmonic (i.e. quadratic) potential. It provides an example of the subcritical and the supercritical Hamiltonian Hopf bifurcation and hence the quantisation of these bifurcations. The bulk of the paper is devoted to the description of the classical integrable system.

Rigid body dynamics is treated in most mechanics textbooks, e.g. [Whi37, LL84, Arn78,

Gol80, MR94]. Of the books devoted specifically to rigid body dynamics we highlight the monumental volumes of Klein & Sommerfeld [KS10], Audin [Aud96] and the recent addition by Borisov & Mamayev [BM18]. Many special cases of rigid body dynamics including the Lagrange top are completely integrable Hamiltonian systems, and as such have been studied in detail in Bolsinov & Fomenko [BF04] and Cushman & Bates [CB15]. For all the references we inevitably missed in this introduction we refer to the extensive bibliography in [BM18].

In modern mechanics the (energy)-momentum map plays a central role. Singularity theory's swallowtail was found as the set of critical values of the energy-momentum map of the Lagrange top in [CK85], also see [CB15]. The meaning of the swallowtail from the point of view of bifurcation theory, specifically the supercritical Hamiltonian Hopf bifurcation in the Lagrange top was described in [CvdM90]. The fact that the swallowtail may make the set of regular values in the image of the energy-momentum map non-simply connected is the essential observation that explains why the Lagrange top does not possess global action variables [Dui80, CD88]. Hamiltonian monodromy of the Lagrange top is described in [Viv03]. Integrable discretisations of the integrable Lagrange top were found in [BS99]. The complex algebraic geometry of the Lagrange top was described in [GZ98], and its bi-Hamiltonian structure in [Tsi08]. In KAM theory perturbations of the Lagrange top give a beautiful example worked out in detail in [HBHN06].

The quantisation of the symmetric top was first done in the early days of quantum mechanics [Rei26] and leads to a hypergeometric equation, also see [LL77]. The study of polar molecules in an electric field leads to a Hamiltonian that is equivalent to the Lagrange top. In the physics literature this is referred to as the Stark effect, and was first studied in [Sch55]. Matrix elements for the numerical computation of the spectrum were given in [Shi63], and nearly 30 years later again in [HO91].

The discovery of quantum monodromy [Dui80] was in the smaller brother of the Lagrange top, the spherical pendulum, in [CD88]. The quantum monodromy in the Lagrange top itself has been studied in [KR03].

While so-called semi-toric systems with two degrees of freedom (somewhat like the spherical pendulum) are now in a precise sense completely understood classically [PVuN09] and quantum mechanically [LFVuN21], the Lagrange top is still out of reach from this point of view. We should mention that many generalisations of the spherical pendulum have been studied, in particular the magnetic spherical pendulum [CB95, CB15], also see [Sak02], and the quadratic spherical pendulum [Zou92, Efs05]. The combination of both is the harmonic Lagrange top, which is the object of this paper. To our knowledge, it has not been considered in the literature in full generality. The so-called Kirchhoff top which has only quadratic terms in the potential has been studied in [Bog92, BZ93]. A general potential with linear and quadratic terms was considered in [Han97] from the point

of view of perturbation theory of the Euler top. The harmonic Lagrange top can also be considered as an example of the general idea described in [DP16], where a semi-toric system is deformed preserving integrability. In particular, we find that the harmonic Lagrange top exhibits the subcritical and the supercritical Hamiltonian Hopf bifurcations.

As mentioned in the beginning, we want to draw attention to the fact that the quantisation of the Lagrange top leads to the confluent Heun equation. The Heun equation is a Fuchsian equation with 4 regular singular points, thus generalising the hypergeometric equation by one singularity, see, e.g., [Ars64, RA95, SL00, DLMF]. An important physical application of the confluent Heun equation appears in the perturbation theory of a rotating black hole in general relativity [Teu73, PT73, Lea86]. In this context, expansions in terms of Jacobi polynomials have been given in [FC77], and series expansion for small potential are given in [Sei89]. As we show below, the harmonic Lagrange top leads to the most general confluent Heun equation, unlike the above application in general relativity, which does not have enough parameters.

After this work was completed we learned that a physical interpretation for the additional quadratic ("harmonic") term in the potential is provided by considering the Lagrange top on a vibrating suspension [Mar09, Mar12]. In this context the focus-focus points in the model have been analysed in [BRS20], also see [BI22]. Some of our results about the threads of focus-focus points in the bifurcation diagram overlap with [BRS20], also see [RS21].

The structure of this paper is as follows. We give an introduction to the Lagrange top in the next section, where we emphasise the description in the spatial frame using quaternions and the corresponding Poisson structure. The various periodic flows and their differences when considering $T^*SO(3)$ or T^*S^3 (the quaternions) is discussed in section 3, and the reductions to two degrees of freedom in section 4. The traditional description in Euler angles is recalled in section 5, which is needed for the quantisation. The main classical results are the description of the critical points in phase space and the corresponding critical values in the image of the energy-momentum map. There are 4 different cases, with one thread (the original Lagrange top), with two threads, with a triangular tube instead of the thread, and a triangular tube shrinking to a thread. In the final section we show that the quantum harmonic Lagrange top leads to the most general confluent Heun equation and compute the spectrum, which is displayed overlayed with (slices) of the classical energy-momentum map. A new method for the computation of the spectrum is presented.

3.2. Heavy Symmetric Top

Consider a general rigid body with a fixed point. Assume that the symmetric inertia tensor I with respect to that point has three distinct eigenvalues I_1, I_2, I_3, the moments of inertia, and assume that a body frame has been chosen in which the tensor of inertia is diagonal.

For the symmetric top with $I_1 = I_2$ the location of the corresponding basis vectors is only defined up to a rotation about the symmetry axis (or figure axis) of the body. In the spatial coordinate frame, the z-axis is parallel to the direction of gravity. Let $\boldsymbol{V}$ be the coordinate vector of a point in the body frame. The orthogonal matrix $R \in SO(3)$ describes how this point is moving in time when viewed in the spatial frame, $\boldsymbol{v} = R\boldsymbol{V}$.

For the free rigid body (Euler top), the fixed point of the body is the centre of gravity of the body. For the Lagrange top, the centre of gravity is on the figure axis but does not coincide with the fixed point of the body, which also lies on said axis. Denote the unit vector along the figure axis of the top by $\boldsymbol{a}$ (in the spatial frame), then the potential energy in the field of gravity is $V = c_1 a_z$. In this paper, we are going to study the more general case

$$V(a_z) = c_1 a_z + c_2 a_z^2 \,.$$

The angular velocity $\boldsymbol{\Omega}$ in the body frame is defined through R by $R^t \dot{R} \boldsymbol{V} = \Omega \times \boldsymbol{V}$ for any vector $\boldsymbol{V}$, or, equivalently, by $\hat{\boldsymbol{\Omega}} = R^t \dot{R}$. The kinetic energy of the rigid body is

$$T = \frac{1}{2} \boldsymbol{\Omega} \cdot I\boldsymbol{\Omega}$$

where I is the diagonal tensor of inertia and $\cdot$ denotes the Euclidean scalar product.

The angular momentum vector is defined by $\boldsymbol{L} = I\boldsymbol{\Omega}$. For the free rigid body $\boldsymbol{l} = R\boldsymbol{L}$ is a constant vector. For the Lagrange top instead there are only two conserved quantities given by

$$l_z = \boldsymbol{l} \cdot \boldsymbol{e}_z, \quad L_3 = \boldsymbol{L} \cdot \boldsymbol{e}_3 = R^t \boldsymbol{l} \cdot \boldsymbol{e}_3 = \boldsymbol{l} \cdot R\boldsymbol{e}_3 = \boldsymbol{l} \cdot \boldsymbol{a} \,.$$

In the spatial frame we have $\boldsymbol{e}_z = (0,0,1)^t$ and in the body frame we have $\boldsymbol{e}_3 = (0,0,1)^t$.

A beautiful global description of the dynamics of rigid bodies uses quaternions $\boldsymbol{x} = (x_0, x_1, x_2, x_3)$ which are coordinates on the double cover of $SO(3)$ which is $S^3 \in \mathbb{R}^4$ given by $x_0^2 + x_1^2 + x_2^2 + x_3^2 = 1$. Define

$$\boldsymbol{x}_\pm = \begin{pmatrix} x_1 & -x_0 & \mp x_3 & \pm x_2 \\ x_2 & \pm x_3 & -x_0 & \mp x_1 \\ x_3 & \mp x_2 & \pm x_1 & -x_0 \end{pmatrix}$$

which satisfy $\boldsymbol{x}_+ \boldsymbol{x}_+^t = id$, $\boldsymbol{x}_- \boldsymbol{x}_-^t = id$, $\boldsymbol{x}_+^t \boldsymbol{x}_+ \boldsymbol{x}_-^t = \boldsymbol{x}_-^t$, and $\boldsymbol{x}_-^t \boldsymbol{x}_- \boldsymbol{x}_+^t = \boldsymbol{x}_+^t$ on the unit sphere. Then an orthogonal 3×3 matrix is given by $R = \boldsymbol{x}_+ \boldsymbol{x}_-^t$ and the last two identities in the previous sentence become $\boldsymbol{x}_+^t R = \boldsymbol{x}_-^t$ and $\boldsymbol{x}_-^t R^t = \boldsymbol{x}_+^t$. The matrices $\boldsymbol{x}_\pm$ relate the angular velocities to the tangent vector of the sphere $\dot{\boldsymbol{x}}$ by $\boldsymbol{\Omega} = 2\boldsymbol{x}_- \dot{\boldsymbol{x}}$ and $\boldsymbol{\omega} = 2\boldsymbol{x}_+ \dot{\boldsymbol{x}}$, see, e.g., [Whi37, Section 16]. To see this, differentiate R with respect to time, observe that

$\dot{\boldsymbol{x}}_+\boldsymbol{x}_-^t = \boldsymbol{x}_+\dot{\boldsymbol{x}}_-^t$, and use $R^t\boldsymbol{x}_+ = \boldsymbol{x}_-$. Substituting $\boldsymbol{\Omega} = 2\boldsymbol{x}_-\dot{\boldsymbol{x}}$ into the expression for T gives

$$T = 2\dot{\boldsymbol{x}}^t(\boldsymbol{x}_-^t I\boldsymbol{x}_-)\dot{\boldsymbol{x}}\,.$$

Differentiating with respect to $\dot{\boldsymbol{x}}$ gives the conjugate momenta $\boldsymbol{p} = 4(\boldsymbol{x}_-^t I\boldsymbol{x}_-)\dot{\boldsymbol{x}}$ on T^*S^3. Using $\boldsymbol{L} = I\boldsymbol{\Omega} = 2I\boldsymbol{x}_-\dot{\boldsymbol{x}}$ we see that

$$\boldsymbol{L} = 2I\boldsymbol{x}_-\dot{\boldsymbol{x}} = 2(\boldsymbol{x}_-\boldsymbol{x}_-^t)I\boldsymbol{x}_-\dot{\boldsymbol{x}} = \frac{1}{2}\boldsymbol{x}_-\boldsymbol{p}\,.$$

Similarly, we have $\boldsymbol{l} = \frac{1}{2}\boldsymbol{x}_+\boldsymbol{p}$. It is valid to use the canonical bracket between $\boldsymbol{x}$ and $\boldsymbol{p}$ because the resulting Hamiltonian automatically preserves $|\boldsymbol{x}| = 1$ and $\boldsymbol{x}\cdot\boldsymbol{p} = 0$.

Now changing from canonical variables $(\boldsymbol{x}, \boldsymbol{p})$ to non-canonical variables $(\boldsymbol{x}, \boldsymbol{L})$ gives the Lie-Poisson structure in the body frame as [BM97, BM18]

$$B_- = \begin{pmatrix} 0 & \frac{1}{2}\boldsymbol{x}_-^t \\ -\frac{1}{2}\boldsymbol{x}_- & \hat{\boldsymbol{L}} \end{pmatrix}, \quad \dot{\boldsymbol{x}} = \tfrac{1}{2}x_-^t\nabla_L H, \quad \dot{\boldsymbol{L}} = -\tfrac{1}{2}x_-\nabla_x H + \boldsymbol{L}\times\nabla_L H\,.$$

Similarly, the Lie-Poisson structure in the space fixed frame is

$$B_+ = \begin{pmatrix} 0 & \frac{1}{2}\boldsymbol{x}_+^t \\ -\frac{1}{2}\boldsymbol{x}_+ & -\hat{\boldsymbol{l}} \end{pmatrix}, \quad \dot{\boldsymbol{x}} = \tfrac{1}{2}x_+^t\nabla_l H, \quad \dot{\boldsymbol{l}} = -\tfrac{1}{2}x_+\nabla_x H - \boldsymbol{l}\times\nabla_l H\,.$$

Both Poisson structures have the Casimir $x_0^2 + x_1^2 + x_2^2 + x_3^2$. The Poisson structure B_+ is found by sandwiching the symplectic structure of the $(\boldsymbol{x}, \boldsymbol{p})$ variables by the Jacobian of the transformation of $(\boldsymbol{x}, \boldsymbol{l})$ and its transpose.

For the Euler top the usual Hamiltonian in the body frame is $H = \frac{1}{2}\boldsymbol{L}\cdot I^{-1}\boldsymbol{L}$, and the complicated integrals are $R\boldsymbol{L}$ (which imply the simple integral $|\boldsymbol{L}|^2$). In the space fixed frame instead we have the complicated Hamiltonian $H = \frac{1}{2}\boldsymbol{l}\cdot RI^{-1}R^t\boldsymbol{l}$ with the simple integrals $\boldsymbol{l}$. We mention the Euler top here to make the point that for general moments of inertia, the description in the body frame is simpler. However, for a round rigid body with $I_1 = I_2 = I_3$ both Hamiltonians are equally simple. Also for a symmetric rigid body with say $I_1 = I_2$, the spatial frame is useful because

$$2T = \boldsymbol{l}\cdot RI^{-1}R^t\boldsymbol{l} = \boldsymbol{l}\cdot\frac{1}{I_1}R(id + \delta\boldsymbol{e}_3\boldsymbol{e}_3^t)R^t\boldsymbol{l} = \frac{1}{I_1}\left(\boldsymbol{l}^2 + \delta L_3^2\right)$$

where $\delta = I_1/I_3 - 1$. The important point is that $L_3 = \boldsymbol{e}_3\cdot\boldsymbol{L} = \boldsymbol{e}_3\cdot R^t\boldsymbol{l} = R\boldsymbol{e}_3\cdot\boldsymbol{l} = \boldsymbol{l}\cdot\boldsymbol{a}$ is the angular momentum about the body's symmetry axis $\boldsymbol{e}_3$ and hence a constant of motion for the symmetric top.

Theorem 3.1. *The Lagrange top (symmetric heavy rigid body with a fixed point on the symmetry*

axis) in coordinates $\boldsymbol{x} \in S^3 \subset \mathbb{R}^4$ and angular momenta $\boldsymbol{l}$ in the space fixed frame has Hamiltonian

$$H = \frac{1}{2I_1}(l_x^2 + l_y^2 + l_z^2 + \delta L_3^2) + V(x_0^2 + x_3^2 - x_1^2 - x_2^2)$$

and Poisson structure B_+, with integrals l_z and

$$L_3 = 2l_x(-x_0x_2 + x_1x_3) + 2l_y(x_0x_1 + x_2x_3) + l_z(x_0^2 + x_3^2 - x_1^2 - x_2^2).$$

The vector fields of l_z and L_3 generate a T^2 action with isotropies. The vector field of the Hamiltonian is

$$X_H = \frac{1}{2I_1}X_{l^2} + \frac{\delta L_3}{I_1}X_{L_3} - \frac{1}{2}(0,0,0,0,\boldsymbol{x}_+\nabla_x V)^t\,. \tag{3.1}$$

The functions H, l_z, L_3 have pairwise vanishing Poisson bracket. The vector fields X_H, X_{L_3} and X_{l_z} are independent almost everywhere.

This theorem is well known for the case of a linear potential, and when using Euler angles it is part of most mechanics textbooks. Instead we offer a global description in the spatial frame with a Poisson structure. In addition, in order to make the connection with the general confluent Heun equation, we consider not just a linear potential (gravity), but in addition a quadratic term. After some preparations in the next sections discussing the torus action, the reduction, and briefly recalling Euler angles, the main technical part is the description of the set of critical values of the energy-momentum map in Theorem 2.

3.3. TORUS ACTION

The vector field generated by L_3 in the space fixed coordinate system is

$$X_{L_3} = B_+\nabla L_3 = \tfrac{1}{2}(\boldsymbol{x}_+^t R\boldsymbol{e}_3, 0, 0, 0)^t = (\tfrac{1}{2}\boldsymbol{x}_-^t\boldsymbol{e}_3, 0, 0, 0)^t \tag{3.2}$$

where we used the identity $\boldsymbol{x}_+^t R = \boldsymbol{x}_-^t$. This vector field can be easily integrated (two harmonic oscillators) to give the flow $\Phi_{L_3}^{\psi}$. This flow rotates (x_0, x_3) and (x_1, x_2) by $\psi/2$ clockwise. However, when the flow acts on R it acts by multiplication by a counterclockwise rotation about the z-axis through ψ (not $\psi/2$!) from the right. Thus L_3 has 2π-periodic flow on $T^*SO(3)$ and hence is an action variable.

The vector field generated by the integral l_z is

$$X_{l_z} = B_+\nabla l_z = (\tfrac{1}{2}\boldsymbol{x}_+^t\boldsymbol{e}_z, -\boldsymbol{l}\times\boldsymbol{e}_z)^t. \tag{3.3}$$

Again, this vector field is easily integrated (three harmonic oscillators) giving the flow $\Phi_{l_z}^{\phi}$. The action on R is by multiplication with a counterclockwise rotation about the z-axis through ϕ from the left. In addition, the momentum vector $\boldsymbol{l}$ is rotated by the same rotation

matrix. Thus l_z has 2π-periodic flow on $T^*SO(3)$ and hence is an action variable.

The vector fields X_{L_3} and X_{l_z} are parallel when $l_x = l_y = 0$ and either $x_0 = x_3 = 0$ or $x_1 = x_2 = 0$. These critical points have $\boldsymbol{l}||\boldsymbol{a}||\boldsymbol{e}_z$ and are called sleeping tops. In the first case $a_z = -1$ (hanging sleeping top), while in the second case $a_z = +1$ (upright sleeping top). The torus action is not free at these points because the rotations coincide. Since $L_3 = \boldsymbol{l} \cdot \boldsymbol{a}$ we see that $L_3 = -l_z$ for the hanging sleeping top and $L_3 = l_z$ for the upright sleeping top. The corresponding critical points of H are two parabolas above $l_z \pm L_3 = 0$.

The vector fields X_{l_z} and X_{L_3} both have 2π periodic flows on $T^*SO(3)$, i.e. they map $\boldsymbol{x}$ to $-\boldsymbol{x}$ after time 2π. When considered as flows on S^3 both flows have period 4π. Now consider the vector fields generated by $l_z \pm L_3$. These are both 2π periodic vector fields on T^*S^3. Points with $l_x = l_y = 0$ and either $x_0 = x_3 = 0$ or $x_1 = x_2 = 0$, respectively, are fixed points of these flows. Nevertheless, they are action variables on T^*S^3. Notice that as flows on $T^*SO(3)$ the orbits of $l_z \pm L_3$ do not all have the same minimal period, since points with $l_x = l_y = 0$ and either $x_0 = x_3$ or $x_1 = x_2$ have minimal period π, while all other non-fixed points have minimal period 2π. The T^2 action on T^*S^3 is of course still not free, the difference is that now the exceptional sets of points are found as those where one of the vector fields vanishes.

The vector field of the spherical Euler top is that of $\boldsymbol{l}^2 = l_x^2 + l_y^2 + l_z^2$. The vector fields of l_x and l_y are permutations to that of l_z given in (3.3). Combining these gives

$$X_{l^2} = (\boldsymbol{x}_+^t \boldsymbol{l}, 0, 0, 0)^t \,.$$

Here the components of $\boldsymbol{l}$ are all constant, and the flow of this vector field is a rotation about the axis $\boldsymbol{l}$. This is also a periodic flow, but the period is not constant. To obtain constant period, we consider the flow generated by $l = \sqrt{\boldsymbol{l}^2}$, which we denote by X_l. This flow commutes with the flows of l_z and L_3, but not with that of H. The flow of $\boldsymbol{l}^2$ leaves $\boldsymbol{l}$ constant and so

$$\begin{aligned}\Phi_l^\alpha &= \exp\left(\frac{\alpha}{2l}\begin{pmatrix} 0 & l_x & l_y & l_z \\ -l_x & 0 & -l_z & l_y \\ -l_y & l_z & 0 & -l_x \\ -l_z & -l_y & l_x & 0 \end{pmatrix}\right) \\ &= \begin{pmatrix} \cos\frac{\alpha}{2} & l_x/l\sin\frac{\alpha}{2} & l_y/l\sin\frac{\alpha}{2} & l_z/l\sin\frac{\alpha}{2} \\ -l_x/l\sin\frac{\alpha}{2} & \cos\frac{\alpha}{2} & -l_z/l\sin\frac{\alpha}{2} & l_y/l\sin\frac{\alpha}{2} \\ -l_y/l\sin\frac{\alpha}{2} & l_z/l\sin\frac{\alpha}{2} & \cos\frac{\alpha}{2} & -l_x/l\sin\frac{\alpha}{2} \\ -l_z/l\sin\frac{\alpha}{2} & -l_y/l\sin\frac{\alpha}{2} & l_x/l\sin\frac{\alpha}{2} & \cos\frac{\alpha}{2} \end{pmatrix}.\end{aligned}$$

When acting with this flow on the rotation matrix R with initial condition $\boldsymbol{x} = (1, 0, 0, 0)$ gives Rodrigues' parametrisation of $SO(3)$ with rotation axis $\boldsymbol{l}/l$ and rotation angle α. Thus

Rodrigues' formula gives the geodesics of the spherical top. When acting with this flow on S^3 it is periodic with period 4π.

The reason we are including this flow is that there is an interesting difference between $SO(3)$ and S^3. On $T^*SO(3)$ the singular T^3 torus action generated by the commuting flows of l_z, L_3, and l is faithful. This means that outside the singularity where $l_z \pm L_3 = 0$ the action on each T^3 obtained by fixing the values of the generators is faithful. By contrast, when considering the T^3 torus action generated by $l_z + L_3$, $l_z - L_3$, and $l + l$ on T^*S^3 the action is not faithful on regular tori. The reason is that when flowing each flow only for angle π, then the first two flows together achieve $\boldsymbol{x} \to -\boldsymbol{x}$, and this is cancelled by the flow $\Phi^{\pi}_{2l} = \Phi^{2\pi}_{l}$.

3.4. REDUCTIONS

The flows of l_z and L_3 are global S^1 actions, and hence allow for regular reduction. It is straightforward to obtain the reduced system from the global system with Poisson structure $B_{\pm}$. The l_z-reduced system gives the well known Euler-Poisson equations, while the L_3-reduced equations are somewhat less well known in classical mechanics (see, e.g., [BS99, CB15, Dul04]). The full reduction is singular because the T^2 action of l_z and L_3 is not free. The standard description of reduction uses zxz-Euler angles, the singular reduction using invariants is in [CB15]. A peculiar property of Euler angles is that the ψ-rotation leaves the figure axis invariant (it acts on the right) while the ϕ-rotation leaves the direction of gravity invariant (it acts on the left), and hence Euler angles are neither space-fixed nor body-fixed. The quantisation of the top (see below) starts out with Euler angles [LL77], but in the end, writing the Hamiltonian using $\boldsymbol{l}^2$ and L_3^2 shows that for the quantum mechanical description the spatial frame is also useful.

The reduction by the symmetry $\Phi^{\psi}_{L_3}$ introduces the coordinates of the axis of the top $\boldsymbol{a} = R\boldsymbol{e}_3$ as new coordinates. This is, in fact, reduction by invariants, since the third column of R is given by $(2(x_0x_2 + x_1x_3), -2x_0x_1 + 2x_2x_3, x_0^2 + x_3^2 - x_1^2 - x_2^2)$ and these are all invariant under the two-oscillator flow $\Phi^{\psi}_{L_3}$. We already noted that $\Phi^{\psi}_{L_3}$ acts on R by multiplication by $R_z(\psi)$ from the right, where $R_z(\psi)$ denotes a counterclockwise rotation about the z-axis by ψ. Hence $RR_z(\psi)\boldsymbol{e}_3 = R\boldsymbol{e}_3 = \boldsymbol{a}$ is invariant. The resulting reduced system has Poisson structure

$$B^r_+ = \begin{pmatrix} 0 & -\hat{\boldsymbol{a}} \\ -\hat{\boldsymbol{a}} & -\hat{\boldsymbol{l}} \end{pmatrix}, \quad \dot{\boldsymbol{a}} = -\boldsymbol{a} \times \nabla_l H, \quad \dot{\boldsymbol{l}} = -\boldsymbol{a} \times \nabla_a H - \boldsymbol{l} \times \nabla_l H\,.$$

Denote the Jacobian of the transformation from $(\boldsymbol{x}, \boldsymbol{l})$ to $(\boldsymbol{a}, \boldsymbol{l})$ by A. Then $B^r_+ = A^t B_+ A$ when expressed in the new variables. The main identity in the reduction from B_+ to B^r_+ is $\frac{1}{2}\frac{\partial \boldsymbol{a}}{\partial \boldsymbol{x}}\boldsymbol{x}^t_+ = \hat{\boldsymbol{a}}$. The Poisson structure B^r_+ has Casimirs $\boldsymbol{a}^2 = 1$ and $\boldsymbol{a} \cdot \boldsymbol{l}$ and the reduced

Hamiltonian is

$$H = \frac{1}{2I_1}(\boldsymbol{l}^2 + \delta(\boldsymbol{a}\cdot\boldsymbol{l})^2) + V(a_z).$$

Since $\boldsymbol{a}\cdot\boldsymbol{l}$ is a Casimir (equal in value to the generator of the symmetry L_3) it does not contribute to the dynamics but merely changes the value of the Hamiltonian.

Note that reduction by the symmetry generated by the integral l_z is more complicated in the spatial frame since the flow is a rotation in $\boldsymbol{x}$ and in l_x, l_y. However, when switching to the body frame then the flow of l_z (written in terms of $\boldsymbol{L}$) is simpler. Reduction is achieved by introducing the invariant of the left action generated by l_z, which is $\boldsymbol{e}_3^t R_z(\phi)R = \boldsymbol{e}_3^t R = \boldsymbol{\Gamma}^t$ with Poisson structure

$$B_-^r = \begin{pmatrix} 0 & \hat{\boldsymbol{\Gamma}} \\ \hat{\boldsymbol{\Gamma}} & \hat{\boldsymbol{L}} \end{pmatrix}, \quad \dot{\boldsymbol{\Gamma}} = \boldsymbol{\Gamma}\times\nabla_L H, \quad \dot{\boldsymbol{L}} = \boldsymbol{\Gamma}\times\nabla_\Gamma H + \boldsymbol{L}\times\nabla_L H\,.$$

The reduction leads to the more familiar Hamiltonian of the Lagrange top given by

$$H = \frac{1}{2I_1}(L_1^2 + L_2^2) + \frac{1}{2I_3}L_3^2 + V(\Gamma_3)$$

where $\boldsymbol{\Gamma}$ is $\boldsymbol{e}_z$ viewed from the body frame. The Poisson structure is B_-^r with the opposite sign than B_+^r. These are the equations usually called Euler-Poisson equations. Their advantage is that this reduction remains valid for an arbitrary rigid body with a fixed point, and this family for appropriate moments of inertia and position of the centre of mass contains the Kovalevskaya top, the Euler top, and all other (non-integrable) tops.

The Hamiltonian Hopf bifurcation in the sleeping top with $\boldsymbol{a}||\boldsymbol{l}||\boldsymbol{e}_z$ respectively $\boldsymbol{\Gamma}||\boldsymbol{L}||\boldsymbol{e}_3$ is best described in the reduced system(s), because the corresponding periodic orbit becomes a relative equilibrium after reduction. It is easy to check that indeed these are equilibria, and linearising the Hamiltonian vector field about these equilibria yields a 6×6 matrix with 2 eigenvalues zero corresponding to the two Casimirs. The characteristic polynomial for the remaining non-trivial eigenvalues is

$$P_+(\lambda) = \lambda^4 + \lambda^2(\kappa^2 - 2f) + f^2 = 0, \quad \kappa = l_z/I_1 = \omega I_3/I_1, \quad f = a_z V'(a_z)/I_1, \quad a_z = \pm 1\,.$$

in the spatial frame and

$$P_-(\lambda) = P_+(\lambda) + \omega(\omega-\kappa)(2\lambda^2 + 2f + \omega(\omega-\kappa)), \quad \omega = l_z/I_3$$

in the body frame. The eigenvalues given by the roots of P_+ in the spatial frame are not the same as the eigenvalues given by the roots of P_- in the body frame because in the latter case the system is described in a frame rotating with angular velocity ω. However, they differ only by $\pm i\omega$. More precisely, let $\lambda_1, \bar{\lambda}_1, \lambda_2, \bar{\lambda}_2$ be the roots of P_+, then the roots of P_- are $\lambda_1 + i\omega, \bar{\lambda}_1 - i\omega, \lambda_2 + i\omega, \bar{\lambda}_2 - i\omega$ such that the Floquet multipliers $\mu = \exp(\lambda T)$ of the

periodic orbit with period $T = 2\pi/\omega$ are the same. The description in the spatial frame gives simpler formulas.

At the Hamiltonian Hopf bifurcation the eigenvalues change from all purely imaginary via a collision on the imaginary axis to a quadruple of complex eigenvalues. This occurs when the discriminant of $P_+(\lambda)$ considered as a quadratic equation in λ^2 changes from positive to negative. The discriminant is given by $\kappa^2(\kappa^2 - 4f)$. When f is negative the eigenvalues are purely imaginary for any κ. When f is positive eigenvalues are purely imaginary when $\kappa^2 > 4f$, while the top is unstable with non-zero real parts of the eigenvalues when $\kappa^2 < 4f$. This is the classical stability condition for the Lagrange top, here obtained for arbitrary potential. At the critical case $\kappa^2 = 4f$ the eigenvalues collide and $\lambda^2 = -\kappa^2/4$.

3.5. Euler Angles

The Poisson structures $B_\pm$ allow for a global description of rigid body dynamics free of coordinate singularities. However, often explicit canonical coordinates are more convenient, and even essential for the quantisation of the problem. Such a coordinate system adapted to the symmetries is given by zxz-Euler angles such that

$$R = R_z(\phi)R_x(\theta)R_z(\psi)\,.$$

The canonically conjugate momenta are denoted by p_ϕ, p_θ, p_ψ, respectively. Then we have that $l_z = p_\phi$ and $L_3 = p_\psi$. The Hamiltonian in these coordinates is

$$H = \frac{1}{2I_1}(2T_{round} + \delta p_\psi^2) + V(\cos\theta)$$

where T_{round} is the kinetic energy of the spherical top with moment of inertia 1:

$$T_{round} = \frac{1}{2}\left(p_\theta^2 + \frac{1}{\sin^2\theta}\left(p_\phi^2 + p_\psi^2 - 2p_\phi p_\psi\cos\theta\right)\right) = \frac{1}{2}\boldsymbol{l}^2\,.$$

Notice that this round metric on $SO(3)$ is a metric of constant curvature and hence up to a covering equivalent to the metric of the round sphere S^3.

Away from the coordinate singularity where the torus action is not free, Euler angles are a smooth local coordinate system. Equilibrium points in θ are determined by $\partial H/\partial\theta = 0$. For later use, we denote this function by H_θ, and similarly the 2nd derivative by $H_{\theta\theta}$.

3.6. Bifurcation diagram

The energy-momentum map from $T^*SO(3)$ to $\mathbb{R}^3$ is given by (l_z, L_3, H) where L_3 is given in terms of $\boldsymbol{x}$ and $\boldsymbol{l}$ as in Theorem 1. The bifurcation diagram of this integrable system is the

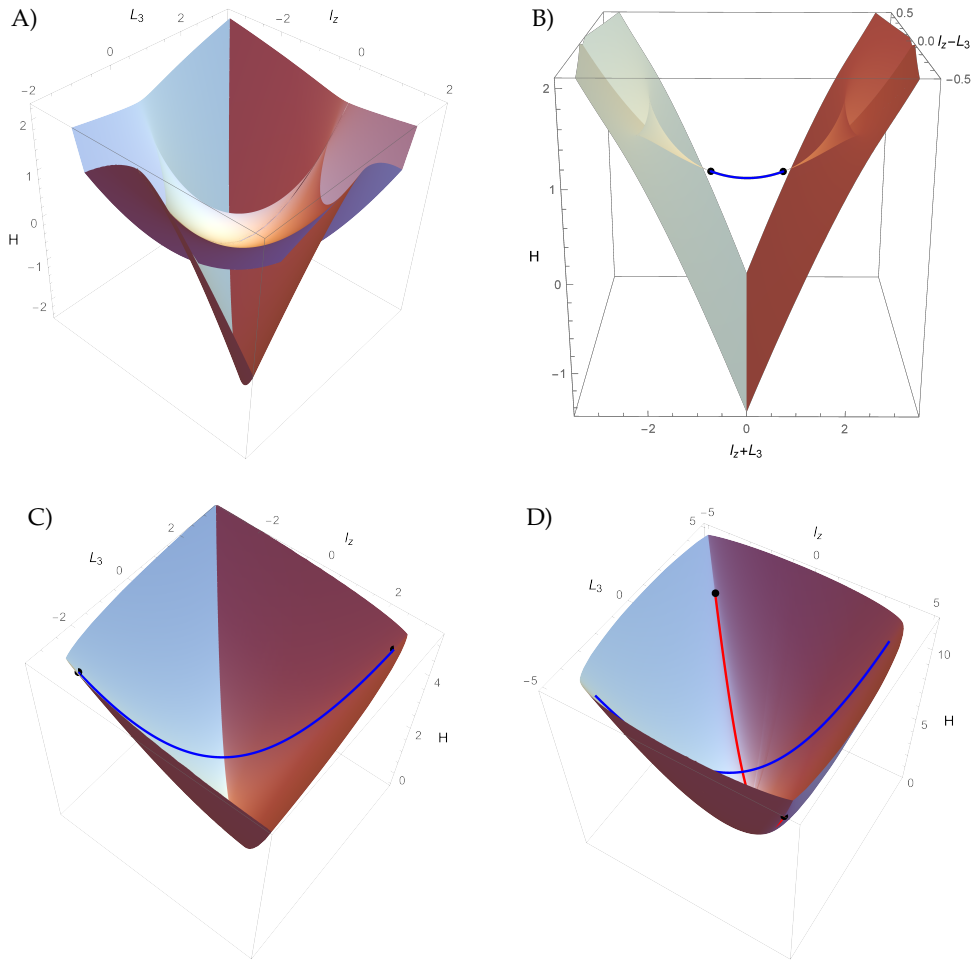

Figure 3.1: Examples of the four topologically different kinds of bifurcation diagrams. A) triangular tube, B) shrinking triangular tube and thread (zoomed in), C) one thread and D) two threads. All figures use $I_1 = 1, \delta = 0, c_1 = 1$. The values of c_2 are $-1.5, -0.48, 0.4, 2.5$ for A,B,C,D, respectively. In A) the ranges for l_z and L_3 are chosen as to cut away parts of the surface facing the viewer. In B) the ranges are even more restricted. The black dots mark the Hamiltonian Hopf bifurcations.

set of critical values of the energy-momentum map. Hence we are interested in the rank of (X_{l_z}, X_{L_3}, X_H). To determine where the rank drops we consider

$$\alpha X_{L_3} + \beta X_{l_z} + \gamma X_H = 0\,. \tag{3.4}$$

Theorem 3.2. *The rank 1 points of the energy-momentum map are given by two parabolas of sleeping tops*

$$(l_z, L_3, H) = \left(m, \pm m, \frac{m^2}{2I_1}(1+\delta) + V(\pm 1)\right)\,. \tag{3.5}$$

The rank 2 points have a rational parametrisation determined by $\boldsymbol{l}(\beta, a_z) = \frac{1}{\beta} I_1 V'(a_z)\boldsymbol{a} + \beta \boldsymbol{e}_z$ *such that for* $a_z \in [-1, 1]$ *and* $\beta \in \mathbb{R}$ *the critical values of the energy-momentum map are*

$$\begin{aligned} l_z(\beta, a_z) &= \frac{1}{\beta} I_1 V'(a_z) a_z + \beta, \\ L_3(\beta, a_z) &= \frac{1}{\beta} I_1 V'(a_z) + \beta a_z, \\ H(\beta, a_z) &= \frac{1}{2I_1}(\boldsymbol{l}(\beta, a_z)^2 + \delta L_3(\beta, a_z)^2) + V(a_z)\,. \end{aligned}$$

Proof. Notice that the last 3 components of X_V can be written as

$$-\tfrac{1}{2}\boldsymbol{x}_+ \nabla_x V(a_z(x)) = -\boldsymbol{a} \times \nabla_a V(a_z) = -\boldsymbol{a} \times \boldsymbol{e}_z V'(a_z)\,.$$

Using $\boldsymbol{x}_-^t \boldsymbol{e}_3 = \boldsymbol{x}_+^t R \boldsymbol{e}_3 = \boldsymbol{x}_+^t \boldsymbol{a}$ in the flow of L_3, (3.4) becomes

$$\begin{pmatrix} \frac{1}{2}\boldsymbol{x}_+^t((\alpha + \gamma\delta L_3)\boldsymbol{a} + \beta \boldsymbol{e}_z + \gamma \boldsymbol{l}) \\ -(\gamma I_1 V^{'} \boldsymbol{a} + \mu \boldsymbol{e}_z + \beta \boldsymbol{l}) \times \boldsymbol{e}_z \end{pmatrix} = \begin{pmatrix} 0 \\ 0 \end{pmatrix}.$$

This means critical points of the momentum map occur when

$$\begin{aligned} (\alpha + \gamma\delta L_3)\boldsymbol{a} + \beta \boldsymbol{e}_z + \gamma \boldsymbol{l} &= 0 \\ \gamma I_1 V^{'} \boldsymbol{a} + \mu \boldsymbol{e}_z + \beta \boldsymbol{l} &= 0. \end{aligned} \tag{3.6}$$

for α, β, γ not all zero. Hence the three vectors $\boldsymbol{a}$, $\boldsymbol{l}$, $\boldsymbol{e}_z$ are co-planar. Since $\boldsymbol{a}$ and $\boldsymbol{e}_z$ never vanish, there is no rank 0 point. We have the following four cases.

1) $\boldsymbol{a} \parallel \boldsymbol{e}_z$. This means $a_x = a_y = 0$ and $a_z = \pm 1$. If $\boldsymbol{l} \neq 0$ and $\boldsymbol{l}$ not parallel to $\boldsymbol{e}_z$, then linear independence (3.6) implies $\alpha = \beta = \gamma = 0$. Hence $\boldsymbol{l} \parallel \boldsymbol{e}_z \parallel \boldsymbol{a}$ (including $\boldsymbol{l} = 0$), and we can use $l_z = m$ as parameter and thus showed the parametrisation of the sleeping tops (3.5). Recall that these are the points where the torus action is not free. All points along these parabolas have rank 1. Parts of these parabolas may be isolated threads of focus-focus type, while others form the edges of the surface of elliptic-elliptic type. The vertices of the parabolas where $m = 0$ and hence $\boldsymbol{l} = 0$ are equilibrium points of X_H with $a_z = \pm 1$.

2) $\boldsymbol{l} \parallel \boldsymbol{e}_z$. Set $\boldsymbol{l} = \lambda \boldsymbol{e}_z$. If $\boldsymbol{a} \parallel \boldsymbol{e}_z$ then this gives the sleeping top solution again. If $\boldsymbol{a}$ is not parallel to $\boldsymbol{e}_z$ then by linear independence, (3.6) implies $\alpha + \gamma\delta L_3 = \beta + \gamma\lambda = 0$ and $I_1 V^{'} = \mu + \beta\lambda = 0$. If $\gamma = 0$ then this forces the trivial solution $\alpha = \beta = 0$ so $\gamma \neq 0$ and $V^{'} = 0$. Since $V^{'} = c_1 + 2c_2 a_z$ this means $a_z = \frac{-c_1}{2c_2} =: a_{z0}$. Normalising $\gamma = -1$ gives $\lambda = \beta$ and hence $\boldsymbol{l} = \beta \boldsymbol{e}_z$, $\boldsymbol{a} = (a_x, a_y, a_{z0})$, $L_3 = \boldsymbol{l} \cdot \boldsymbol{a} = \beta a_{z0}$ and hence using $\beta = m$ as parameter gives

$$(l_z, L_3, H) = \left(m, m a_{z0}, \frac{m^2}{2I_1}(1 + \delta a_{z0}^2) + V(a_{z0}) \right). \tag{3.7}$$

Since $|a_z| \leq 1$ this parabola only exists when $2|c_2| > |c_1|$, while for $2|c_2| = \pm|c_1|$ it merges with the sleeping tops. The vertex of this parabola where $m = 0$ and hence $\boldsymbol{l} = 0$ is an equilibrium point of X_H with $|a_z| \leq 1$. This vertex lies above or below the vertices of the parabolas of sleeping tops (3.5) described in case 1, depending on whether $c_2 < -c_1/2$ or $c_2 > c_1/2$.

3) $\boldsymbol{l} \parallel \boldsymbol{a}$. This forces $\boldsymbol{l} = \lambda \boldsymbol{a} = L_3 \boldsymbol{a}$. If $\boldsymbol{a} \parallel \boldsymbol{e}_z$ then this gives the sleeping top solution again. If $\boldsymbol{a}$ is not parallel to $\boldsymbol{e}_z$ then linear independence and (3.6) implies $\alpha + \gamma(\delta + 1)L_3 = \beta = 0$ and $\gamma I_1 V' + \beta L_3 = \mu = 0$. Again $\gamma = 0$ gives the trivial solution, so we can normalise $\gamma = -1$ and find $\alpha = (1 + \delta)L_3$ and $V' = 0$, as in case 2. Using $L_3 = k$ as parameter gives

$$(l_z, L_3, H) = \left(k a_{z0}, k, \frac{k^2}{2I_1}(\delta + 1) + V(a_{z0}) \right). \tag{3.8}$$

Existence and limiting behaviour is as in case 2. The vertex of this parabola coincides with that of case 2.

4) General case where no pair of vectors is parallel. If $\gamma = 0$ then this gives $\alpha = \beta = 0$ while if $\beta = 0$ then this gives case 2. We now assume $\beta \neq 0$ and $\gamma \neq 0$. Eliminating $\boldsymbol{l}$ from (3.6) and using linear independence gives $\mu = \frac{\beta^2}{\gamma}$ and $\alpha + \gamma\delta L_3 = \frac{\gamma^2}{\beta} I_1 V'$. Using this to eliminate L_3 in (3.6) gives $-\boldsymbol{l} = \frac{\gamma}{\beta} I_1 V^{'} \boldsymbol{a} + \frac{\beta}{\gamma} \boldsymbol{e}_z$. Normalising $\gamma = -1$ computing $l_z = \boldsymbol{l} \cdot \boldsymbol{e}_3$, $L_3 = \boldsymbol{l} \cdot \boldsymbol{a}$, and $\boldsymbol{l}^2 = \boldsymbol{l} \cdot \boldsymbol{l}$ gives the result. Notice that β is the angular velocity of the angle ϕ conjugate of p_ϕ.

■

Note that in cases 2 and 3 the parabolas (3.7) and (3.8) are embedded in the surface of critical values described in case 4. Unlike the parabolas (3.5) the rank of these points is 2. Since V' is linear in a_z we can eliminate a_z in favour of $\tilde{\alpha} = I_1 V'(a_z)/\beta$. Notice that α is the angular velocity of the angle ψ, and $\tilde{\alpha}$ is that angular velocity with $\delta = 0$. As a result we obtain a *polynomial* parametrisation of the critical values of the energy-momentum map which after

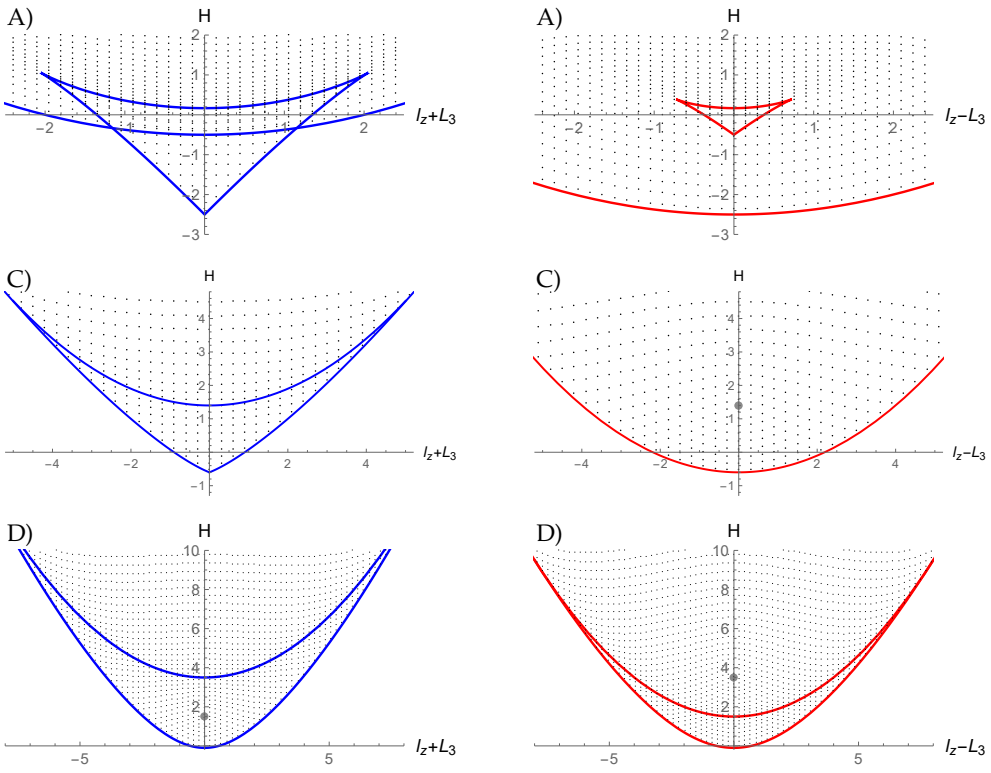

Figure 3.2: Slices through the bifurcation diagram along $l_z - L_3 = 0$ (blue) and $l_z + L_3 = 0$ (red) for Fig. 3.1 A,C,D using $\hbar = (0.075, 0.15, 0.11)$ for the quantum spectrum, respectively.

non-dimensionalisation is given by

$$\big(\beta + a_{z0}\tilde{\alpha}(1-\tilde{\alpha}\beta), \gamma + a_{z0}\beta(1-\tilde{\alpha}\beta), \tfrac{1}{2}(\tilde{\alpha}^2 + \beta^2 + a_{z0}(1-\tilde{\alpha}\beta)(3\tilde{\alpha}\beta+1) + \delta(\tilde{\alpha} + a_{z0}\beta(1-\tilde{\alpha}\beta))^2)\big)$$

with the constraint $-1 \leq a_{z0}(1-\tilde{\alpha}\beta) \leq 1$ on the parameters $\tilde{\alpha}$ and β. When $\delta = 0$ any line determined by fixing α and changing β or vice versa is a planar parabola. This means the surface is doubly foliated by (arcs of) planar parabolas. The two special parabolas (3.7) and (3.8) correspond to vanishing angular momentum $\tilde{\alpha} = 0$ and $\beta = 0$, respectively. Hence for points on (3.7) the top does not rotate about its figure axis while for points on (3.8) the figure axis does not rotate in space. Both are extreme cases of resonant 2-tori where one frequency vanishes. Note that such solutions are impossible in the ordinary Lagrange top with $c_2 = 0$. The parabolas of rank 1 points (3.5) are *not* part of this foliation, instead they mark the endpoints of the parabolic arcs where $a_{z0}(1-\tilde{\alpha}\beta) = \pm 1$.

The rational parametrisation from Theorem 2 is also useful when using the Euler angles. Inserting the parametrisation into the condition for an equilibrium point $H_\theta = 0$ shows that it is identically satisfied. To determine the stability of the equilibrium we evaluate the second derivative $H_{\theta\theta}$ on the rational parametrisation and find

$$H_{\theta\theta}(\beta, a_z) = \beta^2 I_1 - 2a_z V'(a_z) + (1-a_z^2)V''(a_z) + \frac{1}{\beta^2 I_1} V'(a_z)^2 \,. \tag{3.9}$$

The transverse stability of a 2-torus is determined by the sign of $H_{\theta\theta}$ since it gives the curvature of the effective potential. Computing $H_{\theta\theta}$ on the parabolas of sleeping top (3.5) gives $m^2/(4I_1) \mp V'(\pm 1)$, reproducing the classical condition for the Hamiltonian Hopf bifurcation in Lagrange's sleeping top found at the end of section 4. Evaluating $H_{\theta\theta}$ as given in (3.9) on the parabola (3.7) gives $m^2/I_1 + 2c_2(1-a_{z0}^2)$, and on the parabola (3.8) similarly gives $k^2/I_1 + 2c_2(1-a_{z0}^2)$. When $c_2 < -c_1/2$ these are both negative for small m or k, respectively, and hence unstable. These correspond to points on top of the triangular tube, which are hyperbolic. For sufficiently large angular momentum the sign flips, and they are points in the outer envelope surface of critical values. When $c_2 > c_1/2$ the 2nd derivative is always positive, hence in this case rank 2 points correspond to elliptic 2-tori.

Equating $H_{\theta\theta}$ to zero gives a relation between β and a_z which determines degenerate values in the bifurcation diagram. These are the cusp-shaped edges of the triangular tubes in Fig. 1A,B. The most degenerate situation occurs when simultaneously the 2nd and the 3rd θ-derivative of H vanish. This occurs for the special parameter values $a_z = -c_1/(2c_2)$, $\beta^2 = -c_1^2/(8c_2 I_1)$ and $a_z = -c_1/(4c_2)$, $\beta^2 = c_1^2/(2c_2 I_1) - 2c_2/I_1$. When these degenerate values for a_z collide with ± 1 then the degenerate points disappear and the topological structure of the bifurcation diagram changes. This occurs for $c_1 = \pm 2c_2$ and $c_1 = -4c_2$. The plus sign yields imaginary β. The sign of c_1 can be made positive by the original choice of body

coordinate system. This can flip the sign of $c_1 a_z$ in the potential but leaves $c_2 a_z^2$ unchanged. Hence there are 4 topologically distinct cases illustrated in Fig. 1:

A) $c_2/c_1 < -1/2$: triangular tube Fig. 1A;

B) $-1/2 < c_2/c_1 < -1/4$: triangular tube shrinking to a thread Fig. 1B;

C) $-1/4 < c_2/c_1 < 1/2$: one thread Fig. 1C;

D) $c_2/c_1 > 1/2$: two threads Fig. 1D.

To understand the figures corresponding to these 4 cases it helps to consider how they bifurcate into each other. We stress again that we always consider $\delta = 0$, because adding the additional quadratic term in L_3 to the Hamiltonian deforms the bifurcation diagram, but does not essentially change it. Bifurcations similar to those found here have recently been described in [SZ07a, EHM19], in particular also the related quantum monodromy in [SZ07a].

Let us start with the ordinary Lagrange top, $c_2 = 0$, $c_1 = 1$ by choice of coordinate system and normalisation [CK85]. The bifurcation diagram for the harmonic Lagrange top is topologically the same for $-1/4 < c_2/c_1 < 1/2$. It is natural that a small enough quadratic term does not change the nature of the bifurcation diagram since the potential $V(a_z)$ is only changed a little since $|a_z| \leq 1$. The outer surface is a bowl that has at least two corners when cut at constant energy. For high energy there are four corners, while for low energy only two. The transitions are two supercritical Hamiltonian Hopf bifurcations where the sleeping top becomes stable. A thread of critical values detaches at these points of the surface. This thread is shown in blue in Fig. 1C. In Fig. 2 slices through the 3-dimensional bifurcation diagram are shown. Each blue curve is a slice with $l_z - L_3 = 0$ which contains the thread, while in the other slice $l_z + L_3 = 0$ the thread appears as a single isolated point. In these figures we also show the quantum spectrum, see the next section. This situation persists for non-zero c_2 not too large.

For $c_2/c_1 > 1/2$, a second thread emerges from the minimum of H, as shown in Fig. 1D and Fig. 2D. For low energies, the outer surface has no corners at all. For intermediate energy as visible at the top of Fig. 1D, there are 2 corners above where the red thread is attached, but the blue thread is not yet attached and the outer surface nearby is still smooth. For high energies, there are 4 corners.

A more dramatic change occurs when decreasing c_2/c_1 through $-1/4$. All attachment points of the threads in the two cases discussed so far are supercritical Hamiltonian Hopf bifurcations. When passing $-1/4$, the supercritical Hamiltonian Hopf bifurcation turns into a subcritical Hamiltonian Hopf bifurcation. The attachment point is replaced by a tube with triangular cross section that eventually contracts to a point and becomes a thread, as shown in Fig. 1B (zoomed in).

When decreasing c_2/c_1 further, the two subcritical Hamiltonian Hopf bifurcation values collide when $c_2/c_1 = -1/2$, and merge into a triangular tube shown in Fig. 1A and there is no bifurcation any more in the rank 1 points given by (3.5) with $L_3 = +m$. Instead this parabola marks the corner at the bottom of the triangular tube and for higher energies the corner in the outer surface. In this figure, the bounding box is chosen such that it cuts away parts of the surface facing the viewer so that the triangular tube becomes visible. The 0-slices are shown in Fig. 2A. The two bottom surfaces of the tube correspond to elliptic 2-tori, while the top surface of the tube corresponds to hyperbolic 2-tori. The top surface joins the bottom surfaces along a line of cusps where $H_{\theta\theta} = 0$. The merging of the triangular tube with the outer surface is illustrated in additional slices in Fig. 3.3. Consider the red triangle in Fig. 2A. It is obtained by slicing the tube orthogonal to its long direction in the middle. When moving this slice away from the middle the triangle moves up, but the bottom curve below it moves up faster, and eventually the corner of the triangle will pierce through that curve. When viewing the critical values from below the triangular tube pierces through the surface. The first bifurcation in the slice occurs when the top of the triangle (hyperbolic 2-tori) becomes tangent to the curve. This creates a pair of saddle-centre bifurcation of 2-tori and the corresponding critical values in the energy-momentum map are degenerate. In the rightmost slice the two cusps collide and annihilate and the slice becomes smooth. The reason that the two different slices in Fig. 3 appear somewhat similar is that when $c_1 \to 0$ they actually become identical, see Fig. 4 below. In the left pane a perspective view looking down along the H-axis from above is shown, while in the right pane we are looking up along the H-axis from below the surface. This concludes the description of the four generic cases of the bifurcation diagram.

There are 3 degenerate cases separating A,B,C,D from each other. In addition there are two non-generic cases that occur in the limit that $c_1 \to 0$. There are two different limiting cases depending on the sign of c_2. For positive c_2 we recover the case studied in [BZ93], for which the two threads (3.5) intersect at their vertex. The case of negative c_2 is fundamentally different and was not considered in [BZ93]. Again the two parabolas (3.5) intersect at their vertices, but they are now embedded in the surface of critical values and mark its edges, see Fig. 4. In addition the triangular tube becomes symmetric in this limit forming a kind of trampoline. The edge of the trampoline where $H_{\theta\theta} = 0$ is shown in orange. The cuspidal points of the trampoline touch the outer surface where the self-intersection of the surface stops, this is where the parabolas (3.7) and (3.8) (green and purple in Fig. 4) intersect the orange cusps. Viewed from below this point is where the self-intersection of the surface stops and the parabolas become visible as embedded in the smooth outer surface (Fig. 4 right). Slices of the set of critical values for constant energy in this case have D_4 symmetry.

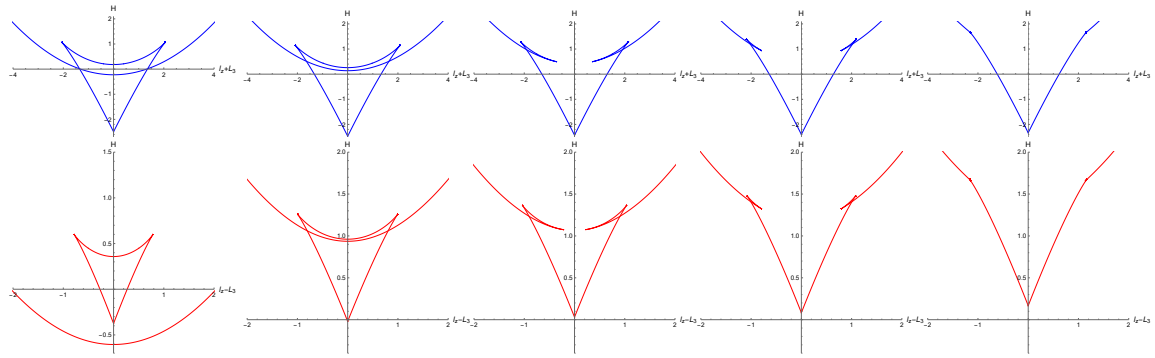

Figure 3.3: Slices of constant $l_z - L_3$ and $l_z + L_3$ near the most degenerate values. Top: slices with constant $l_z - L_3 = (0.200, 0.488, 0.755, 0.888, 1.15)$. Bottom: slices with constant $l_z + L_3 = (1.00, 1.96, 2.06, 2.16, 2.31)$. Parameters are the same as those in Fig. 1A.

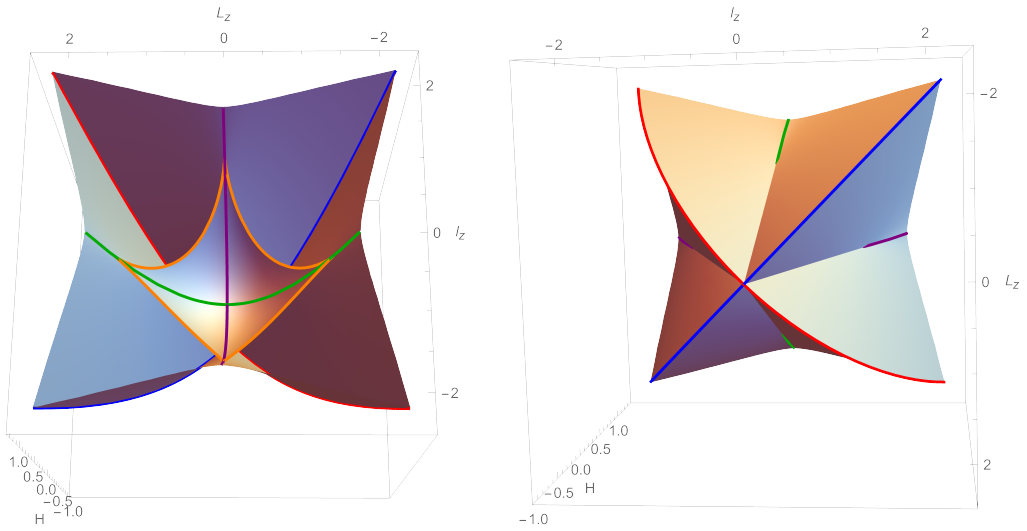

Figure 3.4: Top and bottom view (shown in the left and right pane, respectively) of the limiting case with $c_1 = 0$ and negative $c_2 = -1$. Four parabolas corresponding to (3.5) (red and blue), (3.7) (green), (3.8) (purple) are shown, in addition to the cuspidal edge of the "trampoline" (orange).

3.7. Quantum Mechanics of the Harmonic Lagrange Top

The quantisation of the rigid body is textbook material, see, e.g., [LL77, §103]. The global action variables l_z and L_3 become operators $\hat{l}_z = -i\partial/\partial\phi$ and $\hat{L}_3 = -i\partial/\partial\psi$, measured in units of $\hbar$. We denote the corresponding integer eigenvalues by m and k such that $\hat{l}_z\Psi = m\Psi$ and $\hat{L}_3\Psi = k\Psi$ for a wave function Ψ.

The quantum mechanical harmonic Lagrange top has the Hamiltonian operator

$$\hat{H} = \frac{1}{2I_1}\left(\hat{\boldsymbol{l}}^2 + \delta\hat{L}_3^2\right) + c_1\cos\theta + c_2\cos^2\theta \tag{3.10}$$

where $\hat{\boldsymbol{l}}$ is the total angular momentum operator. Explicitly the first part of the Hamiltonian operator is found as the Laplace-Beltrami operator of the metric T_{round} of the spherical top, hence

$$\hat{\boldsymbol{l}}^2 = -\frac{1}{\sin\theta}\partial_\theta(\sin\theta\,\partial_\theta) + \frac{1}{\sin^2\theta}(m^2 + k^2 - 2mk\cos\theta)\,,$$

where we have already replaced the operators $\hat{l}_z$ and $\hat{L}_3$ by their respective eigenvalues. The equation $\hat{\boldsymbol{l}}^2 f = j(j+1)f$ is a self-adjoint form of the hypergeometric equation. Setting the eigenvalue of $\hat{\boldsymbol{l}}^2$ to $j(j+1)$ for positive integer j, solutions are given by $\sin^{|m+k|}\frac{\theta}{2}\cos^{|m-k|}\frac{\theta}{2}P^{|m+k|,|m-k|}_{j-\max(|k|,|m|)}(\cos\theta)$ where $P_n^{m_1,m_2}$ are the Jacobi polynomials. Up to normalisation and phase factors these are the Wigner-D functions [BLC81]. The equation has regular singular points at $\theta = 0, \pi$ with indices $\pm(m-k)$ and $\pm(m+k)$, respectively. Note that the global quantum numbers m and k appear as indices of regular singular points.

Adding the potential terms, and transforming to $z = \cos\theta$ brings us to the following observation.

Theorem 3.3. *The quantisation of the harmonic Lagrange top leads to the most general confluent Heun equation (aka generalised spheroidal wave equation) which has the self-adjoint form*

$$(-\partial_z((1-z^2)\partial_z + \frac{k^2+m^2-2kmz}{1-z^2} + \tilde{c}_1 z + \tilde{c}_2 z^2 - \lambda)\psi(z) = 0 \tag{3.11}$$

where $z = \cos\theta$ and λ is the spectral parameter related to the energy eigenvalue E of the Hamiltonian by $\lambda = 2I_1E/\hbar^2 - \delta k^2$, $\tilde{c}_1 = c_1 2I_1/\hbar^2$, $\tilde{c}_2 = c_2 2I_1/\hbar^2$,

In the form (3.11) the indices at $z = \pm 1$ are $\pm(m-k)/2$ and $\pm(m+k)/2$. This equation has an irregular singular point at infinity, which is obtained by the confluence of two regular singular points of the Heun equation. The Heun equation is the most general Fuchsian equation with 4 regular singular points. The Heun equation (after normalisation by Möbius transformations) has 6 parameters, 1 position of a pole, 4 indices, and the so called accessory parameter. The pole position is used for the confluence, after which only two regular singular points remain. Hence 2 indices remain as parameters (given by $\pm(m \pm k)/2$).

Two additional parameters describe the behaviour near the irregular singular point, and the accessory parameter remains, so that there is a total of 5 parameters.

To transform into the standard form of the confluent Heun equation, see, e.g., [DLMF], first shift to the standard poles by $z \to (z+1)/2$, and then scale the dependent variable with $\exp(2\sqrt{\tilde{c}_2})z^{|m+k|}(z-1)^{|m-k|}$.

When considering the confluent Heun equation, the usual reference to its application in physics is to Teukolsky's master equation [Teu73], which appears in the perturbation theory around a rotating black hole, i.e. the Kerr metric. However, that equation only has 4 parameters, and one index-parameter is more restricted because it represents the spin of a particle. In this context, eigenvalues λ of the equation have been computed using expansion in Jacobi polynomials in [FC77]. Their results are not applicable to our case because their equation only has 4 parameters. To compute the spectrum in our case we generalise the papers [Shi63], [HO91] which treat the case of a symmetric molecule (i.e. top) in an electric field, hence the Lagrange top (without the harmonic field). To extend their method, which is also an expansion in Jacobi polynomials (or rather the related Wigner D-functions), we need to compute the matrix elements of $\cos^2\theta$. This leads to our final result.

Theorem 3.4. *The spectrum of the harmonic Lagrange top* (3.10) *which is equivalent to the most general confluent Heun equation* (3.11) *can be computed from a penta-diagonal symmetric infinite matrix*

$$\hat{H} = \hat{H}_0 + c_1\hat{H}_1 + c_2\hat{H}_1^2\,. \tag{3.12}$$

For given fixed m, k the operator $\hat{H}_0$ is the diagonal representation of the Hamiltonian without potential and H_1 is the tri-diagonal representation of $\cos\theta$ in terms of Wigner-D basis functions.

Proof. The formulas for $\hat{H}_0$ and $\hat{H}_1$ are given in [Shi63]. We repeat them here for convenience. The diagonal entries of $\hat{H}_0$ are $\frac{\hbar^2}{2I_1}(j(j+1)+\delta k^2)$. The diagonal entries of $\hat{H}_1$ are $a_j = -km/(j(j+1))$ and the off-diagonal entries are $b_j = -\sqrt{(j^2-k^2)(j^2-m^2)/(j^2(4j^2-1))}$. The first entries in the matrix representing the operators have $j = \max(m,k)$. Note that for $m = k = 0$ the diverging terms in b_j cancel and b_0 is defined. It is easy to compute the matrix elements of $\cos^2\theta$. This can be done by noticing that $D_{2,0,0} = \frac{3}{2}\cos^2\theta - \frac{1}{2}$. The matrix representation of $D_{2,0,0}$ can be expressed in terms of Clebsch-Gordan coefficients. However, it is more efficient to use the fact that since $\hat{H}_1$ represents $\cos\theta$ the matrix $\hat{H}_1^2$ represents $\cos^2\theta$. So instead of computing matrix elements of $\cos^2\theta$ from scratch in terms of Clebsch-Gordan coefficients we can simply compute the square of the matrix representation of $\hat{H}_1$. In particular the entries in the 2nd off-diagonal are given by products $b_{j-1}b_j$.

■

The numerical convergence of these expressions is good, and the spectra displayed in Figure 2 were computed from these matrices truncated at twice the maximal needed

quantum number j. The value $j = \max(m, k)$ is called maximal since it is the largest such number for a given value of the basic Hamiltonian $(\hat{H}_0)$. The reason for taking twice this when truncating the infinite matrix is to achieve an optimal balance between performance and computational time. Even though the term δL_3^2 in the Hamiltonian is important for the classical dynamics, its effect on the quantum spectrum is rather trivial, it simply adds δk^2. It does change the spectrum, but the change is simple, and for this reason in the figures we restricted attention to $\delta = 0$, the spherical top. Moreover, from the point of view of the computation of the spectrum of the general confluent Heun equation the term δk^2 is irrelevant.

Why is there a correspondence between the harmonic Lagrange top and the confluent Heun equation? This question may not have a definite answer, but it is suggestive that the harmonic potential is the most general potential for which the classical dynamics can be linearised using the Jacobian of an elliptic curve. This fact appears to be related to the fact that the corresponding quantum system is described by the confluent Heun equation. After adding higher order terms to the potential, the system remains integrable and separable in the same way, but the classical dynamics will involve hyperelliptic curves, and the quantum system will be described by higher order confluent Fuchsian equations. It would be interesting to make this observation more precise.

Chapter 4

Quantum Integrable Systems arising from Separation of Variables on S^3

Abstract

We study the family of quantum integrable systems that arise from separating the Schrödinger equation in all 6 separable orthogonal coordinates on the 3−sphere: ellipsoidal, prolate, oblate, Lamé, spherical and cylindrical. On the one hand each separating coordinate system gives rise to a quantum integrable system on $S^2 \times S^2$, on the other hand it also leads to families of harmonic polynomials in $\mathbb{R}^4$. We show that separation in ellipsoidal coordinates yields a generalised Lamé equation - a Fuchsian ODE with 5 regular singular points. We seek polynomial solutions so that the eigenfunctions are analytic at all finite singularities. We classify eigenfunctions by their discrete symmetry and compute the joint spectrum for each symmetry class. The latter 5 separable coordinate systems are all degenerations of the ellipsoidal coordinates. We perform similar analyses on these systems and show how the ODEs degenerate in a fashion akin to their respective coordinates. For the prolate system we show that there exists a defect in the joint spectrum which prohibits a global assignment of quantum numbers: the system has quantum monodromy. This is a companion paper to [NDD23] where the respective classical systems were studied.

4.1. Introduction

The study of separation of variables yields a vast array of classical and quantum integrable systems that are ripe for exploration. Separation of variables originated with Jacobi and Stäckel [Stä93]. On the quantum side, seminal work was done in the early 20th century by Robertson [Rob27] who showed, for a given orthogonal coordinate system, that the Schrödinger equation is separable if both the classical Hamilton-Jacobi equation is separable and the Robertson condition is satisfied. Work done soon after by Eisenhart [Eis34] showed

that all systems that arise from separation of variables are Stäckel systems and so the corresponding classical integrals obtained will be quadratic in the momenta. Work by Kalnins and Miller in the late 20th century yielded a complete classification of all orthogonal separable coordinates on both $\mathbb{R}^n$ and S^n [KM86]. This work was further summarised in [KKM06], where connections to superintegrability were also drawn. Separation for systems with potential are also well studied. In [KKMP02] invariants for a system that admit separation of variables were constructed. Schöbel and Veselov gave a topology to the space of separable coordinates on the sphere [SV15, Sch16] and identified it with Stasheff polytopes. Previously, our motivation was to study the corresponding integrable systems, which inherit the same topology. In our paper [NDD23], we showed that the space of orthogonally separable coordinates on S^3 induces a family of classical integrable systems on $S^2 \times S^2$ after reduction. Here we seek to broaden this analysis to the space of quantum integrable systems, their corresponding separated ODEs and special functions. In particular, we study 5 families of Fuchsian equations: the generalised Lamé, Heun, Jacobi, Gegenbauer and Legendre differential equations. Similar to our previous work, we aim to understand how degenerations in the coordinate systems descend to the space of integrable systems, and correspondingly ODEs and special functions.

The general idea to start with a super-integrable system and exploit its multiseparability to define interesting Liouville integrable systems by reduction has been exploited in the case of the Kepler problem [DW18] and the harmonic oscillator [CDEW19]. This paper follows the same approach for the geodesic flow on the three dimensional sphere S^3. In this case the space of separable coordinate systems is a Stasheff polytope which is the pentagon shown in Fig. 4.1. This is the parameter space of the family of quantum integrable systems on $S^2 \times S^2$. While the previous examples (Kepler and Harmonic oscillator) also lead to reduced systems on compact symplectic manifolds and hence quantised systems on finite dimensional Hilbert spaces, starting with S^3 separation of variables in the Schrödinger equation leads to Fuchsian equations, while the presence of the potential in the earlier examples lead to confluent Fuchsian equations. Degeneration of parameters in the general separable coordinate system on S^3 to the so-called prolate case (the bottom edge of the pentagon in Fig. 4.1) then leads to a semi-toric family whose quantum mechanics is described by polynomial solutions of the Heun equation. The semi-toric systems on $S^2 \times S^2$ studied in [SZ99, LFP18, ADH19] do not appear to include the prolate system studied here, because the non-trivial integral is a homogeneous polynomial. In fact, all our Liouville integrable systems have integrals that are in general homogeneous quadratics in the momenta, and may degenerate into squares of linear functions of the momenta. Because of this all our integrable systems are related to spherical harmonics on S^3. The ellipsoidal reduced system is related to the Manakov top and has been studied classically and quantum mechanically in [SZ07b].

In our study of these quantum systems, we perform a variety of numerical computations to

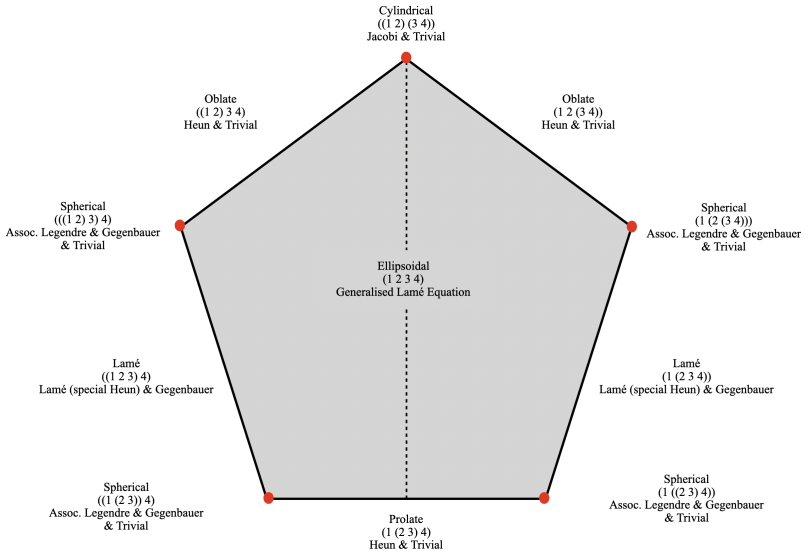

Figure 4.1: Stasheff polytope of orthogonal separable coordinates on S^3 with corresponding ODEs arising from separation.

find the joint spectrum. For all degenerate systems, a power series ansatz yields a three term recurrence relation. Given the necessary quantisation conditions, this recurrence terminates and yields a polynomial as an eigenfunction. The joint spectrum is then computed from the associated tri-diagonal matrix. The ellipsoidal coordinates on S^3 gives the more difficult generalised Lamé equation which has 5 regular singularities. Consequently, the aforementioned methodology falls short and we use the method of computing Heine-Stieltjes polynomials as described in [Ala79, ARZ85, Vol99]. It is interesting to note that for all systems on S^3, the joint spectrum is recovered from finite matrices, with corresponding polynomial eigenfunction. This contrasts with our previous work [DDN22, DDN21] where the spectrum is determined by infinite matrices and the eigenfunctions are given by infinite series. We note that work done by Harnard in [HW95a, HW95b] described obtaining generalised Lamé equations for spheres of arbitrary dimension and obtaining eigenfunctions using the Heine-Stieltjes ansatz.

Another motivation for this work is to suggest a natural family of integrable systems that contains the semi-toric case, but includes deformation to more typical quantum integrable systems. The classification of semi-toric systems is now fully understood classically [PVuN09] and quantum mechanically [LFVuN21]. This line of research was initiated by Duistermaat [Dui80] and the first example of quantum monodromy is due to Cushman and Duistermaat [CD88]. Monodromy, both classical and quantum, is caused by the existence of a non-degenerate focus-focus critical value in the classical system [VuN99]. Many important examples of integrable systems in physics do have monodromy, see, e.g. [CD88, SZ99, DDN21, DW18, DDN22]. In this paper, we obtain a semi-toric system through separation of the geodesic flow on S^3 in prolate coordinates. This system thus

arises as a degeneration of a more general 2 parameter family corresponding to the inside of the pentagon in Fig. 4.1.

The outline of this paper is as follows. In Section 4.2 we describe the ellipsoidal-spherical coordinates, the most general orthogonal separable coordinates on S^3. The ODEs that arise from separating the Schrödinger equation in these coordinates are known as the generalised Lamé equation. The joint spectrum is computed, along with the corresponding quantised actions and their symmetry classes. The first degenerate system is analysed in Section 4.3.1 with the prolate coordinates. Separation yields a semi-toric system whose monodromy matrix we compute. This contrasts with the oblate system in Section 4.3.2 which, while similar to prolate coordinates, does not possess monodromy and instead has hyperbolic singularities. Section 4.3.3 studies the Lamé coordinates (an extension of ellipsoidal coordinates on S^2 onto S^3) while Sections 4.3.4 and 4.3.5 focus on the spherical and cylindrical systems respectively. All these results are visualised by the Stasheff polytope in Fig. 4.1. In the appendix we recall some results on S^2 for the only two separable coordinates: ellipsoidal and spherical.

4.2. Ellipsoidal Coordinates and the Generalised Lamé Equation

Let $\boldsymbol{x} \coloneqq (x_1, x_2, x_3, x_4)$ be Cartesian coordinates on $\mathbb{R}^4$ and consider the unit sphere $S^3 \subset \mathbb{R}^4$ where $S^3 = \left\{(x_1, x_2, x_3, x_4) \in \mathbb{R}^4 \,|\, x_1^2 + x_2^2 + x_3^2 + x_4^2 = 1\right\}$. The geodesic flow on S^3 is a constrained system on $T^*\mathbb{R}^4$ with corresponding momentum $\boldsymbol{y} = (y_1, y_2, y_3, y_4)$ such that $\boldsymbol{x} \cdot \boldsymbol{x} = 1$ and $\boldsymbol{x} \cdot \boldsymbol{y} = 0$. Set

$$H = \frac{1}{2} \sum_{i>j} \ell_{ij}^2$$

to be the Hamiltonian of the geodesic flow where the angular momentum in the (i, j) plane is given by $\ell_{ij} \coloneqq x_i y_j - x_j y_i$ and the symplectic structure is $\sum_i dx_i \wedge dy_i$.

Let a homogeneous polynomial $\Psi_D(x_1, x_2, \ldots, x_n)$ of degree D be a solution to Laplace's equation in $\mathbb{R}^n$,

$$\Delta \Psi_D = \sum \partial_i^2 \Psi_D = 0\,.$$

By definition Ψ_D is called a *harmonic* polynomial. Introduce the radius $r = \sqrt{\sum x_i^2}$ and some local coordinates s on the sphere S^{n-1}. The Laplacian in such a coordinate system is

$$\Delta_{\mathbb{R}^n} = \frac{\partial^2}{\partial r^2} + \frac{n-1}{r} \frac{\partial}{\partial r} + \frac{1}{r^2} \Delta_{S^{n-1}}\,.$$

Now rewrite the harmonic polynomial as $\Psi_D(\boldsymbol{x}) = r^D \psi_D(s)$ and thus define the spherical

harmonic $\psi_D : S^{n-1} \to \mathbb{R}$. Inserting this into the above Laplacian gives

$$-\Delta_{S^{n-1}}\psi_D = D(D-2+n)\psi_D\,,$$

so we see that spherical harmonics are eigenfunctions of the Laplace-Beltrami operator on the sphere. For $n = 3$ on S^2 these are the usual spherical harmonics typically denoted by Y_{lm}, for the case of general n see, e.g., [ABR01]. The above Hamiltonian can be canonically quantised which leads to $\hat{\ell}_{ij} = -i\hbar(x_i\partial_j - x_j\partial_i)$. This again gives the Laplace-Beltrami operator on S^{n-1} and hence

$$2\hat{H}\Psi_D = D(D-2+n)\Psi_D\,.$$

In the following we will speak of both the spherical harmonic ψ_D in local coordinates s on the sphere S^{n-1}, and the corresponding harmonic polynomial Ψ_D in global Cartesian coordinates $\boldsymbol{x}$ on $\mathbb{R}^n$, as eigenfunctions of the Laplace-Beltrami operator. These considerations apply to any dimension n, but in the following we will consider $n = 4$ only.

Ellipsoidal-spherical (also known as sphero-conal or spherical ellipsoidal) coordinates $\boldsymbol{s} \coloneqq (s_1, s_2, s_3)$ on S^3 are defined as the roots of

$$T(s) = \sum_{i=1}^{4} \frac{x_i^2}{s - e_i}$$

where $0 \leq e_j \leq s_j \leq e_{j+1}$ for all $j = 1, 2, 3$ and the e_i are called the semi-major axes. This is by analogy with ellipsoidal coordinates on the tri-axial ellipsoid which are different and defined through $T(s) = 1$. We will only use ellipsoidal-spherical coordinates in the following and call them ellipsoidal for short since no confusion can arise. The transformation to ellipsoidal coordinates is found by solving $T(s_j) = 0$ where $j = 1, 2, 3$ together with $r^2 = \sum_{i=1}^{4} x_i^2 = 1$ to give

$$x_i^2 = \frac{\prod_{j=1}^{3}(s_j - e_i)}{\prod_{k\neq i}(e_k - e_i)}. \tag{4.1}$$

From [NDD23] we have the following result.

Lemma 11. *The Hamiltonian H for the geodesic flow on S^3 separates in ellipsoidal coordinates (4.1) to give integrals*

$$\eta_1 = \sum_{i<j}\left(\ell_{ij}^2 \sum_{k\neq i,j} e_k\right), \qquad \eta_2 = \sum_{i<j}\left(\ell_{ij}^2 \prod_{k\neq i,j} e_k\right). \tag{4.2}$$

The triple (H, η_2, η_2) is a Liouville integrable system on T^*S^3.

Consider the following linear coordinate transformation

$$\begin{aligned} X_1 &= \frac{1}{\sqrt{2}}(\ell_{12}+\ell_{34}) & Y_1 &= \frac{1}{\sqrt{2}}(\ell_{12}-\ell_{34}) \\ X_2 &= \frac{1}{\sqrt{2}}(\ell_{13}-\ell_{24}) & Y_2 &= -\frac{1}{\sqrt{2}}(\ell_{13}+\ell_{24}) \\ X_3 &= \frac{1}{\sqrt{2}}(\ell_{14}+\ell_{23}) & Y_3 &= \frac{1}{\sqrt{2}}(\ell_{14}-\ell_{23}). \end{aligned}$$

Since $\sqrt{H}$ generates an S^1 flow with constant period, we are able to reduce by the flow of $\sqrt{H}$ to $S^2 \times S^2$ with local coordinates $(\boldsymbol{X}, \boldsymbol{Y}) = (X_1, X_2, X_3, Y_1, Y_2, Y_3)$ and Casimirs $\boldsymbol{X} \cdot \boldsymbol{X} = \boldsymbol{Y} \cdot \boldsymbol{Y} = 1$. Again, from [NDD23] we have the following result.

Lemma 12. *The original integrable system (H, η_1, η_2) on T^*S^3 descends to a two degree of freedom integrable system $(\eta_1(\boldsymbol{X}, \boldsymbol{Y}), \eta_2(\boldsymbol{X}, \boldsymbol{Y}))$ on $S^2 \times S^2$ with Poisson structure*

$$B_{\boldsymbol{X},\boldsymbol{Y}} = \begin{pmatrix} \hat{\boldsymbol{X}} & \boldsymbol{0} \\ \boldsymbol{0} & \hat{\boldsymbol{Y}} \end{pmatrix} \tag{4.3}$$

where, for a vector $\boldsymbol{v} \in \mathbb{R}^3$, the corresponding antisymmetric hat matrix $\hat{\boldsymbol{v}}$ is given by

$$\hat{\boldsymbol{v}}\boldsymbol{u} = \boldsymbol{v} \times \boldsymbol{u}, \qquad \forall \boldsymbol{u} \in \mathbb{R}^3. \tag{4.4}$$

When written in terms of $\boldsymbol{X}$ and $\boldsymbol{Y}$ on $S^2 \times S^2$ the system can be quantised through Berezin-Toeplitz quantisation in the same way it was done in [LFP18, LF23]. The quantisation is the same, but the operators are different. In their case the global S^1 integral is linear and the commuting second integral has linear and quadratic terms, while the integrals η_1, η_2 are both homogeneous quadratic. In later chapters on degenerate coordinate systems (e.g. the prolate case) linear integrals will also appear, in particular the global S^1 actions are linear in $\boldsymbol{X}, \boldsymbol{Y}$. We will not use Berezin-Toeplitz quantisation, but instead employ separation of variables, so that the connection to spherical harmonics and special functions remains.

Quantising through separation of variables reduces the quantisation problem to the problem of finding polynomial solutions of a single 2nd order Fuchsian ODE. It would be interesting to study in detail the relationship between the two approaches. The one thing that we do use from the Berezin-Toeplitz approach is the fact that $\hbar$ is the inverse of an integer. This also appears naturally through the separation of variables, but would be harder to justify without reference to the Berezin-Toeplitz approach, because separation of variables does not clearly execute the reduction to a system with compact phase space.

To construct a quantised version of the Hamiltonian we derive the diagonal metric tensor g in ellipsoidal coordinates on the $3-$sphere given by (4.1). This is an orthogonal coordinate

systems, so the off-diagonal entries of the metric vanish. The diagonal entries of the metric are

$$g_{jj} = \frac{-(s_j - s_k)(s_j - s_m)}{4(s_j - e_1)(s_j - e_2)(s_j - e_3)(s_j - e_4)}$$

where k and m are the two unique distinct indices different from j. Denote the determinant of the metric by $g = \prod g_{jj}$. The inverse metric with upper indices has entries $g^{jj} = 1/g_{jj}$. Thus the Laplace-Beltrami operator on S^3 in these coordinates is given by

$$\Delta = -\frac{1}{\sqrt{g}} \sum \partial_i (\sqrt{g}\, g^{jj} \partial_i) \,.$$

When quantising with the semi-classical parameter $\hbar$ the corresponding stationary Schrödinger equation is given by

$$-\hbar^2 \Delta \psi = \tilde{E} \psi \,. \tag{4.5}$$

As already remarked, it is possible to quantise in the original Euclidean coordinates and replace ℓ_{ij} with $x_i \partial_j - x_j \partial i$, see [Gur95, Tot94]. We need separation of variables, however, and hence obtain commuting operators via the Stäckel matrix of the system. The classical commuting integrals (4.2) are obtained from separation of variables in the Hamilton-Jacobi equation. The same separation works for the Schrödinger equation because the sphere has constant curvature, and hence the Robertson condition is satisfied, see, e.g. [KKM18].

The reduction to a two degree of freedom integrable system is achieved on the quantum level by fixing the eigenvalue of the Laplace-Beltrami operator, which for S^3 is $E = D(D+2)$ for non-negative integer D.

Theorem 4.1. *There are three commuting 2nd order differential operators $(\hat{H}, \hat{\eta}_1, \hat{\eta}_2)$ on S^3 with rational coefficients, whose classical limit are the integrals (H, η_1, η_2) given in (4.2).*

Proof. A Stäckel matrix for ellipsoidal coordinates is given by

$$\sigma_{\text{el}} = \frac{1}{4} \begin{pmatrix} -\frac{s_1^2}{A(s_1)} & -\frac{s_1}{A(s_1)} & -\frac{1}{A(s_1)} \\ -\frac{s_2^2}{A(s_2)} & -\frac{s_2}{A(s_2)} & -\frac{1}{A(s_2)} \\ -\frac{s_3^2}{A(s_3)} & -\frac{s_3}{A(s_3)} & -\frac{1}{A(s_3)} \end{pmatrix} . \tag{4.6}$$

where $A(z) = \prod_{k=1}^{4} (z - e_k)$. Note that the metric and Stäckel matrix (4.6) are related by

$$\frac{1}{g_{jj}} = \frac{\det(\Omega_j)}{\det(\sigma_{\text{el}})}$$

where Ω_j is the minor formed by deleting the j^{th} row and first column of σ_{el}.

Denote the rows of the inverse of the Stäckel matrix by r^1, r^2, r^3. By definition of the Stäckel matrix the first row contains the diagonal entries of the metric $g^{jj} = r^{1j}$ with upper indices.

Then the commuting operators are

$$\hat{\eta}_{k-1} = -\frac{1}{\sqrt{g}} \sum_i \partial_i (\sqrt{g}\, r^{ki} \partial_i), \quad k = 1, 2, 3.$$

where $\hat{H} = \hat{\eta}_0$ corresponding to the first row of the inverse of the Stäckel matrix is the Laplace-Beltrami operator. The corresponding classical integrals are $\eta_{k-1} = \sum r^{ki} p_i^2$ as defined in (4.2) in Cartesian coordinates. Here p_i are the canonical curvilinear momenta conjugate to the coordinates s_i. We denote the eigenvalues of $(\hat{H}, \hat{\eta}_1, \hat{\eta}_2)$ by $(E, \lambda_1, \lambda_2)$.

■

The system of ellipsoidal coordinates on the sphere is used in the separation of the quantised C. Neumann system, see e.g. [Gur95, Gur08] and also [BT06b, BT05, BT06a]. Our system before reduction is the Neumann system without potential, and hence formulas in [Gur95] can be specialised to our case. The reduction step (or fixing the eigenvalue of the Schrödinger operator) does not make sense for the Neumann system, because unlike the geodesic flow on S^3 it is not a superintegrable system.

It is also possible to obtain the operators $\hat{\eta}_i$ by canonical quantisation of the angular momentum operators expressed in ellipsoidal coordinates using

$$\ell_{ij} = 2x_i(s)x_j(s)(e_i - e_j) \sum_{k=1}^{3} c_{ij}(s_k) p_k, \quad c_{ij}(s_k) = \frac{\prod_{n \neq i,j}(s_k - e_n)}{\prod_{m \neq k}(s_k - s_m)}$$

where $x_i(s)$ as given in (4.1). This equation is linear in momenta and can be quantised by replacing $p_k \to -i\hbar\partial_{s_k}$. In this way the classical commuting integrals expressed in terms of ℓ_{ij} can be directly converted into the corresponding quantum operators. However, the calculation using the Stäckel matrix is much simpler.

The inverse of the Stäckel matrix is used to define the commuting operators, while the Stäckel matrix itself determines how the spectral parameters enter the separated equation(s), which is the content of

Lemma 13. *In ellipsoidal coordinates (4.1) on S^3, the Schrödinger equation (4.5) separates into*

$$\psi_j'' + \frac{1}{2}\left(\frac{1}{s_j - e_1} + \frac{1}{s_j - e_2} + \frac{1}{s_j - e_3} + \frac{1}{s_j - e_4}\right)\psi_j' + \frac{-Es_j^2 + \lambda_1 s_j - \lambda_2}{4(s_j - e_1)(s_j - e_2)(s_j - e_3)(s_j - e_4)}\psi_j = 0 \tag{4.7}$$

for all $j = 1, 2, 3$ with $E := \frac{\tilde{E}}{\hbar^2}$, λ_1 and λ_2 are spectral parameters and $\psi = \psi_1\psi_2\psi_3$ where $\psi_j = \psi(s_j)$.

Proof. Let

$$f_j := \frac{\partial}{\partial s_j} \log(g^{jj}\sqrt{\det(g)}).$$

Following [Gur95] the equation (4.5) separates into

$$\psi_j'' + f_j\psi_j' + \sum_{k=1}^{3} c_{k-1}(\sigma_{\text{el}})_{jk}\psi_j = 0$$

where $(c_0, c_1, c_2) = (-E, \lambda_1, -\lambda_2)$ are spectral parameters. Computing the relevant quantities gives (4.7).

■

Equation (4.7) is known as the generalised Lamé equation. This is a second order Fuchsian equation with 4 finite regular singular points which can be writen as

$$\frac{d^2w}{dz^2} + \left(\sum_{j=1}^{4} \frac{\gamma_j}{z - e_j}\right)\frac{dw}{dz} + \left(\sum_{j=1}^{4} \frac{q_j}{z - e_j}\right) w = 0 \tag{4.8}$$

where $\sum_{j=1}^{4} q_j = 0$ and the q_j are known as the accessory parameters. Often, we write the multiplicative term of (4.8) over a common denominator, i.e.

$$\sum_{j=1}^{4} \frac{q_j}{z - e_j} = \frac{c_0 z^2 + c_1 z + c_2}{4\Pi_{j=1}^{4}(z - e_j)}. \tag{4.9}$$

The exponents at the pole e_j are $(0, 1-\gamma_j)$ while those at infinity are (α, β) defined by

$$\alpha + \beta + 1 = \sum_{j=1}^{4} \gamma_j, \quad \alpha\beta = \sum_{j=1}^{4} e_j q_j. \tag{4.10}$$

From (4.10) it is clear that there are two free (so-called) accessory parameters, while the more well known Lamé equation only has one, see [DLMF] 31.14 for more detail. These two free parameters turn out to be the spectral parameters, i.e. the eigenvalues of $\hat{\eta}_1$ and $\hat{\eta}_2$. For some other examples of occurrences of the generalised Lamé equation, see [Paw07, MRSD06, CKL19] and the references therein.

In this paper, we seek polynomial solutions of (4.5) giving harmonic polynomials on S^3 in Cartesian coordinates. Ellipsoidal coordinates are singular along co-dimension one submanifolds of S^3, and these coordinate singularities translate to the singularities of the Fuchsian ODE (4.8). Solutions to the separated equations that are analytic at all finite singularities correspond to polynomial solutions in the local coordinates s_i, possibly after

factoring out single powers of $x_k(s)$ to achieve all possible discrete symmetries in the original coordinates. Thus polynomial solutions of the Fuchsian ODEs in local coordinates lead to polynomial solutions in the original cartesian coordinates. The quantisation conditions at the level of the Fuchsian equation *are* the conditions that enforce a polynomial separated eigenfunction $\psi(s)$. In general these are conditions for each factor $\psi_j(s_j)$ of the separated eigenfunction $\psi(s) = \prod \psi_j(s_j)$, but it turns out that in the present highly symmetric case the three equations are the same equation, just evaluated on different intervals $e_j \leq s_j \leq e_{j+1}$, and hence a single polynomial gives three $\psi_j(s_j)$ and hence the complete eigenfunction $\psi(s)$. In cases of more degenerate coordinate systems discussed in the next section there will actually be different equations for the different coordinates.

It is known from 31.15 of [DLMF] and [Vol99] that for every vector $\boldsymbol{n} = (n_1, n_2, n_3)$ of non negative integers, there are uniquely determined real values of (c_0, c_1, c_2) such that (4.8) has polynomial solutions with n_j zeros in the interval (e_j, e_{j+1}) for all $j = 1, 2, 3$. Such solutions $S_d(z)$ of degree d where $d = n_1 + n_2 + n_3$ are known as Heine-Stieltjes polynomials.

From [Vol99] we have the following Lemma for the spectral parameter c_0.

Lemma 14. *Let $S_d(z)$ be a Heine-Stieltjes polynomial solution to (4.8) of degree d over the interval $[e_1, e_4]$. Then*

$$\frac{1}{4}c_0 = -d(d-1+\sum_{i=1}^{4}\gamma_i) = \alpha\beta \tag{4.11}$$

and $(\alpha, \beta) = (-d, (-1+d+\sum \gamma_i))$. Further, let $K(d)$ be the space of all such polynomials that satisfy (4.8). Then, we have

$$dim(K(d)) \coloneqq \binom{d+2}{2}. \tag{4.12}$$

Note that α is a negative integer in order to obtain polynomial solutions. We also have from [Vol99] the following Lemma relating polynomial solutions of the Schrödinger equation in Cartesian coordinates to products of Heine-Stieltjes polynomials.

Proposition 15. *The product $S_d(s_1)S_d(s_2)S_d(s_3)$, where $S_d(s)$ is a Heine-Stieltjes polynomial solution to (4.7) of degree d, when expressed in the original Cartesian coordinates using (4.1), is a homogeneous polynomial of degree $\tilde{D} \coloneqq 2d$ in the variables x_i given by*

$$\Phi_{\tilde{D}}(\boldsymbol{x}) \coloneqq \left(\prod_{i=1}^{4}\prod_{k=1}^{d}(z_k - e_i)\right)\prod_{k=1}^{d}\sum_{i=1}^{4}\frac{x_i^2}{z_k - e_i}, \tag{4.13}$$

where z_k are the roots of $S_d(z)$.

In Cartesian coordinates there are 16 discrete symmetry classes of eigenfunctions corres-

ponding to parity about each of the x_i axes. Let $\boldsymbol{\mu} = (\mu_1, \mu_2, \mu_3, \mu_4)$ with $\mu_i \in \{0, 1\}$ where $\mu_i = 1$ denotes a wavefunction odd about the respective axis and even otherwise. By (4.13) the wave function $\Phi_{\tilde{D}}(\boldsymbol{x})$ is quadratic in all x_i, and hence cannot give any odd symmetry. In order to find these other symmetries, consider the change of dependent variable in (4.7) given by

$$\phi_j = \prod_i (s_j - e_i)^{\mu_i/2} \psi_j. \tag{4.14}$$

This corresponds to multiplication by $x_1^{\mu_1} x_2^{\mu_2} x_3^{\mu_3} x_4^{\mu_4}$ in Cartesian coordinates. This yields the transformed generalised Lamé equation

$$\phi_j'' + \left(\frac{\tilde{\gamma}_1}{z - e_1} + \frac{\tilde{\gamma}_2}{z - e_2} + \frac{\tilde{\gamma}_3}{z - e_3} + \frac{\tilde{\gamma}_4}{z - e_4} \right) \phi_j' + \frac{(u_0 - E)z^2 + (u_1 + \lambda_1)z + (u_2 - \lambda_2)}{4(z - e_1)(z - e_2)(z - e_3)(z - e_4)} \phi_j = 0 \tag{4.15}$$

where

$$\tilde{\gamma}_m = \begin{cases} \frac{3}{2} & \text{if } \mu_m = 1 \\ \frac{1}{2} & \text{if } \mu_m = 0 \end{cases} \tag{4.16}$$

and the u_j are shown in Table 4.1 for a given symmetry class $\boldsymbol{\mu}$. Note that in the table we adopted the notation where (μ_i) represents symmetry classes where only one μ_i is 1 (i.e. $(1, 0, 0, 0), (0, 1, 0, 0)$ etc). Similarly, (μ_i, μ_j) represents all classes which are odd about two axes and so forth for (μ_i, μ_j, μ_k).

Denote by $S_d^{\boldsymbol{\mu}}(z)$ solutions to (4.15) for the symmetry class $\boldsymbol{\mu}$. Repeating the same reasoning used to obtain (4.13), we let the product $S_d^{\boldsymbol{\mu}}(s_1) S_d^{\boldsymbol{\mu}}(s_2) S_d^{\boldsymbol{\mu}}(s_3)$, when converted to Cartesian coordinates, be given by $\Phi_{\tilde{D}}^{\boldsymbol{\mu}}(\boldsymbol{x})$. Finally, we set

$$\Psi_D^{\boldsymbol{\mu}}(\boldsymbol{x}) \coloneqq x_1^{\mu_1} x_2^{\mu_2} x_3^{\mu_3} x_4^{\mu_4} \Phi_{\tilde{D}}^{\boldsymbol{\mu}}(\boldsymbol{x}) \tag{4.17}$$

where $D = \tilde{D} + \sum_{i=1}^4 \mu_i$. Note that $\Phi_{\tilde{D}}(\boldsymbol{x})$ in (4.13) is the special case of (4.17) with $\boldsymbol{\mu} = (0, 0, 0, 0)$.

Symmetry	u_2	u_1	u_0
$(0, 0, 0, 0)$	0	0	0
(μ_i)	$e_j e_k + e_j e_m + e_k e_m$	$-2(e_j + e_k + e_m)$	3
(μ_i, μ_j)	$e_i e_k + e_i e_m + e_j e_k + e_j e_m + 4 e_k e_m$	$-2(e_i + e_j) - 6(e_k + e_m)$	8
(μ_i, μ_j, μ_k)	$e_i e_j + e_i e_k + e_j e_k + 4(e_i e_m + e_j e_m + e_k e_m)$	$-6(e_i + e_j + e_k + 2e_m)$	15
$(1, 1, 1, 1)$	$4(e_1 e_2 + e_1 e_3 + e_2 e_3 + e_1 e_4 + e_2 e_4 + e_3 e_4)$	$-12(e_1 + e_2 + e_3 + e_4)$	24

Table 4.1: Coefficients u_j in (4.15) for each symmetry class.

Theorem 4.2. *The function $\Psi_D^{\boldsymbol{\mu}}(\boldsymbol{x})$ given by (4.17) is an eigenfunction of the Schrödinger operator*

(4.5). *The energy eigenvalue E is given by*

$$E = D(D+2) \tag{4.18}$$

where $D = 2d + \sum_{i=1}^{4} \mu_i$ is the degree of the harmonic polynomial Ψ_D.

Proof. We have

$$\Delta(\Psi_D^{\boldsymbol{\mu}}(\boldsymbol{x})) = \Delta(\Phi_{\tilde{D}}^{\boldsymbol{\mu}}(\boldsymbol{x})) + \sum_{j=1}^{4} \frac{2\mu_j}{x_j} \frac{\Phi_{\tilde{D}}^{\boldsymbol{\mu}}(\boldsymbol{x})}{\partial x_j}. \tag{4.19}$$

From [Vol99], we know that since $\Phi_{\tilde{D}}^{\boldsymbol{\mu}}(\boldsymbol{x})$ satisfy (4.15) for the appropriate parameter choices in Table 4.1, they also satisfy the right hand side of (4.19). Hence, $\Psi_D^{\boldsymbol{\mu}}(\boldsymbol{x})$ are solutions of (4.5). To compute the energy for a given symmetry class $\boldsymbol{\mu}$, we note that the shift u_2 in Table 4.1 is simply $U(U+2)$ where $U = \sum_{i=1}^{4} \mu_i$. Combining this with (4.11) and using $E = -c_0$ gives

$$E = U(U+2) + 4d(d+1+U) \tag{4.20}$$

which simplifies to $E = D(D+2)$ for each class.

■

For more discussion on the representation theory of the above, including the irreducible representations of $SO(4)$, see the works of Harnard [HW95b, HW95a] and Gurarie [Gur95].

From (4.17) we observe the following

Proposition 16. *For polynomial solutions to (4.5) of fixed degree D corresponding to energy $E = D(D+2)$, only 8 of the 16 total discrete symmetry classes can be present. If E is even, then the $(0,0,0,0)$, $(1,1,1,1)$ and all symmetry classes even about 2 of the x_i axes are present. Similarly, if E is odd, then the remaining 8 symmetry classes odd about and odd number of x_i are present.*

We refer to solutions which are even about an even (odd) number of axes (with even (odd) energies) as "even" ("odd") solutions. In particular, the even symmetry classes are

$$\mathcal{S}_E = \{(0,0,0,0), (1,1,0,0), (1,0,1,0), (1,0,0,1), (0,1,1,0), (0,1,0,1), (0,0,1,1), (1,1,1,1)\} \tag{4.21}$$

and the odd symmetry classes are

$$\mathcal{S}_O = \{(0,0,0,1), (0,0,1,0), (0,1,0,0), (1,0,0,0), (1,1,1,0), (1,1,0,1), (1,0,1,1), (0,1,1,1)\}. \tag{4.22}$$

Using the above results, we also have the following Lemma, which shows that all eigenfunctions are obtained in this way.

Lemma 17. *The total number of eigenstates N for a polynomial solution to (4.5) of degree D is given by*

$$N = (D+1)^2 \tag{4.23}$$

Proof. Without loss of generality, we prove this for D even (i.e. "even" solutions). From (4.12), we know that the total number of eigenstates for the $(0,0,0,0)$ symmetry class is $\binom{d+2}{2} = \binom{\frac{D+4}{2}}{2}$. For a fixed D, we similarly have the total number of states for an element of the (μ_i, μ_j) class as $\binom{\frac{D+2}{2}}{2}$ and for the $(1,1,1,1)$ class we obtain $\binom{\frac{D}{2}}{2}$. The result follows since

$$N = \binom{\frac{D+4}{2}}{2} + 6\binom{\frac{D+2}{2}}{2} + \binom{\frac{D}{2}}{2} = (D+1)^2.$$

In Table 4.2 we show the number of eigenstates per symmetry class and energy parity.

■

Symmetry	Number of States	Energy Parity
$(0,0,0,0)$	$\binom{(D+4)/2}{2}$	Even
(μ_i)	$\binom{(D+3)/2}{2}$	Odd
(μ_i, μ_j)	$\binom{(D+2)/2}{2}$	Even
(μ_i, μ_j, μ_k)	$\binom{(D+1)/2}{2}$	Odd
$(1,1,1,1)$	$\binom{D/2}{2}$	Even

Table 4.2: Number of states for each symmetry class and energy parity.

Recall that the basis of our study is separation of variables on the 3−sphere. It is no surprise then that the total energy (4.18) and number of eigenstates (4.23) precisely coincide with standard results for spherical harmonics on the sphere, see, e.g. [ABR01]. To compute the joint spectrum of (λ_1, λ_2) in (4.7) for all 16 discrete symmetry classes, we employ the following Lemma from [ARZ85].

Lemma 18. *Let S_d be a Heine-Stieltjes polynomial of degree d and denote its (real) roots by $z_1, \ldots, z_d$. If, in (4.8), the $\gamma_j > 0$ and $e_j \in \mathbb{R}$ with $e_j < e_{j+1}$ for all j, then every root is a*

solution to the system of equations

$$\sum_{j=1}^{4} \frac{\gamma_j/2}{z_k - e_j} + \sum_{j=1, j\neq k}^{d} \frac{1}{z_k - z_j} = 0, \quad k = 1, \ldots, d\,. \tag{4.24}$$

For each solution $z_1, \ldots, z_d$ the accessory parameters q_j are given by

$$q_j = \gamma_j \sum_{k=1}^{d} \frac{1}{z_k - e_j}, \quad j = 1, 2, 3, 4\,,$$

and in terms of these the spectral parameters (λ_1, λ_2) are

$$\lambda_1 = -4 \sum e_i e_j (q_k + q_m) \tag{4.25a}$$

$$\lambda_2 = 4 \sum e_i e_j e_k q_m \tag{4.25b}$$

where the sums are over all i, j, k, m that are pairwise distinct.

This well known Lemma is surprising in the sense that the system of equations (4.24) determines the eigenfunction S_d and joint spectrum (λ_1, λ_2) simultaneously. Comparing (4.25a), (4.25b) and the classical equation (4.2), the degrees in e_j are different. The reason for this is that q_j for fixed energy is of degree -1 in e_j, as can be seen from (4.11). Note that the solution to the nonlinear equations (4.24) is such that automatically $\sum q_i = 0$ and $\sum q_i e_i = \alpha\beta = -d(d - 1 + \sum \gamma_i)$, combining (4.11) and (4.10).

We can use the value of $\hbar$ to scale the energy eigenvalue to 1 in the semiclassical limit $\hbar \to 0$, and similar scalings for the other eigenvalues. After the scaling, changing $\hbar$ changes the number of states, but not the size of the image of the momentum map. Recall the definition of $E = \frac{\tilde{E}}{\hbar^2}$ and the discrete values of $E = D(D + 2)$ given in (4.18). To scale such that $\tilde{E}$ is exactly 1 would require $\hbar = 1/\sqrt{D(D + 2)}$, which is, however, not an integer. The reduced symplectic manifold is $S^2 \times S^2$ and hence compact, and therefore we require $\hbar$ to be the inverse of an integer. Thus

$$\hbar = \frac{1}{\sqrt{D(D + 2) + 1}} = \frac{1}{D + 1} \tag{4.26}$$

so that $1/\hbar^2$ is exactly the number of states in the reduced compact system. With this definition of $\hbar$ we find

$$\tilde{E} = E\hbar^2 = \frac{D(D + 2)}{(D + 1)^2} = 1 - \hbar^2$$

where the last equality is exact.

Using (4.24) with the 16 forms of the generalised Lamé equation, we produce examples of the joint spectrum shown in Fig. 4.2 with $D = 18$ (a) and $D = 19$ (b). We also show that the

boundary of the joint spectrum is given by the classical momentum map (solid black lines). For their derivation, see [NDD23].

In our numerics, we seed roots z_k randomly in the appropriate intervals (e_j, e_{j+1}) as outlined in [Vol99]. Standard root finding techniques like Newton's method are then used to find accurate solutions to (4.24). Larger values of D result in substantially longer computation time.

Since we have the freedom to choose the quadratic integrals via an affine transformation, we can give a clearer representation of the spectrum, as shown in Fig. 4.3 a) and b) with the hyperbolic-hyperbolic point centred at the origin. This clearly shows three regions with a $\mathbb{Z}^2$ lattice.

Note that lattice points in these regions are actually two points, representing period doubling. Classically, this corresponds to two tori in the pre-image of the classical momentum map. Moving from these chambers into the fourth (bounded by the curve), we see a halving of visible dots as we see period doubling occurring again. This phenomena has been described in more detail in [SZ07b].

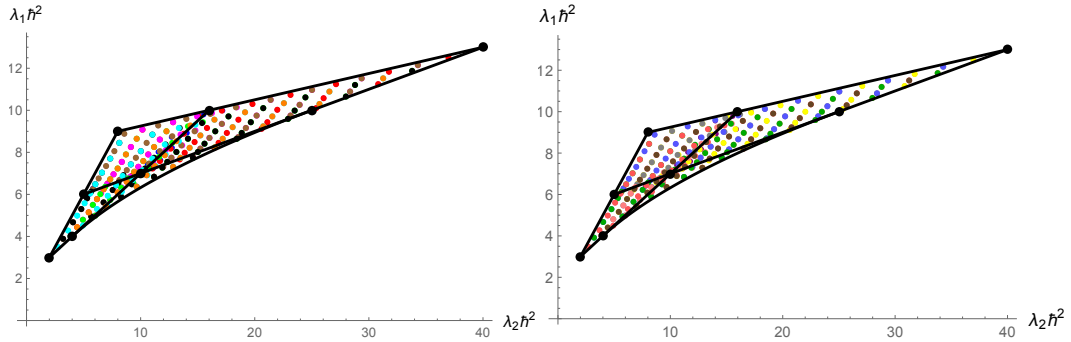

Figure 4.2: a) Joint spectrum (λ_1, λ_2) where $(e_1, e_2, e_3, e_4) = (1, 2, 5, 8)$ with $D = 18$ and b) $D = 19$. A direct correspondence between the coloured dots and symmetry classes is shown in Table 4.3.

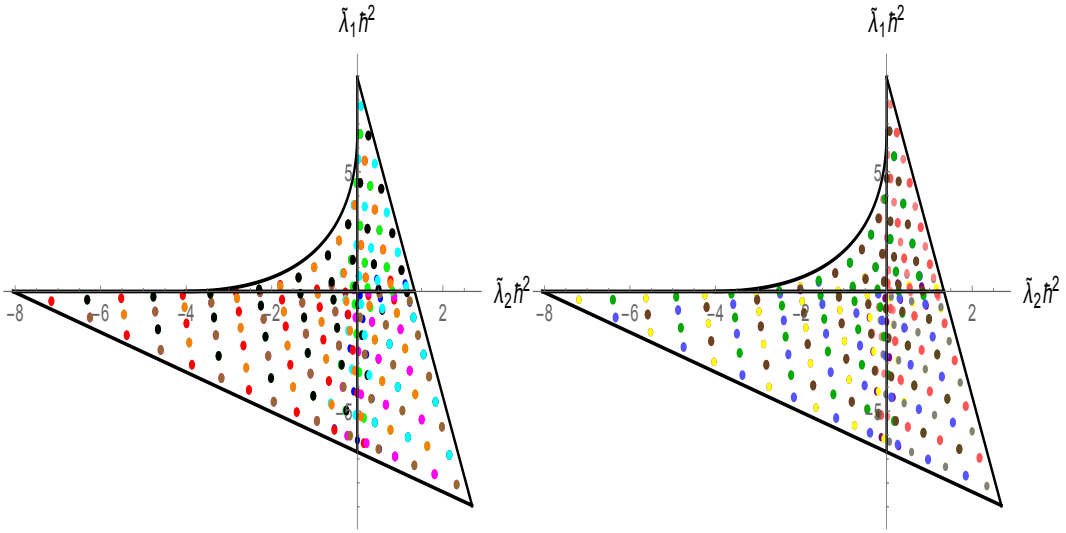

Figure 4.3: Spectra corresponding to Fig. 4.2 a) and b) after performing an affine transformation to map the hyperbolic-hyperbolic point to the origin.

$\boldsymbol{\mu}$	Colour a)	$\boldsymbol{\mu}$	Colour b)
$(0,0,0,0)$	Blue	$(1,0,0,0)$	Purple
$(1,1,0,0)$	Red	$(0,1,0,0)$	Yellow
$(1,0,1,0)$	Magenta	$(0,0,1,0)$	Grey
$(1,0,0,1)$	Green	$(0,0,0,1)$	Pink
$(0,1,1,0)$	Brown	$(1,1,1,0)$	Light Blue
$(0,1,0,1)$	Black	$(1,1,0,1)$	Dark Green
$(0,0,1,1)$	Cyan	$(0,1,1,1)$	Light Red
$(1,1,1,1)$	Orange	$(1,0,1,1)$	Dark Brown

Table 4.3: Symmetry class corresponding to each coloured eigenstate shown in Figure 4.2.

Equipped with the joint spectrum (λ_1, λ_2), we can investigate the corresponding action variables. Using the Stäckel matrix (4.6) and the results of [Gur95] and [NDD23], we have the following Lemma.

Lemma 19. *The three continuous, classical actions (J_1, J_2, J_3) are given by*

$$J_1 = \frac{1}{\pi}\int_{e_1}^{\min(R_1,e_2)} p(z)dz \quad J_2 = \frac{1}{\pi}\int_{\max(R_1,e_2)}^{\min(R_2,e_3)} p(z)dz \quad J_3 = \frac{1}{\pi}\int_{\max(R_2,e_3)}^{e_4} p(z)dz \tag{4.27}$$

where the momentum $p(z)$ is given by

$$p^2 = \frac{-\tilde{E}z^2 + \lambda_1 z - \lambda_2}{4(z-e_1)(z-e_2)(z-e_3)(z-e_4)},$$

and R_1, R_2 denote the roots of p^2 with $0 \leq R_1 \leq R_2$.

It was shown in [NDD23] that the 3 actions are linearly dependent, continuous and satisfy

the following Lemma.

Lemma 20. *The actions are constrained by the following relation*

$$J_1 + J_2 + J_3 = \sqrt{\tilde{E}}. \tag{4.28}$$

The fact that H can be written as a function of the sum of the actions in (4.28) follows from the fact that H is superintegrable. In Fig. 4.4 a) and b) we show the actions of the even and odd spectra in Fig. 4.2 a) and b) respectively, computed using (4.27) with $\tilde{E} = 1$. Similar plots for each symmetry class can be found in Appendix A.3.

The classical action variables even though continuous are complicated functions, and defining corresponding quantum mechanical operators may be difficult. Thus presenting the joint spectrum in the space of action variables is not done by quantising these functions. Instead we take the eigenvalues of the operators $(\hat{H}, \hat{\eta}_1, \hat{\eta}_2)$ and map them to (J_1, J_2, J_3) with the previous Lemma. In this way a striking representation of the joint spectrum inside an equilateral triangle is obtained. Is shown in [NDD23] this triangle is rigid even when passing to degenerate coordinates systems. Note that this triangle is not Delzant (our system is not toric to begin with), but it seems to serve a similar role for our class of quantum integrable systems. Near each corner of the triangle the lattice is approximately $\mathbb{N}^2$ with basis vectors given by the sides of the triangle. The action triangle is a natural global representation because there are three elliptic-elliptic equilibrium points in the reduced system, so that it represents three different $\mathbb{Z}^2$ lattices in one moment map.

Among the degenerate systems discussed in the next section the cylindrical coordinate system does lead to a toric system on $S^2 \times S^2$ with a square as Delzant polytope. The triangle appears as the quotient of the square by discrete symmetry group $\mathbb{Z}^2 \times \mathbb{Z}^2$ acting by reflection across the diagonals of the square, see below.

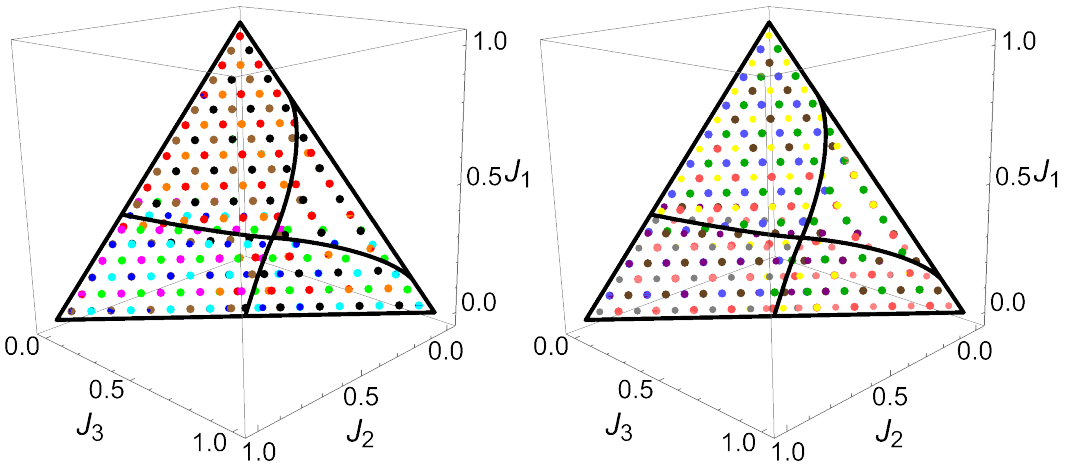

Figure 4.4: Joint spectrum in action variables in the ellipsoidal case corresponding to the joint spectra shown in Fig 4.2 a) and b) respectively.

4.3. Degenerate Systems

We now study the degenerate systems arising from the generalised ellipsoidal coordinates (1234). We originally focus on the prolate, oblate and Lamé coordinates; these correspond to the edges of the Stasheff polytope shown in Fig. 4.1. Further degenerations of these yield the spherical and cylindrical coordinates, represented by the corners of the polytope.

We will show that the separated ODEs for these coordinates can be obtained by smoothly degenerating those of the generalised ellipsoidal coordinates (i.e. the generalised Lamé equation). In doing this, we prove the following theorem which is the quantum analogue of Theorem 3 of [NDD23]:

Theorem 4.3. *For each pair of parentheses in the labelled Stasheff polytope (see Fig. 4.1) that enclose two adjacent numbers, the corresponding quantum integrable system has an $SO(2)$ symmetry and a corresponding ODE that can be transformed to a trivial ODE with trigonometric solutions.*

For each pair of parentheses that enclose three adjacent numbers, the corresponding quantum integrable system has a global $SO(3)$ symmetry and a corresponding ODE that can be transformed to the Gegenbauer equation (hypergeometric type). This applies also when there is a pair of parentheses inside.

If there are two pairs of parentheses (corresponding to the edges of the Stasheff polytope) then one ODE is of Heun type (Fuchsian with 4 regular singular points).

If there are three pairs of parentheses (corresponding to the corners of the Stasheff polytope) then one ODE is of hypergeometric type (Fuchsian with 3 regular singular points). For spherical coordinates

this can be transformed to the associated Legendre equation and for cylindrical coordinates this is the Jacobi equation.

For the above Theorem, systems which enclose three adjacent numbers refers to either the Lamé or spherical systems. If there is a pair of parentheses inside, then this specifically means the latter. If there are two pairs of parentheses on the edge of the polytope, then this could either be the prolate or oblate systems.

Note that a single ODE of Heun type gives solutions for *two* factors of the eigenfunction ψ. In the general ellipsoidal case treated in the previous section the single Fuchsian ODE with 4 finite regular singular points gives *three* such factors. Any ODE of hypergeometric type (including the trivial trigonometric one) gives a solution for a single factor of the eigenfunction. Hence another way of stating which ODEs occur for the various cases is this: On the inside/edges/corners of the Stasheff polytope the highest Fuchsian ODE has 5/4/3 regular singular points, accounting for 3/2/1 of the factors of the eigenfunctions. The remaining 0/1/2 ODEs are of hypergeometric type.

4.3.1. Prolate Coordinates and the Heun Equation

Prolate coordinates on S^3 are a degeneration of ellipsoidal coordinates arising from limiting the middle two semi major axes to each other, i.e. $e_3 \to e_2^+$. We normalise the e_i according to $(e_1, e_2 = e_3, e_4) = (0, 1, a)$.

From [KM86], an explicit representation of prolate coordinates is

$$\begin{aligned} x_1^2 &= \frac{s_1 s_3}{a} & x_2^2 &= -\frac{(s_1-1)\,s_2\,(s_3-1)}{a-1} \\ x_3^2 &= \frac{(s_1-1)\,(s_2-1)\,(s_3-1)}{a-1} & x_4^2 &= \frac{(a-s_1)\,(a-s_3)}{(a-1)a} \end{aligned} \tag{4.29}$$

where $0 \le s_1, s_2 \le 1 \le s_3 \le a$ and a possible Stäckel matrix is given by

$$\sigma_{\text{pro}} = \frac{1}{4}\begin{pmatrix} -\frac{1}{(s_1-1)(s_1-a)} & -\frac{1}{(s_1-1)s_1(s_1-a)} & -\frac{1-a}{(s_1-1)^2 s_1(s_1-a)} \\ 0 & 0 & -\frac{1}{(s_2-1)s_2} \\ -\frac{1}{(s_3-1)(s_3-a)} & -\frac{1}{(s_3-1)s_3(s_3-a)} & -\frac{1-a}{(s_3-1)^2 s_3(s_3-a)} \end{pmatrix}. \tag{4.30}$$

From [NDD23] we have the following result.

Lemma 21. *Separating the Hamilton-Jacobi equation in prolate coordinates and subsequently reducing by $\sqrt{H}$ gives a semi-toric integrable system on $S^2 \times S^2$ with integrals*

$$G = a\ell_{12}^2 + a\ell_{13}^2 + \ell_{14}^2 \qquad M = \ell_{23}^2$$

and Poisson structure $B_{\boldsymbol{X},\boldsymbol{Y}}$ as given in (4.3).

To obtain the separated equations, we use the Stäckel matrix (4.30) and the metric tensor for prolate coordinates (4.29), and follow the same methodology as described in Lemma 13. For all future systems studied in this paper, this same technique is used to obtain the separated ODEs. This gives the following.

Lemma 22. *Separating the Schrödinger equation (4.5) in prolate coordinates (4.29) gives the following separated equations*

$$\psi_j'' + \frac{1}{2}\left(\frac{1}{s_j} + \frac{2}{s_j-1} + \frac{1}{s_j-a}\right)\psi_j' + \frac{-Es_j^2 + \left(\lambda + E + (a-1)m^2\right)s_j - \lambda}{4s_j(s_j-1)^2(s_j-a)}\psi_j = 0 \quad \text{for } j = 1,3 \tag{4.31a}$$

$$\psi_j'' + \frac{1}{2}\left(\frac{1}{s_j} + \frac{1}{s_j-1}\right)\psi_j' + \frac{m^2}{4s_j(1-s_j)}\psi_j = 0 \qquad \text{for } j = 2 \tag{4.31b}$$

where (m, λ) are spectral parameters.

We observe that the separated equation in (4.31b) is of hypergeometric type, but via the coordinate transformation $s_2 = \cos^2\phi$ we recover the trivial ODE

$$\psi_2''(\phi) + m^2 = 0. \tag{4.32}$$

To ensure a smooth globally defined solution on S^3, we enforce periodic boundary conditions. This yields a discrete spectral parameter $m \in \mathbb{Z}$ representing the quantised angular momentum in the (x_2, x_3) plane with solutions $e^{im\phi}$ to (4.32).

In [NDD23] we showed that the classical integrals for the degenerate systems are obtained by a smooth degeneration of the coordinates. The following Lemma shows how the ODEs (4.31a) and (4.31b) naturally arise from the generalised Lamé equation (4.7) in a similar fashion.

Lemma 23. *The separated equations for ψ_j in (4.31a) and (4.31b) can be obtained by smoothly degenerating the generalised Lamé equation (4.7).*

Proof. As noted in [NDD23], the canonical transformation from ellipsoidal to prolate coordinates is given by

$$e_3 = e_2 + \varepsilon, \qquad s_2 = e_2 + \varepsilon\tilde{s}_2, \qquad p_2 = \frac{\tilde{p}_2}{\varepsilon}, \tag{4.33}$$

in the limit $\varepsilon \to 0$ where $\tilde{s}_2 \in [0,1]$ and $\tilde{p}_2$ is its conjugate momenta. We normalise the semi-major axes with $(e_1, e_2 = e_3, e_4) = (0, 1, a)$ and set

$$\lambda = \lambda_2, \qquad m^2 = \frac{1}{a-1}(\lambda_1 - \lambda_2 - E).$$

For the equations in s_1 and s_3, the first derivative terms trivially degenerate while for the multiplicative term, substituting (4.33) into (4.7) and taking the limit $\varepsilon \to 0$ gives (4.31a).

Repeating the same process for the equations in s_2 gives the desired result.

■

Note that the Stäckel matrix used to obtain the separation constants is not unique and so neither are the arising ODEs. Another choice of Stäckel matrix would result in a different (yet equivalent - up to a linear combination of the eigenvalues and operators) set of ODEs since the separation constants would be different. The first derivative term is specific to the coordinates and so is independent of the choice of Stäckel matrix.

Equation (4.31a) is an example of a Heun equation; a Fuchsian 4 ODE with regular singularities at $0, 1, a$ and ∞:

$$W'' + \left(\frac{\gamma}{z} + \frac{\delta}{z-1} + \frac{\varepsilon}{z-a}\right) W' + \frac{\alpha\beta z - q}{z(z-1)(z-a)} W = 0 \tag{4.34}$$

where $\alpha + \beta + 1 = \gamma + \delta + \varepsilon$. The corresponding Riemann symbol is given by

$$\mathcal{S}_{\text{Heun}} = \begin{pmatrix} 0 & 1 & a & \infty \\ 0 & 0 & 0 & \alpha; z \\ 1-\gamma & 1-\delta & 1-\varepsilon & \beta \end{pmatrix}. \tag{4.35}$$

Lemma 24. *By the change of dependent variable $\psi_j = (z-1)^{|m|/2} W_j$, (4.31a) can be written in the form of (4.34) where $\gamma = \varepsilon = \frac{1}{2}, \delta = 1 + |m|, q = \frac{1}{4}(a|m| - \lambda)$ and*

$$\alpha, \beta = \frac{1}{2}\left(1 \pm \sqrt{1+E} + |m|\right). \tag{4.36}$$

Specifically, we have

$$W_j'' + \left(\frac{1}{2z} + \frac{1+|m|}{2(z-1)} + \frac{1}{2(z-a)}\right) W_j' + \frac{(-E + |m|(|m|+2))z - (a|m| - \lambda)}{4z(z-1)(z-a)} W_j \tag{4.37}$$

The solution $H\ell(a, q; \alpha, \beta, \gamma, \delta; z)$ that corresponds to exponent 0 about $z = 0$ such that $H\ell(a, q; \alpha, \beta, \gamma, \delta; 0) = 1$ is called a Heun function. We use the notation from [DLMF]. Assuming $\gamma \notin -\mathbb{N}$, the Heun function can be expanded as an infinite series

$$H\ell(a, q; \alpha, \beta, \gamma, \delta; z) = \sum_{i=0}^{\infty} c_i z^i \tag{4.38}$$

where $|z| < 1$ and $c_0 = 1$. Substituting (4.38) into (4.34) gives the following Lemma taken

from [RA95].

Lemma 25. *The coefficients c_i in (4.38) satisfy the following three term recurrence relation*

$$A_i c_{i+1} - (B_i + q)c_i + C_i c_{i-1} = 0 \tag{4.39}$$

where, for $i \geq 1$:

$$\begin{aligned} A_i &= a(i+1)(i+\gamma) \\ B_i &= i\left[(i-1+\gamma)(a+1) + a\delta + \varepsilon\right] \\ C_i &= (i-1+\alpha)(i-1+\beta) \end{aligned} \tag{4.40}$$

subject to the conditions $c_0 = 1$ and

$$a\gamma c_1 - q c_0 = 0. \tag{4.41}$$

From (4.40) it is clear that $\alpha = -d$ where $d \in \mathbb{N}$ forces $C_{d+1} = 0$ and the three term recurrence (4.39) truncates (4.38) to a polynomial of degree d. These solutions, analytic at all three finite singularities $z = 0, 1, a$ are known as Heun polynomials and will be denoted by $Hp(a, q; \alpha, \beta, \gamma, \delta; z)$. In the general ellipsoidal case Heine-Stieltjes polynomials were computed by solving a non-linear system of equations for the roots of the eigenfunctions. In the Heun case the above recursion gives a different and simpler method for computing the eigenfunctions and eigenvalues. In the remainder of this section we show how to obtain the corresponding harmonic polynomials in $\mathbb{R}^4$ and how to compute the various discrete symmetry classes of eigenfunctions.

Using a technique similar to the ellipsoidal case and outlined by [Vol99], we have the following Lemma.

Lemma 26. *Let $Hp_d(z)$ be a Heun polynomial solution to (4.37) of degree d and denote by $z_1, \ldots, z_d$ its roots. The product $Hp_d(s_1)Hp_d(s_3)$, expressed in the original Cartesian coordinates, is given by*

$$Hp_d(s_1)Hp_d(s_3) = \prod_{k=1}^{d} z_k(z_k - a)\left[\frac{x_1^2}{z_k} - r^2 + x_4^2\frac{1-a}{z_k - a}\right] \tag{4.42}$$

where $r^2 = x_1^2 + x_2^2 + x_3^2 + x_4^2$.

Proof. Firstly, we claim that

$$(\theta - s_1)(\theta - s_3) = \theta(\theta - a)\left(r^2 - \frac{x_1^2}{\theta} + \frac{(a-1)}{\theta - a}x_4^2\right) \tag{4.43}$$

for all $\theta \neq 0, a$. Both the left and right hand sides of (4.43) are monic quadratic functions of θ. Further, both expressions have roots at $\theta = s_1, s_3$. This is easily verified for the right hand side by using the coordinate transform (4.29) and the condition $r^2 = 1$.

Let $Hp_d(z)$ be a Heine-Stieltjes polynomial of degree d with roots $z_1, z_2, \ldots, z_d$ in factored form, i.e.

$$Hp_d(z) = (z_1 - z)(z_2 - z)\ldots(z_d - z). \tag{4.44}$$

Combining (4.43) with (4.44) gives the desired result.

■

Note that we have solved the canonical Heun equation (4.34). To write the combined solution to (4.31a) and (4.31b), we include the normalisation factor by recalling $\psi_1 = (1-s_1)^{|m|/2}W_1$. For the s_3 equation, since $s_3 \geq 1$ we have $\psi_3 = (s_3-1)^{|m|/2}W_3$. Hence, the combined solution to (4.5) in prolate coordinates is the product

$$\psi_1\psi_2\psi_3 = (1-s_1)^{|m|/2}(s_3-1)^{|m|/2}Hp_d(s_1)Hp_d(s_2)e^{im\phi}. \tag{4.45}$$

This yields the following Lemma.

Lemma 27. *Expressed in Cartesian coordinates, the product $\psi_1\psi_2\psi_3$ in (4.45) can be written as the following $\tilde{D}$ degree homogeneous polynomial where $\tilde{D} = 2d + |m|$:*

$$\Phi_{\tilde{D}}(\boldsymbol{x}) = (a-1)^{|m|/2}\left(x_2 + i\,\mathrm{sign}(m)x_3\right)^{|m|}\prod_{k=1}^{d} z_k(z_k - a)\left[\frac{x_1^2}{z_k} - r^2 + x_4^2\frac{1-a}{z_k - a}\right] \tag{4.46}$$

and $m \in [-\tilde{D}, \tilde{D}]$ is an integer.

Proof. Using the definition of prolate coordinates in (4.29) we obtain

$$(1-s_1)^{m/2}(s_3-1)^{m/2} = \left[(a-1)(x_2^2 + x_3^2)\right]^{m/2}.$$

We also know that $e^{im\phi} = \left(\frac{x_2+ix_3}{\sqrt{x_2^2+x_3^2}}\right)^m$. Combining this with (4.42) and (4.45) gives the product in (4.46). For homogeneity, given that $r^2 = \sum_{i=1}^4 x_i^2$, it is clear that all terms in (4.46) are of degree $\tilde{D} = 2d + |m|$.

■

Like in the ellipsoidal case, there are 16 discrete symmetry classes of $\Phi_{\tilde{D}}$ corresponding to parity about each of the x_i axes. However, we note that a simple parity flip of either x_2 or x_3 for the the complex phase $(x_2 + ix_3)^m$ would not necessarily yield a materially different wave function depending on the parity of m.

To address this, we note that for odd m we have $\Re(x_2 + ix_3)^m = x_2P(x_2^2, x_3^2)$ and $\Im(x_2 + ix_3)^m = x_3Q(x_2^2, x_3^2)$ where P and Q are some polynomials of degree $(m-1)/2$. These therefore give solutions which are odd about the x_2 (x_3) axes and even about x_3 (x_2)

respectively. Similarly, we note that for even m we have $\Re(x_2 + ix_3)^m = \tilde{P}(x_2^2, x_3^2)$ and $\Im(x_2+ix_3)^m = x_2x_3\tilde{Q}(x_2^2, x_3^2)$ where $\tilde{P}$ and $\tilde{Q}$ are polynomials of degree $m/2$ and $(m-2)/2$ respectively. The former give solutions which are even about both x_2 and x_3 and the latter those which are odd about both of these axes.

In the following discussion, we only focus on the discrete symmetries about the x_1 and x_4 axes. This is because symmetries about the x_2 and x_3 axes are encoded in taking the real and imaginary components of the wave function, in conjunction with a parity choice of m, as just described. This is similar in other degenerate systems (oblate, spherical, etc).

Let $\boldsymbol{\mu} = (\mu_1, \mu_4)$ where $\mu_i \in \{0, 1\}$ and μ_i being 1 (0) denotes a solution odd (even) about the x_i axis. For these symmetries, we consider the change of dependent variable in (4.37) given by $\phi_1 = s_1^{\mu_1/2}(a - s_1)^{\mu_1/2}W_1$ and $\phi_3 = s_3^{\mu_4/2}(a - s_3)^{\mu_4/2}W_3$ which corresponds to multiplication of the total wavefunction by $x_1^{\mu_1}x_4^{\mu_4}$. Doing so gives a resulting Heun equation with parameters shown in Table 4.4.

Denote by $Hp_d^{\boldsymbol{\mu}}(z)$ solutions to (4.34) corresponding to the $\boldsymbol{\mu}$ symmetry class. Let the product $Hp_d^{\boldsymbol{\mu}}(s_1)Hp_d^{\boldsymbol{\mu}}(s_3)e^{im\phi}$, when converted back to Cartesian coordinates, be given by $\Phi_{\tilde{D}}^{\boldsymbol{\mu}}(\boldsymbol{x})$. As with the ellipsoidal case, we set

$$\Psi_D^{\boldsymbol{\mu}}(\boldsymbol{x}) \coloneqq x_1^{\mu_1}x_4^{\mu_4}\Phi_{\tilde{D}}^{\boldsymbol{\mu}}(\boldsymbol{x}) \tag{4.47}$$

where $D \coloneqq \tilde{D} + \mu_1 + \mu_4$ and $m \in [-D, D]$ is an integer for all symmetry classes. Note that (4.46) is a special case of $\Psi_D^{\boldsymbol{\mu}}(\boldsymbol{x})$ with $\boldsymbol{\mu} = (0, 0)$.

Lemma 28. *The $\Psi_D^{\boldsymbol{\mu}}(\boldsymbol{x})$ are D degree, homogeneous harmonic polynomials and the energy eigenvalue is given by $E = D(D + 2)$.*

Proof. The proof that $\Psi_D^{\boldsymbol{\mu}}(\boldsymbol{x})$ satisfy (4.5) is identical to the ellipsoidal case. For the energy eigenvalue, we note that a necessary condition for polynomial solutions is for the three-term recurrence relation (4.39) to vanish. This forces $C_i = 0$ in (4.40), leading to the condition

$$\alpha = -d + \frac{1}{2}(\mu_1 + \mu_4). \tag{4.48}$$

Substituting (4.48) into the expression for α in (4.36) gives the desired result.

■

From (4.48) we observe that for the $(0, 0)$ and $(1, 1)$ symmetry classes, α is a negative integer while for the $(0, 1)$ and $(1, 0)$ classes, α is a negative half integer. Further, we note that fixing a value of E (in turn fixing D) enforces a parity relationship between E and m for a given symmetry class. For even (odd) E, m must be even (odd) for the $(0, 0)$ and $(1, 1)$ classes while m must be odd (even) for the others.

(μ_1, μ_4)	$\tilde{\alpha}$	$\tilde{\beta}$	$\tilde{\gamma}$	$\tilde{\delta}$	$\tilde{\varepsilon}$	$\tilde{q}$
$(0,0)$	α	β	γ	δ	ε	q
$(1,0)$	$\alpha+1-\gamma$	$\beta+1-\gamma$	$2-\gamma$	δ	ε	$(1-\gamma)(a\delta+\varepsilon)+q$
$(0,1)$	$\alpha+1-\varepsilon$	$\beta+1-\varepsilon$	γ	δ	$2-\varepsilon$	$\gamma(1-\varepsilon)+q$
$(1,1)$	$2+\alpha-\gamma-\varepsilon$	$2+\beta-\gamma-\varepsilon$	$2-\gamma$	δ	$2-\varepsilon$	$q+2+a\delta-\varepsilon-\gamma(1+a\delta)$

Table 4.4: Parameters of (4.34) for the various symmetry classes.

(μ_1, μ_4)	E even	E odd
$(0,0)$	$\left(\frac{D}{2}+1\right)^2$	$\left(\frac{D+1}{2}\right)\left(\frac{D+3}{2}\right)$
$(1,0)$	$\left(\frac{D}{2}+1\right)\frac{D}{2}$	$\left(\frac{D+1}{2}\right)^2$
$(0,1)$	$\left(\frac{D}{2}+1\right)\frac{D}{2}$	$\left(\frac{D+1}{2}\right)^2$
$(1,1)$	$\left(\frac{D}{2}\right)^2$	$\left(\frac{D+1}{2}\right)\left(\frac{D-1}{2}\right)$

Table 4.5: Number of states for each symmetry class and each parity of E.

As in the ellipsoidal case, we can compute the total number of states for a fixed energy E as well as that for each symmetry class.

Lemma 29. *Fix an energy $E = D(D+2)$. Then the total number of eigenstates is given by*

$$N = (D+1)^2. \tag{4.49}$$

The total number of eigenstates for each symmetry class is shown in Table 4.5.

Proof. Assume D is even and consider the $(\mu_1, \mu_4) = (0,0)$ symmetry class; the other cases are proven in a similar manner. We observe that $|m|$ ranges over the $D+1$ values $-D, -D+2, \ldots, 0, \ldots, D-2, D$ since $|m|$ is required to be an even integer based on our condition for α. For a fixed energy and the relationship between d and $|m|$ this enforces, we have a total of $\frac{D-|m|}{2}+1$ states for a given m.

Summing the total number of states over all possible values of m gives

$$N^{even}_{(0,0)} = \left(\frac{D}{2}+1\right) + 2\times\left(\frac{D}{2}+\left(\frac{D}{2}-1\right)+\cdots+1\right) = \left(\frac{D}{2}+1\right)^2.$$

Repeating a similar procedure for all other symmetry classes gives the desired result. Regardless of the parity of D, summing over each column of Table 4.5 gives (4.49).

■

As with the ellipsoidal case, we have $\hbar$ as the inverse of an integer, namely $\hbar = \frac{1}{D+1}$. The joint spectrum $(m\hbar, \lambda\hbar^2)$ is obtained for fixed $\tilde{E}$ and total degree d by numerically computing the eigenvalues of the matrix (4.40) to obtain d eigenvalues q and hence λ for given m. We use Mathematica's `Eigenvalue[]` command and the numerics is fast and

accurate for moderately large $D = 2d + |m| \approx 20$. Since the matrices (4.40) are not self adjoint, substantially larger d results in non-trivial numerical error.

An example of the joint spectrum is shown in Fig. 4.5 a) below. We have chosen $D = 20$ giving $\hbar = \frac{1}{21}$ and a total of $(20+1)^2 = 441$ total eigenstates. The blue, orange, red and cyan points correspond to the $(0,0),(1,0),(0,1),(1,1)$ symmetry classes respectively. Since we have chose an even value of E (and thus D) we observe states of the $(0,0)$ and $(1,1)$ symmetry classes only along even m. Similarly, along odd m only the $(1,0)$ and $(0,1)$ states are present. Had we chosen an odd E then orange/red dots would be seen along even m and vice versa. We also show the classical boundary of the momentum map in black. As mentioned, this is a semi-toric system and an isolated rank-2 critical point of focus-focus variety is located at $(m\hbar, \lambda\hbar^2) = (0,1)$. This is shown as the magenta dot.

From the same reasoning used to obtain (4.27), we obtain the following formulae for the actions

$$J_{1,pro} = \frac{1}{\pi}\int_0^{\min(r_1,1)} p_1 ds_1 \quad J_{2,pro} = \frac{1}{\pi}\int_0^{1} p_2 ds_2 \qquad J_{3,pro} = \frac{1}{\pi}\int_{\max(1,r_2)}^{a} p_3 ds_3 \tag{4.50}$$

where, using (4.30), for $j = 1, 3$

$$p_j^2 = \frac{\tilde{E}s_j^2 + \left(\lambda + \tilde{E} + (a-1)m^2\right)s_j - \lambda}{4s_j(s_j-1)^2(s_j-a)} \tag{4.51}$$

and (r_1, r_2) denote the roots of p_j^2 with $0 \le r_1 \le 1 \le r_2 \le a$. Note that J_2 simplifies to $m = |\ell_{23}|$. Like for the ellipsoidal system, the prolate actions also satisfy (4.28). The action map for the prolate system is shown in Fig. 4.5 b) where the magenta dot corresponding to the focus-focus point is located at $\frac{2}{\pi}(\sin^{-1}(\frac{1}{a}), 0, \frac{\pi}{2} - \sin^{-1}(\frac{1}{a}))$. Eigenstates with $m = 0$ have $J_1 = 0$ and are hence on the boundary of the triangle. The reason for this is that the discrete symmetry reduced action variables in the quantum setting would require to impose Neumann boundary conditions.

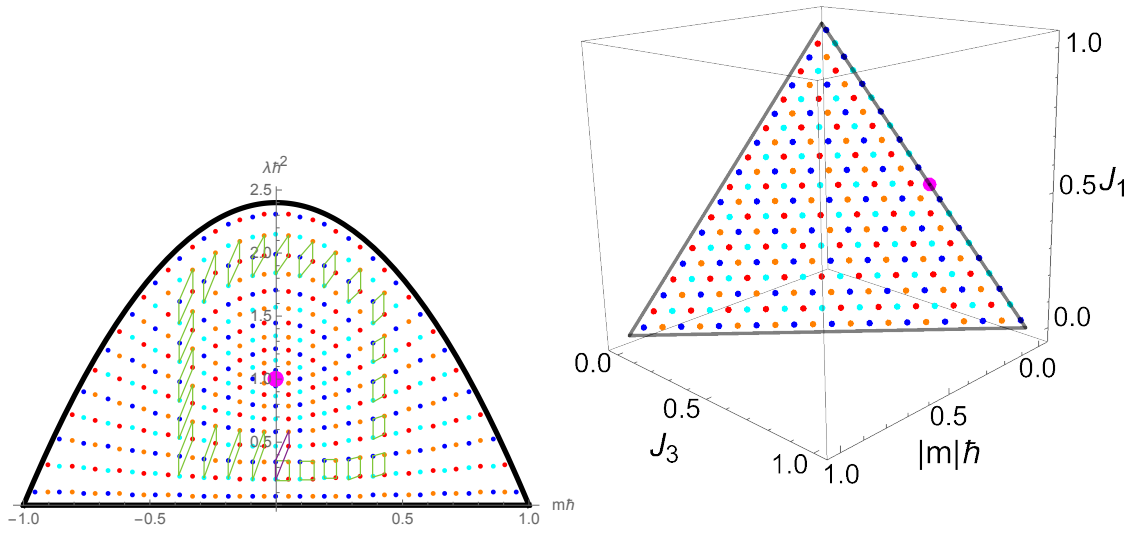

Figure 4.5: a) Prolate spectrum with $D = 20$, $a = 2.4$ and a total of 21^2 eigenstates. Different symmetry classes are represented with different colours. Note the focus-focus critical value shown in magenta. b) Action map corresponding to the joint spectrum.

Since the classical integrable system is semi-toric and has a focus-focus point, we expect the corresponding joint spectrum to exhibit quantum monodromy. This is shown in Fig. 4.5 a). A unit cell is parallel transported around the focus-focus critical value. Denote the basis vectors of this unit cell as v_1 (vertical) and v_2 (horizontal). As the cell completes a full loop, we observe a basis transformation where v_1 remains unchanged but v_2 is updated to $v_2 + 2v_1$. In a similar vein to our previous work [DDN21], we have the following basis transformation

$$\begin{pmatrix} v_1' \\ v_2' \end{pmatrix} = \begin{pmatrix} 1 & 0 \\ \omega & 1 \end{pmatrix} \begin{pmatrix} v_1 \\ v_2 \end{pmatrix} \tag{4.52}$$

where $\omega = 2$. As was observed in [DDN21], when considering the symmetry classes one at a time, $\omega = 1$ whereas combining them two at a time gives $\omega = 2$. Finally, in Fig. 4.6 we show the projection of the joint spectrum in the action variables onto either the (m, J_1) or (m, J_3) axes (and plotting the signed m instead of $|m|$). The resulting polygons are two different representations of the semi-toric polygon invariant with the cut above and below the focus-focus point.

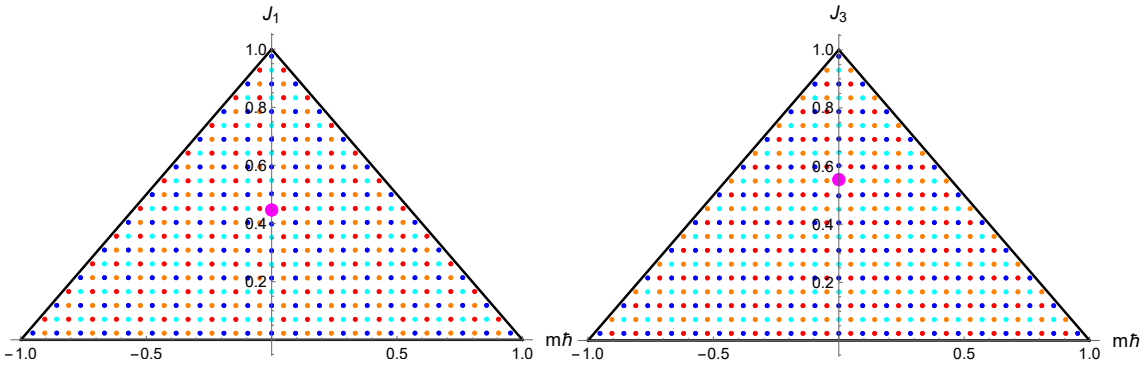

Figure 4.6: a) The semi-toric polygon in the prolate case $D = 20$, $a = 2.4$; projection of the actions onto the (m, J_1) axes, b) Projection onto the (m, J_3) axes.

4.3.2. Oblate Coordinates

Degenerating either the two largest $(e_3 = e_4)$ or smallest $(e_1 = e_2)$ semi major axes gives rise to the oblate coordinates on S^3. They are equivalent under sending $e_i \to -e_i$ and then translating and scaling. In this paper we only address the former case and normalise the e_i with $(e_1, e_2, e_3 = e_4) = (0, 1, a)$.

From [KM86], an explicit representation of oblate coordinates is

$$\begin{aligned} x_1^2 &= \frac{s_1 s_2}{a} & x_2^2 &= \frac{-(s_1-1)(s_2-1)}{a-1} \\ x_3^2 &= \frac{(s_1-a)(s_2-a)s_3}{a(a-1)} & x_4^2 &= \frac{(s_1-a)(s_2-a)(1-s_3)}{a(a-1)} \end{aligned} \tag{4.53}$$

where $0 \leq s_1, s_2 \leq 1 \leq s_3 \leq a$. A possible Stäckel matrix is given by

$$\Phi_{\text{obl}} = \frac{1}{4}\begin{pmatrix} -\frac{1}{(s_1-1)(s_1-a)} & -\frac{1}{(s_1-1)s_1(s_1-a)} & \frac{(1-a)a}{(s_1-1)s_1(s_1-a)^2} \\ -\frac{1}{(s_2-1)(s_2-a)} & -\frac{1}{(s_2-1)s_2(s_2-a)} & \frac{(1-a)a}{(s_2-1)s_2(s_2-a)^2} \\ 0 & 0 & -\frac{1}{(s_3-1)s_3} \end{pmatrix}. \tag{4.54}$$

From [NDD23] and similar to the prolate system, we have the following.

Lemma 30. *Separating the Hamilton Jacobi equation in oblate coordinates using the Stäckel matrix (4.54) and subsequently reducing by H gives a two degree of freedom integrable system on $S^2 \times S^2$ with integrals*

$$G_{obl} = a\ell_{12}^2 + \ell_{13}^2 + \ell_{14}^2 \qquad M = \ell_{34}^2$$

and Poisson structure $B_{\boldsymbol{X},\boldsymbol{Y}}$ as given in (4.3).

Using (4.54) and a computation similar to the prolate case we have the following Lemma.

Lemma 31. *Separating the Schrödinger equation (4.5) in oblate coordinates (4.53) gives the following ODEs*

$$\psi_j'' + \frac{1}{2}\left(\frac{1}{s_j} + \frac{1}{s_j - 1} + \frac{2}{s_j - a}\right)\psi_j' + \frac{-Es_j^2 + \left(\lambda + aE - (a-1)m^2\right)s_j - a\lambda}{4s_j(s_j-1)(s_j-a)^2}\psi_j = 0 \quad \text{for } j = 1, 2 \tag{4.55a}$$

$$\psi_j'' + \frac{1}{2}\left(\frac{1}{s_j} + \frac{1}{s_j - 1}\right)\psi_j' + \frac{m^2}{4s_j(1-s_j)}\psi_j = 0 \qquad \text{for } j = 3 \tag{4.55b}$$

where (m, λ) are spectral parameters.

Again, the equation for ψ_3 in (4.55b) can be converted to the trivial equation (4.32) using the same transformation as for prolate. This yields a discrete spectral parameter $m \in \mathbb{Z}$ which represents quantised angular momentum in the (x_3, x_4) plane with solutions $e^{im\phi}$. As with the prolate system, the separated ODEs can also be obtained by degenerating the generalised Lamé equation.

Lemma 32. *The separated equations for the oblate system (4.55a) and (4.55b) smoothly degenerate from those of the ellipsoidal system.*

Proof. The proof is identical to that of prolate but uses the transformation

$$(e_4, s_3, p_3) = (e_3 + \varepsilon, e_3 + \varepsilon\tilde{s}_3, \frac{\tilde{p}_3}{\varepsilon})$$

and taking the limit as $\varepsilon \to 0$. For more detail, see [NDD23].

■

Equation (4.55a) is an example of a Heun equation.

Lemma 33. *By the change of dependent variable $\psi_j = (z-a)^{|m|/2}W_j$, (4.55a) can be written in the form of (4.34) where $\gamma = \delta = \frac{1}{2}, \varepsilon = 1 + |m|, q = \frac{1}{4}\left(|m| - \lambda\right)$ and α, β as in (4.36). In particular, we have*

$$W_j'' + \left(\frac{1}{2z} + \frac{1}{2(z-1)} + \frac{1+|m|}{z-a}\right)W_j' + \frac{(-E + |m|(|m|+2))z - (|m| - \lambda)}{4z(z-1)(z-a)}W_j. \tag{4.56}$$

Let $Hp_d(z)$ be a Heun polynomial solution to (4.56) of degree d and let $z_1, \ldots, z_d$ be its roots. Many of the results for prolate apply for the oblate system which we state in the following Lemma.

Lemma 34. *The combined solution to (4.55a) and (4.55b) is the product*

$$\psi_1\psi_2\psi_3 = (a - s_1)^{m/2}(a - s_2)^{m/2}Hp_d(s_1)Hp_d(s_2)e^{im\phi}. \tag{4.57}$$

(μ_1,μ_2)	$\tilde{\alpha}$	$\tilde{\beta}$	$\tilde{\gamma}$	$\tilde{\delta}$	$\tilde{\varepsilon}$	$\tilde{q}$
$(0,0)$	α	β	γ	δ	ε	q
$(1,0)$	$\alpha+1-\gamma$	$\beta+1-\gamma$	$2-\gamma$	δ	ε	$q+(1-\gamma)(a\delta+\varepsilon)$
$(0,1)$	$\alpha+1-\delta$	$\beta+1-\delta$	γ	$2-\delta$	ε	$q+(1-\gamma)(a\delta+\varepsilon)$
$(1,1)$	$\alpha+2-\gamma-\delta$	$\beta+2-\gamma-\delta$	$2-\gamma$	$2-\delta$	ε	$q+2a(1-\gamma)+2(1-\gamma)\varepsilon$

Table 4.6: Parameters of (4.34) for the various symmetry classes of the oblate system.

Expressed in the original Cartesian coordinates using (4.53), (4.57) is a homogeneous polynomial of total degree $\tilde{D}=2d+|m|$ given by

$$\Phi_{\tilde{D}}=(a(a-1))^{m/2}\left(x_3+i\text{sign}(m)x_4\right)^{|m|}\prod_{k=1}^{d}z_k(z_k-1)\left(r^2-\frac{x_1^2}{z_k}a-\frac{a-1}{z_k-1}x_2^2\right). \tag{4.58}$$

Proof. The proof follows the same logic as used for the prolate system. To obtain (4.58), we note the use of the following identity:

$$(\theta-s_1)(\theta-s_2)=\theta(\theta-1)\left(r^2-\frac{x_1^2}{\theta}a-\frac{a-1}{\theta-1}x_2^2\right),$$

which holds since both sides are monic quadratic polynomials in θ that vanish at $\theta=s_1,s_2$. Using the definition of oblate coordinates in (4.53) and observing that $e^{im\phi}=\left(\frac{x_3+ix_4}{\sqrt{x_3^2+x_4^2}}\right)^m$, the result follows.

■

As with the prolate system, we only consider the 4 discrete symmetry classes about the x_1 and x_2 planes. Let $\boldsymbol{\mu}=(\mu_1,\mu_2)$ where $\mu_i\in\{0,1\}$ and μ_1 (μ_2) being 1 (0) denotes a solution odd (even) about the x_1 (x_2) axis. To investigate these symmetries, consider the change of dependent variable in (4.56) given by $\phi_1=s_1^{\mu_1/2}(a-s_1)^{\mu_1/2}W_1$ and $\phi_2=s_2^{\mu_2/2}(a-s_2)^{\mu_2/2}W_2$ which corresponds to multiplication by $x_1^{\mu_1}x_2^{\mu_2}$. This change of variables leads to a Heun equation (4.34) with parameters given in Table 4.6. As in the prolate example, denote by $Hp_d^{\boldsymbol{\mu}}(z)$ solutions to (4.34) for the symmetry class $\boldsymbol{\mu}$ and let the product $Hp_d^{\boldsymbol{\mu}}(s_1)Hp_d^{\boldsymbol{\mu}}(s_2)e^{im\phi}$, when converted back into Cartesian coordinates, be given by $\Phi_{\tilde{D}}^{\boldsymbol{\mu}}(\boldsymbol{x})$. Set

$$\Psi_D^{\boldsymbol{\mu}}(\boldsymbol{x}):=x_1^{\mu_1}x_2^{\mu_2}\Phi_{\tilde{D}}^{\boldsymbol{\mu}}(\boldsymbol{x}) \tag{4.59}$$

where $D=\tilde{D}+\sum_{i=1}^{2}\mu_i$. Again, (4.58) is a special case with $\boldsymbol{\mu}=(0,0)$. Following the same argument used in prolate, we have the following Lemma.

Lemma 35. *The $\Psi_D^{\boldsymbol{\mu}}(\boldsymbol{x})$ are D degree homogeneous, harmonic polynomials and the energy eigenvalue is given by $E=D(D+2)$.*

For a given energy the total number of eigenstates is computed using the same methodology as for the prolate case.

Lemma 36. *For a fixed value of D, the total number of eigenstates is given by $N = (D+1)^2$. The number of states for each symmetry class given in Table 4.6 is the same as that shown in Table 4.5.*

Using the three term recurrence (4.40) and the same methodology for prolate, we find the joint spectrum. In Fig. 4.7 a) we show the joint spectrum $(m\hbar, \lambda\hbar^2)$ for $D = 20$ and $a = 2.4$. As in the prolate system, we have $\hbar = \frac{1}{D+1}$ and a total of 441 total eigenstates. The blue, red, orange and cyan points correspond to the $(0,0), (1,0), (0,1)$ and $(1,1)$ symmetry classes respectively.

We also show the classical outline of the momentum map in black. Unlike the prolate system, this is not a semi-toric system. One interesting feature of the joint spectrum is the existence of period doubling. A quantum consequence of this is the near-degeneracy in the upper chamber.

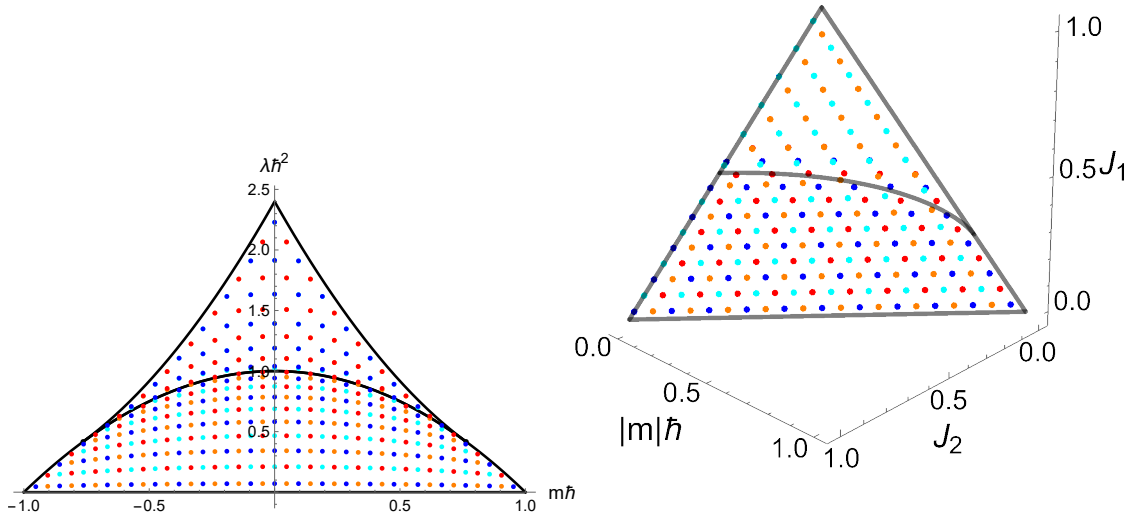

Figure 4.7: a) Joint spectrum of the oblate system $(m\hbar, \lambda\hbar^2)$ for $D = 20$ and $a = 2.4$ showing a total of 441 states. b) Corresponding action map. Note that light blue (cyan) and orange states are hidden by the nearby degenerate red and blue states in the upper chamber.

To compute the actions, we use the same methodology as for the prolate system. Doing so gives the following three continuous actions:

$$J_1 = \frac{2}{\pi}\int_0^{\min(r_1,1)} p_1 ds \qquad J_2 = \frac{2}{\pi}\int_{\max(r_1,1)}^{\min(r_2,a)} p_2 ds \qquad J_3 = |\ell_{34}|$$

where

$$p_i^2 = \frac{-\tilde{E}s_i^2 + (\tilde{E}a + g - (a-1)m^2)s_i - ag}{4s_i(s_i-1)(s_i-a)^2}$$

for $i = 1, 2$, $r_2 \geq 1$ and $0 \leq r_1 \leq r_2 \leq a$. The action map corresponding to the joint spectrum in Fig. 4.7 a) is shown in b). Again, we note that $J_1 + J_2 + J_3 = 1$.

4.3.3. LAMÉ COORDINATES

The Lamé coordinates are unique compared to the other singly degenerate coordinate systems (oblate, prolate) since they are an extension of ellipsoidal coordinates from S^2 onto S^3. Consequently, while prolate and oblate coordinates have symmetry group $SO(2)$, the Lamé coordinates have the larger symmetry group $SO(3)$.

As with oblate, there are two possible (yet equivalent) ways to define Lamé coordinates. Either the largest three e_i become equal, or the smallest three. We choose the former and define Lamé coordinates by

$$\begin{aligned} x_1^2 &= s_1 & x_2^2 &= \frac{(1-s_1)(s_2-f_1)(s_3-f_1)}{(f_2-f_1)(f_3-f_1)} \\ x_3^2 &= \frac{(s_1-1)(f_2-s_2)(f_2-s_3)}{(f_1-f_2)(f_2-f_3)} & x_4^2 &= \frac{(s_1-1)(f_3-s_2)(f_3-s_3)}{(f_2-f_3)(f_3-f_1)} \end{aligned} \tag{4.60}$$

where $0 \leq s_1 \leq 1$ and $0 \leq f_1 \leq s_2 \leq f_2 \leq s_3 \leq f_3$ with real parameters f_i.

A possible Stäckel matrix is given by

$$\sigma_{\text{Lamé}} = \frac{1}{4}\begin{pmatrix} \frac{1}{s_1(1-s_1)} & \frac{-1}{s_1(1-s_1)^2} & 0 \\ 0 & \frac{1}{(f_3-s_2)(s_2-f_2)} & \frac{1}{(f_3-s_2)(s_2-f_2)(s_2-f_1)} \\ 0 & \frac{1}{(f_3-s_3)(s_3-f_2)} & \frac{1}{(f_3-s_3)(s_3-f_2)(s_3-f_1)} \end{pmatrix} \tag{4.61}$$

with corresponding integrals obtained by separation as

$$F = \ell_{12}^2 + \ell_{13}^2 + \ell_{14}^2, \qquad G = f_1\ell_{34}^2 + f_2\ell_{24}^2 + f_3\ell_{23}^2.$$

As in the other coordinates, reduction by H gives a two degree of freedom integrable system (F, G) on $S^2 \times S^2$ with Poisson structure $B_{\boldsymbol{X},\boldsymbol{Y}}$. The integral F is a result of the $SO(3)$ symmetry. Using (4.61) and the same methodology used in the previous systems, we obtain the following separated ODEs

$$\psi_1'' + \frac{1}{2}\left(\frac{1}{s_1} + \frac{3}{s_1-1}\right)\psi_1' + \frac{f - Es_1}{4s_1(1-s_1)^2}\psi_1 = 0 \tag{4.62a}$$

$$\psi_k'' + \frac{1}{2}\left(\frac{1}{z-f_1} + \frac{1}{z-f_2} + \frac{1}{z-f_3}\right)\psi_k' + \frac{(f-E)z + g}{4(z-f_1)(z-f_2)(z-f_3)}\psi_k = 0 \qquad k = 2, 3 \tag{4.62b}$$

The separated equations can also be obtained by smoothly degenerating the generalised Lamé equation.

Lemma 37. *Equations* (4.62a) *and* (4.62b) *arise from smoothly degenerating the separated generalised Lamé equations in* (4.7).

Proof. From [NDD23], it is known that the transformation

$$(e_1, e_2, e_3, e_4) = \left(-\frac{1}{\varepsilon}, f_1, f_2, f_3\right) \tag{4.63}$$

$$(s_1, p_1) = \left(f_2 - \frac{s_1}{\varepsilon}, \varepsilon p_1\right) \tag{4.64}$$

defines a canonical transformation that smoothly degenerates the classical ellipsoidal system into that for Lamé. Further, applying (4.63) and taking the limit as $\varepsilon \to 0$ gives

$$(\eta_1, \eta_2) = \left(-\frac{2H - F}{\varepsilon}, -\frac{G}{\varepsilon}\right). \tag{4.65}$$

Substituting (4.63), (4.64) and (4.65) into (4.7) and and considering dominating terms of ε gives the degenerated ODEs (4.63) and (4.64).

■

Equation (4.62a) has regular singularities at $s_1 = 0, 1, \infty$ meaning that it is of the hypergeometric type. We observe that the form as written in (4.62a) is not canonical. The roots of the indicial equation at $s_1 = 1$ are

$$r_\pm = \frac{1}{4}\left(-1 \pm \sqrt{1 + 4E - 4f}\right), \tag{4.66}$$

where $r_- < 0 < r_+$. To change (4.62a) into canonical form, we make the change of dependent variable $\psi_1 \to y(1 - s_1)^{r_+}$ followed by the change of independent variable $s_1 = x_1^2$, yielding the well known Gegenbauer equation

$$(1 - x_1^2)y'' - (2u + 1)x_1 y' + n(n + 2u)y = 0 \tag{4.67}$$

where $u = \frac{1}{2}(1 + \sqrt{1 + 4E - 4f})$ and

$$n = -\frac{1}{2}\left(\sqrt{4E - 4f + 1} - \sqrt{4E + 4} + 1\right). \tag{4.68}$$

From [AS92, MF53], it is known that polynomial solutions to (4.67) occur when n is an integer. These are known as the Gegenbauer polynomials $C_n^u(x_1)$ where n denotes the degree of the polynomial.

The equation in the s_2, s_3 variables is known as the Lamé equation, a special case of the Heun equation. As with the previous degenerate cases, we simplify by mapping (f_1, f_2, f_3) to $(0, 1, a)$ where $a > 1$. The parameters (f_1, f_2, f_3) in (4.62b) can be mapped to $(0, 1, a)$ by a

Möbius transformation, then the Riemann symbol is given by

$$\mathcal{S}_{2,3} = \begin{pmatrix} 0 & 1 & a & \infty \\ 0 & 0 & 0 & \alpha; z \\ 1/2 & 1/2 & 1/2 & \beta \end{pmatrix}$$

where $\alpha, \beta = \frac{1}{4}\left(1 \pm \sqrt{1 + 4E - 4f}\right)$ and $q = g/4$. The Lamé equation is typically written as follows [BE55]:

$$W'' + \frac{1}{2}\left(\frac{1}{\xi} + \frac{1}{\xi - 1} + \frac{1}{\xi - k^{-2}}\right) W' + \frac{bk^{-2} - \nu(\nu+1)\xi}{4\xi(\xi-1)(\xi - k^{-2})} W = 0 \tag{4.69}$$

where $k = \frac{1}{\sqrt{a}}$, $b = g/a$ and $\nu = \frac{1}{2}\left(\sqrt{4E - 4f + 1} - 1\right) = 2\beta - 1$ with $\nu \geq -1/2$ and $0 < k < 1$. Polynomial solutions of the Lamé equation are known as Lamé polynomials [ASSU14] and we denote them as $Lp_d(z)$ where the subscript d signifies the solution's degree. Note that ν being a non negative integer is a necessary condition for polynomial solutions.

Lemma 38. *Solutions to (4.62b) are polynomial iff $E = \tilde{D}(\tilde{D}+2)$ where $\tilde{D} = 2d + n$ is an integer.*

Proof. From [Vol99] we know that polynomial solutions are only obtainable for (4.62b) if

$$\frac{f - E}{4} = -d(d + \frac{1}{2}). \tag{4.70}$$

Combining (4.70) and (4.68) gives the result.

■

Using (4.70), we know that r_+ in (4.66) simplifies to d, $\nu = 2d, \alpha = -d, \beta = 2d + \frac{1}{2}$ and $u = 2d + 1$. Denote the full solution $\psi = \psi_1\psi_2\psi_3$ to (4.62a) and (4.62b) as

$$\psi = (1 - s_1)^d C_n^{2d+1}(x_1) Lp_d(s_2) Lp_d(s_3). \tag{4.71}$$

We have the following Lemma.

Lemma 39. *Expressed in the original Cartesian coordinates, ψ is a homogeneous polynomial of degree $\tilde{D}$. Specifically, we can rewrite (4.71) as*

$$\Phi_{\tilde{D}}(\boldsymbol{x}) = r^n C_n^{2d+1}\left(\frac{x_1}{r}\right) \prod_{i=1}^{3}\prod_{k=1}^{d}(z_k - f_i) \prod_{k=1}^{d}\sum_{i=1}^{3}\frac{x_{i+1}^2}{z_k - f_i} \tag{4.72}$$

where the z_k are the roots of the Lamé polynomials Lp_d, $(f_1, f_2, f_3) = (0, 1, a)$ and $r^2 = \sum_i x_i^2$.

Proof. From the definition of the Lamé coordinates (4.60), it is easily seen that

$$(z_k - s_2)(z_k - s_3) = \frac{(z_k - f_1)(z_k - f_2)(z_k - f_3)}{1 - x_1^2}\left(\frac{x_2^2}{z_k - f_1} + \frac{x_3^2}{z_k - f_2} + \frac{x_4^2}{z_k - f_3}\right).$$

Taking the product over all d roots and using $r^2 = 1$ along with $s_1 = x_1^2$ gives (4.72). To prove homogeneity, we note that

$$C_n^{2d+1}(x_1) = r^n C_n^{2d+1}(\frac{x_1}{r}) \tag{4.73}$$

and so the argument of the Gegenbauer polynomial will be of degree 0. We observe that r^n will be of degree n in the x_i and $C_n^{2d+1}(\frac{x_1}{r})$ will only consist of terms whose powers have the same parity as n. Thus, we have shown that (4.72) is homogeneous and polynomial.

■

As with the previous systems, let $\boldsymbol{\mu} = (\mu_2, \mu_3, \mu_4)$ where $\mu_i \in \{0, 1\}$ denote a symmetry class where $\mu_i = 0$ represent the wavefunction odd about the x_i axis and even otherwise. Consider the change of dependent variable

$$\phi_j = \prod_{i=1}^{3}(s_j - f_i)^{\mu_{i+1}/2}\psi_j \tag{4.74}$$

where $j = 2, 3$ in (4.62b). This is equivalent to multiplying the original solution by $x_2^{\mu_2}x_3^{\mu_3}x_4^{\mu_4}$. Note that performing this change of variables in the Lamé equation (4.62b) results in a Heun equation of the form (4.34) with parameters for each symmetry class $\boldsymbol{\mu}$ as shown in Table 4.7.

For the Gegenbauer equation (4.67), we note that the independent variable is x_1 and so parity about this axis is determined simply by the parity of the Gegenbauer polynomial $C_n^u(x_1)$, which is determined by n. We let $\mu_1 = 1$ if n is odd and $\mu_1 = 0$ otherwise.

For a given symmetry class $\boldsymbol{\mu}$, denote by $Lp_d^{\boldsymbol{\mu}}(z)$ solutions to (4.34) with parameters given in Table 4.7. We consider the product $\Phi_{\tilde{D}}^{\boldsymbol{\mu}}(\boldsymbol{x}) = C_n^{2d+1+U}(x_1)Lp_d^{\boldsymbol{\mu}}(s_2)Lp_d^{\boldsymbol{\mu}}(s_3)$ where $U = \sum_{i=1}^{3}\mu_{i+1}$. Finally, we set

$$\Psi_D^{\boldsymbol{\mu}}(\boldsymbol{x}) := x_2^{\mu_2}x_3^{\mu_3}x_4^{\mu_4}\Phi_{\tilde{D}}^{\boldsymbol{\mu}}(\boldsymbol{x}) \tag{4.75}$$

where $D = n + \tilde{D} + U$. As before, (4.72) is a special case of (4.75) with $\boldsymbol{\mu} = (0, 0, 0)$.

Lemma 40. *The $\Psi_D^{\boldsymbol{\mu}}(\boldsymbol{x})$ are homogeneous polynomial eigenfunctions of the original Laplacian (4.5) and the energy is given by $E = D(D + 2)$.*

Proof. Proving $\Psi_D^{\boldsymbol{\mu}}(\boldsymbol{x})$ is an eigenfunction follows the same argument as the previous cases. To compute the energy for a given symmetry class $\boldsymbol{\mu}$, we combine the parameters of Table

4.7 with the results of [Vol99] to get a more general form of (4.70), namely

$$\frac{f - E + U(U+1)}{4} = -d(d + 1/2 + U). \tag{4.76}$$

Combining (4.76) and (4.68) gives the result for E. Similarly, we have that $u = 2d + 1 + U$.

■

$\boldsymbol{\mu}$	$\tilde{\alpha}$	$\tilde{\beta}$	$\tilde{\gamma}$	$\tilde{\delta}$	$\tilde{\varepsilon}$	$\tilde{q}$
$(0,0,0)$	α	β	γ	δ	ε	q
$(1,0,0)$	$\alpha+1-\gamma$	$\beta+1-\gamma$	$2-\gamma$	δ	ε	$q+(1-\gamma)(a\delta+\varepsilon)$
$(0,1,0)$	$\alpha+1-\delta$	$\beta+1-\delta$	γ	$2-\delta$	ε	$q-a\gamma(\delta-1)$
$(0,0,1)$	$\alpha+1-\varepsilon$	$\beta+1-\varepsilon$	γ	δ	$2-\varepsilon$	$q+\gamma(1-\varepsilon)$
$(1,1,0)$	$\alpha-\gamma-\delta+2$	$\beta-\gamma-\delta+2$	$2-\gamma$	$2-\delta$	ε	$q-a(\gamma+\delta-2)-\gamma\varepsilon+\varepsilon$
$(1,0,1)$	$\alpha-\gamma-\varepsilon+2$	$\beta-\gamma-\varepsilon+2$	$2-\gamma$	δ	$2-\varepsilon$	$q-\gamma(a\delta+1)+a\delta-\varepsilon+2$
$(0,1,1)$	$\alpha-\delta-\varepsilon+2$	$\beta-\delta-\varepsilon+2$	γ	$2-\delta$	$2-\varepsilon$	$q+\gamma(-a\delta+a-\varepsilon+1)$
$(1,1,1)$	$\alpha-\gamma-\delta-\varepsilon+3$	$\beta-\gamma-\delta-\varepsilon+3$	$2-\gamma$	$2-\delta$	$2-\varepsilon$	$q-a(\gamma+\delta-2)-\gamma-\varepsilon+2$

Table 4.7: Symmetry class $\boldsymbol{\mu}$ and corresponding Heun (Lamé) equation parameters for which the resulting polynomial is an eigenfunction.

From the above, it is clear that for a fixed energy E, only 8 of the 16 discrete symmetry classes for the Lamé system can be present. If E is even, then the symmetry classes $\mathcal{S}_E$ given in (4.21) are present. Conversely, if E is odd, we have the remaining 8 symmetry classes $\mathcal{S}_O$ from (4.22). Note that while we have omitted μ_1 from the definition of $\boldsymbol{\mu}$ in our discussion of the Lamé systems so far, this symmetry is accounted for in the parity of n which is set by the value of D. When addressing all symmetry classes below, we will write $\tilde{\boldsymbol{\mu}} = (\mu_1; \mu_2, \mu_3, \mu_4)$ to highlight this fact.

We have the following observation.

Lemma 41. *Chebyshev polynomials of the second kind are the eigenfunction corresponding to the joint spectrum point* $(f, g) = (1 - \hbar^2, 0)$.

Proof. For $\boldsymbol{\mu} = (0,0,0)$, we have from (4.76) the relation $f = E - 4d(d + 1/2)$. When $d = 0$ one obtains $f = E$ which gives $f = 1 - \hbar^2$ (after normalisation by $\hbar$) and $g = 0$. This gives Chebyshev polynomials of the second kind $U_n(x_1)$ since $U_n(x_1) = C_n^1(x_1)$. Note that in the limit $\hbar \to 0$ this joint spectrum point becomes the degenerate point $(1, 0)$ for the classical system.

■

Lamé Polynomial	Corresponding Symmetry $\boldsymbol{\mu}$
$Ec_{2d}^{2m}(z,k^2)$	$(0,0,0)$
$Ec_{2d+1}^{2m+1}(z,k^2)$	$(1,0,0)$
$Es_{2d+1}^{2m+1}(z,k^2)$	$(0,1,0)$
$Ec_{2d+1}^{2m}(z,k^2)$	$(0,0,1)$
$Es_{2d+1}^{2m+2}(z,k^2)$	$(1,1,0)$
$Ec_{2d+2}^{2m+1}(z,k^2)$	$(1,0,1)$
$Es_{2d+2}^{2m+1}(z,k^2)$	$(0,1,1)$
$Es_{2d+3}^{2m+2}(z,k^2)$	$(1,1,1)$

Table 4.8: Lamé polynomials solutions to (4.77) and their corresponding symmetries given in Table 4.7.

The Lamé equation (4.69) can be transformed by the change of independent variable $\xi = \text{sn}^2(z,k)$ into the following form:

$$W'' + (b - \nu(\nu+1)k^2\text{sn}^2(z,k))W = 0. \tag{4.77}$$

This form of the Lamé equation has regular singular points at $2pK+(2q+1)iK'$ where K, K' are the complete elliptic integrals of the first kind with moduli k and $\sqrt{1-k^2}$ respectively and $p, q \in \mathbb{Z}$.

From [ASSU14], it is known that there are 8 polynomial solutions to (4.77) if ν is a non-negative integer. These are shown in Table 4.8 where $m = 0, 1, \ldots, \nu$ and Ec_d^m, Es_d^m are known as the Lamé functions [EMOT55]. Since $\xi = s_i = \text{sn}^2(z,k)$, we are able to connect these eigenfunctions to $Lp_d^{\boldsymbol{\mu}}(z)$ as given in Table 4.7.

The total number of states for each symmetry class is shown in Table 4.9 below. Here we use the notation $(\mu_1;\mu)$ to represent a state with parity given by μ_1 about the x_1 axis and odd about one remaining axis given by μ. E.g. $(1;\mu)$ represents the classes $(1;0,0,1), (1;0,1,0), (1;1,0,0)$. Similarly, we have $(\mu_1;\mu,\nu)$ and so forth. The number of states are computed using similar methods to those shown in the prolate case.

Summing the relevant entries for a given parity of the energy shows that the total number of states for a given energy $E = D(D+2)$ is given by $(D+1)^2$. To compute the joint spectrum for a given E, we use the parameters shown in Table 4.7 and the recurrence relationship given in Lemma 25. An example for even and odd energies is shown in Fig. 4.8. As with the other cases such as ellipsoidal and prolate, we have $\hbar = \frac{1}{D+1}$. As with the prolate and oblate systems, since the matrices involved are not self adjoint, larger values of D lead to numerical instability.

	Number of States	E
$(1;\mu)$	$D(D+2)/8$	Even
$(1;1,1,1)$	$D(D-2)/8$	Even
$(0;0,0,0)$	$(D+2)(D+4)/8$	Even
$(0;\mu,\nu)$	$D(D+2)/8$	Even
$(1;0,0,0)$	$(D+1)(D+3)/8$	Odd
$(1;\mu,\nu)$	$(D+1)(D-1)/8$	Odd
$(0;\mu)$	$(D+1)(D+3)/8$	Odd
$(0;1,1,1)$	$(D+1)(D-1)/8$	Odd

Table 4.9: Number of states per symmetry class and corresponding energy parity.

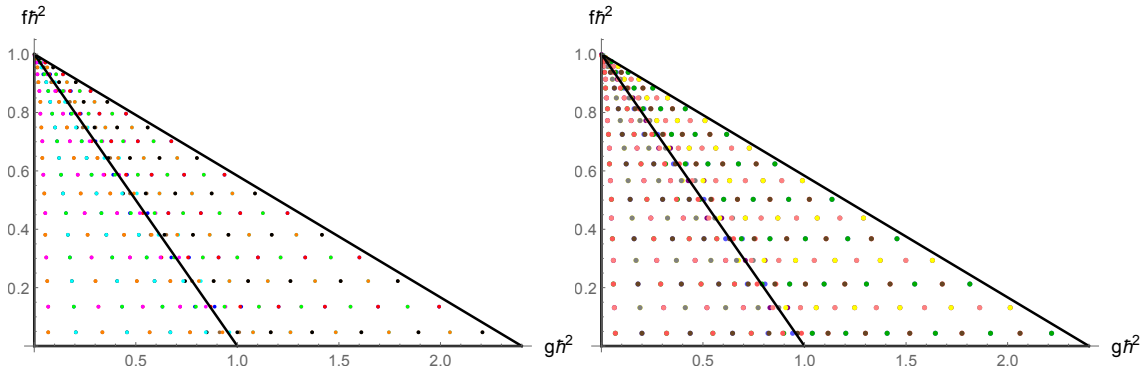

Figure 4.8: Joint spectrum (f, g) in the Lamé case with $(f_1, f_2, f_3) = (0, 1, 2.4)$ for a) even energy with $D = 20$ and b) odd energy with $D = 21$ thereby representing all 16 symmetry classes. Correspondence between the coloured dots and symmetry class are the same for the ellipsoidal system shown in Table 4.3.

The actions of the Lamé system are given by the following

$$J_1 = \frac{2}{\pi}\int_0^f p_1 ds, \quad J_2 = \frac{2}{\pi}\int_{f_1}^{\min(r_2,f_2)} p_2 ds, \quad J_3 = \frac{2}{\pi}\int_{\max(f_2,r_2)}^{f_3} p_3 ds$$

where $r_2 = \frac{g}{1-f}$ and

$$p_1^2 = \frac{f - \tilde{E}s_1}{4(s_1-1)^2 s_1} \quad p_i^2 = \frac{(f-\tilde{E})s_i + g}{4(s_i - f_3)(s_i - f_2)(s_i - f_1)}$$

for $i = 2, 3$. The first action simplifies to

$$J_1 = 1 - \sqrt{1-f}. \tag{4.78}$$

The image of spectra shown in Fig. 4.8, under the action map is shown in Fig. 4.9. Unlike the prolate and oblate cases, there are no states on the boundary. There is a single state located near the top corner $(f, g) = (1 - \hbar^2, 0)$.

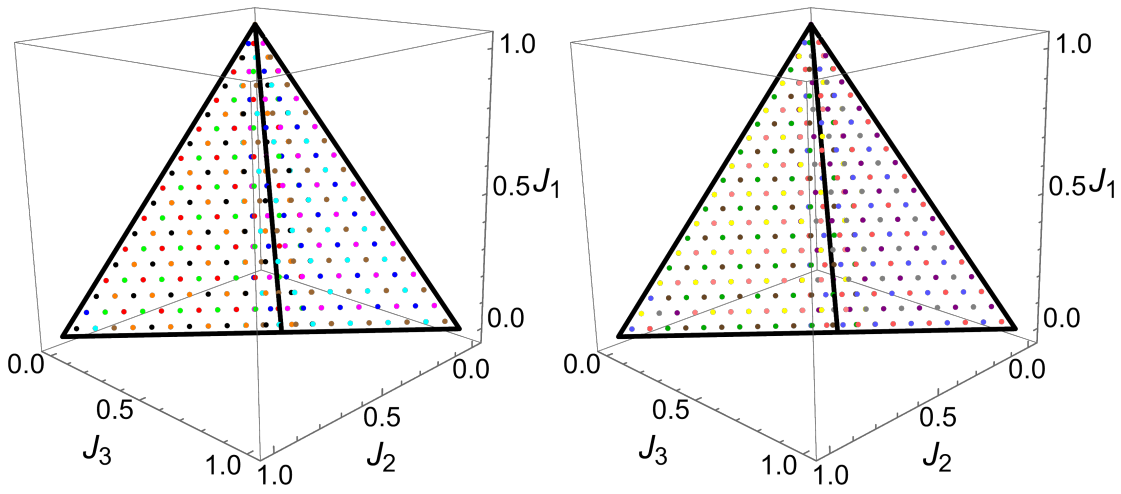

Figure 4.9: Joint spectrum in the Lamé case in action variables corresponding to the joint spectra shown in Fig. 4.8 a) and b).

4.3.4. Spherical Coordinates

Spherical coordinates (also known as poly-spherical coordinates) are a further degeneration of prolate, oblate or Lamé coordinates and possess both an $SO(2)$ and $SO(3)$ symmetry. Unlike prolate coordinates, spherical coordinates - despite having a global S^1 action - are not semi-toric since they have a degenerate point. This point corresponds to the critical values at which the global action is not differentiable, and the pre-image of the critical value is a sphere. We will see that there is a simple eigenfunction built from Chebyshev polynomials that is related to this sphere.

Spherical coordinates can be obtained from the Lamé case by setting either $f_1 = f_2$ or $f_2 = f_3$. These result in different coordinate systems, respectively called the 12 and 23 spherical systems and are related to each other via a permutation of coordinates. Similarly, setting $a = 1$ in both the prolate and oblate cases gives the 23 and 12 spherical systems respectively. See [NDD23] for more details.

In this paper we focus on the 23 spherical system, defined by

$$\begin{aligned} x_1^2 &= s_1 & x_2^2 &= (1-s_1)s_2 \\ x_3^2 &= (1-s_1)(1-s_2)s_3 & x_4^2 &= (1-s_1)(1-s_2)(1-s_3), \end{aligned} \tag{4.79}$$

where $0 \leq s_k \leq 1$ for all $k = 1, 2, 3$. Unlike the previously described systems, the spherical coordinates are relatively simple and separation can be done "by hand", without the use of a Stäckel matrix. The classical integrals obtained by separation are (F, ℓ_{34}^2) where $F = \ell_{12}^2 + \ell_{13}^2 + \ell_{14}^2$. Note this is the same F as in the Lamé system. The separated ODEs are

$$\psi_1'' + \frac{1}{2}\left(\frac{3}{s_1-1} + \frac{1}{s_1}\right)\psi_1' + \frac{\lambda - Es_1}{4s_1(1-s_1)^2}\psi_1 = 0 \tag{4.80a}$$

$$\psi_2'' + \left(\frac{1}{2s_2} + \frac{1}{s_2-1}\right)\psi_2' + \frac{(\lambda-E)(s_2-1)-m}{4s_2(1-s_2)^2}\psi_2 = 0 \tag{4.80b}$$

$$\psi_3'' + \frac{1}{2}\left(\frac{1}{s_3} + \frac{1}{s_3-1}\right)\psi_3' + \frac{m}{4s_3(1-s_3)}\psi_3 = 0. \tag{4.80c}$$

The equation for ψ_3 (4.80c) can be converted to the trivial equation (4.32) with the coordinate transformation $s_3 = \cos^2(\phi)$. Using this and periodic boundary conditions, we find that $m \in \mathbb{Z}$ and $\psi_3 = e^{im\phi}$ where $\phi = \arctan(\frac{x_3}{x_4})$.

As for the previous degenerate systems, we have the following Lemma.

Lemma 42. *The system of separated equations in* (4.80a), (4.80b), (4.80c) *can be obtained from either those of the Lamé system* (4.62a), (4.62b) *or those of the oblate system* (4.55a), (4.55b).

Proof. For the Lamé system (4.62a), (4.62b), the transformation $(s_3, p_3) \to (f_2 + \tilde{s_3}\varepsilon, \tilde{p_3}/\varepsilon)$ is canonical. This, coupled with $f_3 \to f_2 + \varepsilon$ and a corresponding transformation of the integrals followed by the normalization $(f_1, f_2) = (0, 1)$ yields the result. For the oblate direction, a similar method with $(a, s_3, p_3) = (1+\varepsilon, 1+\varepsilon\tilde{s_3}, \tilde{p_3}/\varepsilon)$ in (4.55a) and (4.55b) gives the result.

■

Next, we turn our attention to the non trivial equations. For ψ_1 in (4.80a), we observe that it is of hypergeometric type. It has 3 regular singularities - two finite poles at $s_1 = 0, 1$ and the third at infinity. To assist in finding polynomial solutions, we transform the equation for ψ_1 using the change of dependent variable $\psi_1 = (1-s_1)^{\frac{1}{4}(-1+X)}W_1$ where $X = \sqrt{1+4E-4\lambda}$, followed by the change of independent variable $s_1 = x_1^2$. This yields the Gegenbauer equation

$$(1-x_1^2)W_1'' - 2x_1(2u+1)W_1' + n(n+2u)W_1 = 0 \tag{4.81}$$

where $u = \frac{1}{2}(1+X)$ and

$$n = -\frac{1}{2}(1 - 2\sqrt{1+E} + X). \tag{4.82}$$

Gegenbauer polynomial solutions to (4.81), denoted by $C_n^u(x_1)$, are obtained when n_1 is a non negative integer.

Repeating a similar process for ψ_2 in (4.80b), we again note the equation is hypergeometric with regular singularities at $0, 1$ and infinity. The change of independent variable $s_2 = x^2 :=$

$\frac{x_2^2}{\tilde{r}^2}$ where $\tilde{r} := x_2^2 + x_3^2 + x_4^2$ gives the Associated Legendre equation written as follows

$$(1-x^2)\psi_2'' - 2x\psi_2' + \left(\ell(\ell+1) - \frac{m^2}{1-x^2}\right)\psi_2 = 0 \tag{4.83}$$

where $\ell(\ell+1) = E - \lambda$, i.e.

$$\ell = \frac{1}{2}(-1 + \sqrt{1 + 4E - 4\lambda}). \tag{4.84}$$

In (4.83), ℓ and m are referred to as the degree and order respectively of the Associated Legendre equation. Non trivial non singular solutions $P_\ell^m(x)$ are yielded when both ℓ and m are integers. Further, said solutions are polynomial only if m is an even integer. For polynomial solutions, both n and ℓ from (4.82) and (4.84) respectively must be integers. Solving these simultaneously for E gives

$$E = D(D+2) \tag{4.85}$$

where $D = \ell + n$. Using (4.85) with (4.84) gives analytic values of the eigenvalue λ as

$$\lambda = D(D+2) - \ell(\ell+1) \tag{4.86}$$

Using (4.86), we also have

$$X = 2\ell + 1 \tag{4.87}$$

along with $u = \ell + 1$. Combining the above, we have the following Lemma.

Lemma 43. *For a fixed value of $D = n + \ell$, the combined wavefunction solution to (4.5), expressed in Cartesian coordinates, is the homogeneous polynomial given by the product*

$$\Psi_D(\boldsymbol{x}) = r^n \tilde{r}^\ell \left(\frac{x_3 + ix_4}{\sqrt{x_3^2 + x_4^2}}\right)^m C_n^{\ell+1}\left(\frac{x_1}{r}\right) P_\ell^m\left(\frac{x_2}{\tilde{r}}\right) \tag{4.88}$$

where $\tilde{r}^2 = r^2 - x_1^2$.

Proof. First, we note as before $e^{im\phi} = (\frac{x_3+ix_4}{\sqrt{x_3^2+x_4^2}})^m$. The associated Legendre polynomials $P_\ell^m(x)$ can be written in the form (see, e.g., [DLMF, 14.7])

$$P_\ell^m(x) = \frac{(-1)^m}{2^\ell \ell!}(1-x^2)^{m/2}\frac{d^{\ell+m}}{dx^{\ell+m}}(x^2-1)^\ell. \tag{4.89}$$

Thus the denominator $\sqrt{x_3^2 + x_4^2}^m$ in the Lemma cancels with $\tilde{r}^m(1 - x_2^2/\tilde{r}^2)^{m/2}$. The remaining terms produce a homogeneous degree $\ell - m$ polynomial in x_2 and $\tilde{r}^2 - x_2^2 = x_3^2 + x_4^2$. We note that $r^n C_n^{\ell+1}(\frac{x_1}{r})$ is homogeneous of degree n and so it follows that (4.88) is homogeneous of degree $D = n + \ell$.

■

Let $\boldsymbol{\mu} = (\mu_1, \mu_2)$ where $\mu_i \in \{0, 1\}$ and μ_1 (μ_2) being 1 (0) denotes a solution odd (even) about the x_1 (x_2) axis. As with the Lamé system, we note that both the Gegenbauer and Associated Legendre equations have independent variables x_1 and x_2 respectively and thus their parity about these axes will be determined by that of n and $\ell - m$ respectively. Consequently, a fixed value of D enforces a relationship between n, ℓ and m.

We note that $\ell = 0$ forces $D = n$ and $m = 0$. Consequently, we recover Chebyshev polynomials of the second kind as $C_n^1(x_1) = U_n(x_1)$. The corresponding state on the joint spectrum is $(m, \lambda) = (0, 1 - \hbar^2)$, which becomes the classical degenerate point in the limit of $\hbar \to 0$. Depending on the parity of E, this corresponds to either the $(0, 0)$ symmetry (if E is even) or $(1, 0)$ if E is odd.

Fixing an energy E allows us to compute the joint spectrum for the spherical system. An example of the joint spectrum (m, λ) is shown in Fig. 4.10 a). The degenerate point is shown in magenta at $(0, 1)$.

From [NDD23], it is known that the actions of the spherical system are given as follows:

$$J_1 = 1 - \sqrt{1 - f} \qquad J_2 = \sqrt{1 - f} - m \qquad J_3 = m \tag{4.90}$$

where f is a value of the integral F. In Fig. 4.10 b) we show the corresponding action map to the joint spectrum shown in a).

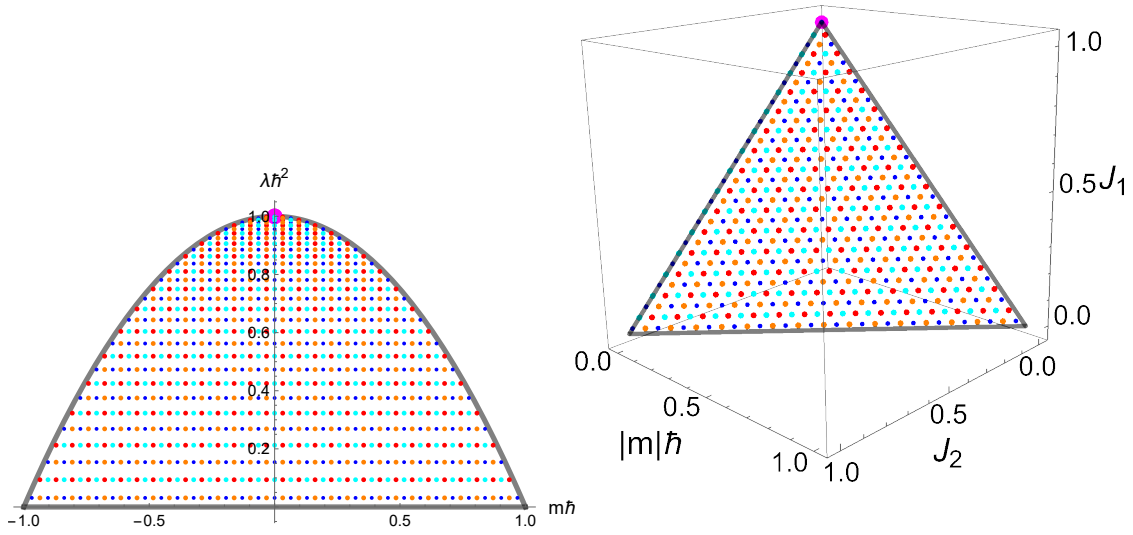

Figure 4.10: a) The joint spectrum in the spherical case with $D = 30$. Blue, red, orange and cyan represent the $(0, 0), (1, 0), (0, 1)$ and $(1, 1)$ symmetries respectively. There are $31^2 = 961$ states in total. b) The corresponding spectrum in action variables (4.90).

4.3.5. CYLINDRICAL COORDINATES

Cylindrical (or Hopf, or doubly cylindrical) coordinates are a further degeneration of oblate coordinates, found by setting $e_1 = e_2$ in addition to $e_3 = e_4$. The relationship between Cartesian and cylindrical coordinates is given by

$$\begin{aligned} x_1^2 &= s_1 s_2 & x_2^2 &= s_2(1-s_1) \\ x_3^2 &= s_3(1-s_2) & x_4^2 &= (1-s_2)(1-s_3). \end{aligned} \tag{4.91}$$

The separated equations are given by

$$\psi_1'' + \frac{1}{2}\left(\frac{1}{s_1} + \frac{1}{s_1-1}\right)\psi_1' + \frac{m_1^2}{4s_1(1-s_1)}\psi_1 = 0 \tag{4.92a}$$

$$\psi_2'' + \left(\frac{1}{s_2-1} + \frac{1}{s_2}\right)\psi_2' + \frac{m_1(s_2-1) - (m_2 + E(s_2-1))s_2}{4s_2^2(1-s_2)^2}\psi_2 = 0 \tag{4.92b}$$

$$\psi_3'' + \frac{1}{2}\left(\frac{1}{s_3} + \frac{1}{s_3-1}\right)\psi_3' + \frac{m_2^2}{4s_3(1-s_3)}\psi_3 = 0 \tag{4.92c}$$

where m_1, m_2 are spectral parameters. The equations in ψ_1 and ψ_3 in (4.92a) and (4.92c) are reducible to the trivial equation (4.32) with the trigonometric transformation used for the previous systems. This, along with periodic boundary conditions, give $m_1, m_2 \in \mathbb{Z}$ with solutions $\psi_1 = e^{im_1\phi_1}$ and $\psi_3 = e^{im_2\phi_3}$ where $\phi_1 = \arctan(\frac{x_2}{x_1})$ and $\phi_3 = \arctan(\frac{x_4}{x_3})$.

In (4.92b), the equation in ψ_2 is of hypergeometric type. The change of dependent variable $\psi_2 = s_2^{\frac{|m_1|}{2}}(1-s_2)^{\frac{|m_2|}{2}}y$ and independent $s_2 = \frac{1-x}{2}$ variables yields

$$y'' + \left(\frac{1+|m_1|}{x-1} + \frac{1+|m_2|}{x+1}\right)y' + \frac{-E + 2|m_1|(|m_2|+1) + m_1^2 + m_2^2 + 2|m_2|}{4(x^2-1)}y = 0$$

whose Riemann symbol is given by

$$\mathcal{S}_{\text{Cyl}} = \begin{pmatrix} -1 & 1 & \infty \\ 0 & 0 & \frac{1}{2}\left(-\sqrt{E+1} + |m_1| + |m_2| + 1\right); x \\ -|m_2| & -|m_1| & \frac{1}{2}\left(\sqrt{E+1} + |m_1| + |m_2| + 1\right) \end{pmatrix}.$$

Polynomial solutions to ψ_2 are obtained when an index at infinity vanishes. This leads to the condition

$$\frac{1}{2}\left(-\sqrt{E+1} + |m_1| + |m_2| + 1\right) = -d \tag{4.93}$$

which gives the quantised energy

$$E = D(D+2)$$

where $D = 2d + |m_1| + |m_2|$. These solutions, denoted by $P_d^{(|m_1|,|m_2|)}(x)$, are the well known

Jacobi polynomials.

The combined wavefunction solution to (4.5) is therefore

$$\psi = P_d^{(|m_1|,|m_2|)}(x) e^{im_1\phi_1} e^{im_2\phi_3}. \tag{4.94}$$

Lemma 44. *For a given $D = 2d + |m_1| + |m_2|$, the total wave function (4.94) in the original Cartesian coordinates is a harmonic homogeneous polynomial of degree D given by*

$$\Psi_D = r^{2d}(x_1 + i\,\mathrm{sign}(m_1)x_2)^{|m_1|}(x_3 + i\,\mathrm{sign}(m_2)x_4)^{|m_2|} P_d^{(|m_1|,|m_2|)}\left(\frac{x_3^2 + x_4^2 - x_1^2 - x_2^2}{r^2}\right). \tag{4.95}$$

Proof. Using the definition of cylindrical coordinates in (4.91), we note that $s_2 = x_1^2 + x_2^2$. Since $x = 1 - 2s_2$ and $r^2 = \sum_i x_i^2$, the argument of the Jacobi polynomial follows. Similarly, rewriting the exponential terms in (4.95) using this definition and cancelling terms gives the final result. To prove homogeneity, we note that the argument of the Jacobi polynomial is of degree 0 and so the final degree of Ψ_D will be $|m_1| + |m_2| + 2d = D$.

■

Note that for $m_1 = m_2 = 0$ we recover the Legendre polynomials $P_d^0(x) = P_d^{(0,0)}(x)$. For $m_1 = m_2$ we recover Gegenbauer polynomials $C_d^l(x)/P_d^{(l+1/2,l+1/2)} = const$, i.e. they are the same up to normalisation, see, e.g. [Sze75].

Since there are two continuous S^1 symmetries, the discrete symmetries of (4.95) are represented by the parity of m_1 and m_2. Note that $D - 2d = |m_1| + |m_2|$ has the same parity as D and E. In particular this implies that $m_1 = m_2 = 0$ is only possible for even D and E.

An example of the joint spectrum is given in Fig. 4.11 a) with $D = 20$. The total number of eigenstates is $(D+1)^2 = 441$.

Two of the spectral parameters are trivial angular momenta: $(J_1, J_3) = (|m_1|, |m_2|)$. As $J_1 + J_2 + J_3 = 1$, the remaining action J_2 is easily found. In Fig. 4.11 b) an example of the action map for the corresponding spectrum in a) is shown.

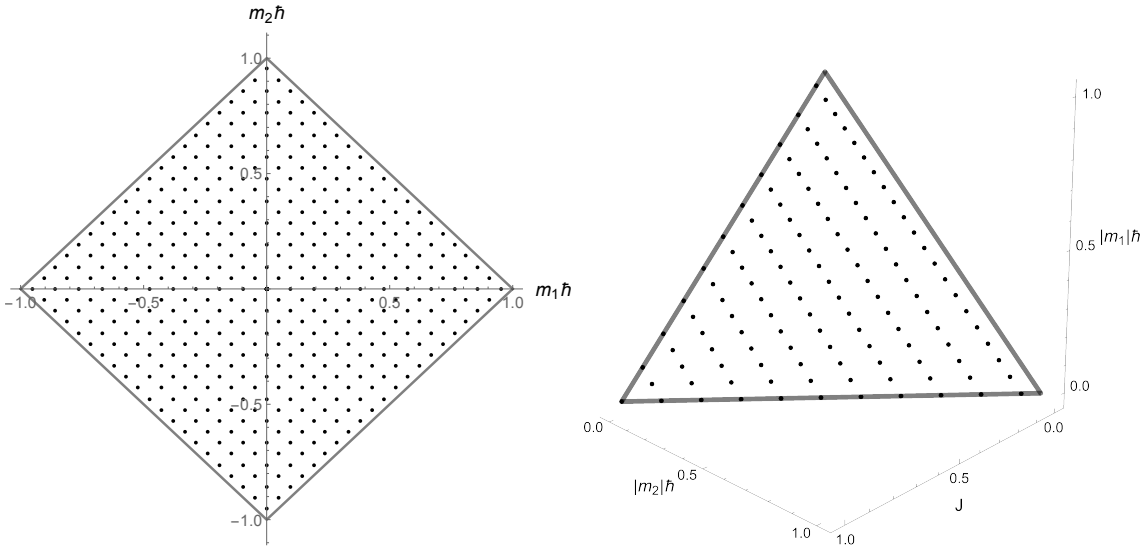

Figure 4.11: a) Joint spectrum with $D = 20$. b) Corresponding action map.

Chapter 5

Conclusion and Further Work

In this thesis we have studied the connections between separable integrable systems, their corresponding quantum systems and the resulting special function solutions. In doing so, we have made connections that reveal deep insights about both the classical and quantum mechanics, along with their respective discrete and continuous symmetries. A common theme throughout all chapters has been the study of both classical and quantum monodromy. We hope that the examples in this thesis will be instrumental to further work in this field.

In Chapter 2 we studied the free particle on $\mathbb{R}^3$. Separating the Schrödinger equation in prolate spheroidal coordinates yields the spheroidal wave equation, a special case of the confluent Heun equation. Employing symmetry reduction, quantum operators on $L_2(S^2)$ whose joint spectrum exhibit quantum monodromy were obtained. Taking the semi-classical limit, a semi-toric integrable system on T^*S^2 was recovered. This possesses a non degenerate focus-focus point, thereby proving the existence of both classical and quantum monodromy. To our knowledge, this is the first analysis of quantum monodromy using well known asymptotic expansions for the eigenvalues of the spheroidal wave equation.

Our study of the free particle and the spheroidal wave equation leads us to the question: what classical system would, when quantised, generate the most general confluent Heun equation? This inquiry motivates the work of Chapter 3. Here, we investigate the Harmonic Lagrange Top which is the well known Lagrange Top with an added quadratic potential. Separating the Schrödinger equation yields the most general confluent Heun equation, known in the physics literature as the Teukolsky master equation. We show that the quantum operators obtained by this separation have a joint spectrum which also exhibits quantum monodromy. However, unlike for the free particle system, this feature is only present for certain parameter choices related to the moments of inertia of the Lagrange Top.

We turn our attention in Chapter 4 to geodesic flow on S^3 as a natural extension to our free particle work on $\mathbb{R}^3$. Here, we separate the Schrödinger equation in the 6 orthogonal

separable coordinates on S^3: ellipsoidal, prolate, oblate, Lamé, spherical and cylindrical. Unlike the free particle and Harmonic Lagrange Top, for all 6 coordinate systems, the separated ODEs on S^3 (a compact manifold) are Fuchsian type, i.e., all singularities are regular. The most general of these separable coordinates are the ellipsoidal coordinates and the ODEs that arise are known as the generalised Lamé equation. All other ODEs that arise were shown to be obtained via degeneration from the generalised Lamé equation. We obtained a variety of special function solutions, namely the generalised Lamé wave functions, Heun and Gegenbauer polynomials. Numerical computations yielded the joint spectra of each quantum system. Finally, the monodromy that arises from the system obtained by separation in prolate coordinates is studied. Unlike the free particle and Harmonic Lagrange Top, the ODEs here are Heun equations.

Our work on S^3 can be expanded to higher dimensional spaces, in particular S^4. In doing so, a more general notion of monodromy can be defined and investigated. Further study can also be done investigating the connection between the confluent equations obtained on the non compact manifolds for the free particle and Harmonic Lagrange Top, and those obtained by separation on S^3.

Chapter A

Appendix

A.1. Ellipsoidal Coordinates on S^2

In these remaining sections we compare our results on S^3 to the more familiar S^2. Ellipsoidal coordinates on S^2 are defined as follows:

$$x_1^2 = \frac{(s_1-e_1)(s_2-e_1)}{(e_2-e_1)(e_3-e_1)} \quad x_2^2 = \frac{(s_1-e_2)(s_2-e_2)}{(e_1-e_2)(e_3-e_2)} \quad x_3^2 = \frac{(s_1-e_3)(s_2-e_3)}{(e_1-e_3)(e_2-e_3)}. \tag{A.1}$$

where $0 \leq e_1 \leq s_1 \leq e_2 \leq s_2 \leq e_3$. Separating (4.5) in these coordinates gives the following separated equations

$$\psi_i'' + \frac{1}{2}\left(\frac{1}{s_i-e_1} + \frac{1}{s_i-e_2} + \frac{1}{s_i-e_3}\right)\psi_i' + \frac{-Es_i+\lambda}{4(s_i-e_1)(s_i-e_2)(s_i-e_3)}\psi_i = 0 \tag{A.2}$$

for $i = 1, 2$. Equations (A.2) for $i = 1, 2$ are the Lamé equations studied in section 4.3.3 and so we denote their polynomial solutions by $Lp_d(s_i)$. Classically, the integrals obtained by separation are

$$(I_1, I_2) = (\ell_{12}^2 + \ell_{13}^2 + \ell_{23}^2, e_3\ell_{12}^2 + e_2\ell_{13}^2 + e_1\ell_{23}^2).$$

A combined solution to (4.5) in ellipsoidal coordinates is given by

$$\psi = Lp_d(s_1)Lp_d(s_2) \tag{A.3}$$

where there are $d = n_1 + n_2$ total roots of ψ with n_1 occurring in the interval $[e_1, e_2]$ and n_2 in $[e_2, e_3]$.

Lemma 45. *Written in Cartesian coordinates, ψ in (A.3) is a homogeneous $\tilde{\ell} := 2d$ degree polynomial*

$$\Phi_{\tilde{l}} = \left(\prod_{i=1}^{3}\prod_{k=1}^{d}(z_k - e_i)\right)\prod_{k=1}^{d}\sum_{i=1}^{3}\frac{x_i^2}{z_k - e_i} \tag{A.4}$$

where the z_k are solutions of

$$\sum_{i=1}^{3} \frac{1/4}{z_k - e_i} + \sum_{j=1, j\neq k}^{d} \frac{1}{z_k - z_j} = 0.$$

Inspecting (A.4), it is clear there are 8 symmetry classes in total (even/odd parity about each of the x_i axes). Let $\boldsymbol{\mu} \coloneqq (\mu_1, \mu_2, \mu_3)$ where $\mu_i \in \{0, 1\}$ represent a symmetry class of the solution (A.4) where $\mu_i = 1$ signifies a solution odd about the x_i axis and even otherwise. As with the S^3 ellipsoidal case, we consider these symmetries by performing the change of variables

$$\phi_j = \prod_{i=1}^{3} (s_j - e_i)^{\mu_i/2} \psi_j \tag{A.5}$$

in (A.2). Let solutions to the transformed (A.2) for a given symmetry class $\boldsymbol{\mu}$ be given by $\Phi_{\tilde{l}}^{\boldsymbol{\mu}}(\boldsymbol{x})$ and set

$$\Psi_{\ell}^{\boldsymbol{\mu}}(\boldsymbol{x}) \coloneqq x_1^{\mu_1} x_2^{\mu_2} x_3^{\mu_3} \Phi_{\tilde{l}}^{\boldsymbol{\mu}}(\boldsymbol{x}) \tag{A.6}$$

We then have the following Lemma.

Lemma 46. *The $\Psi_{\ell}^{\boldsymbol{\mu}}(\boldsymbol{x})$ are eigenfunctions of the Schrödinger equation (4.5) and the energy is given by $E = \ell(\ell+1)$ where $\ell \coloneqq 2d + \sum_{i=1}^{3} \mu_i$.*

Similar to the S^3 ellipsoidal and Lamé system, for a fixed value of ℓ, only four of these symmetries appear at any time. When ℓ is even, these are the $(0,0,0), (1,1,0), (1,0,1), (0,1,1)$ classes (blue, purple, orange, gray respectively in Fig. A.1 a)) while for odd ℓ we have the $(1,0,0), (0,1,0), (0,0,1), (1,1,1)$ classes (red, green, cyan, brown). Note that E is always even.

We demonstrate an example of this in Fig. A.1 a) and b) with $\ell = 20$ and $\ell = 19$ respectively and $(e_1, e_2, e_3) = (0, 1, 2.4)$. The joint spectrum is obtained using the same three term recurrence relations from Lemma 25 used to find the prolate, oblate and Lamé spectra.

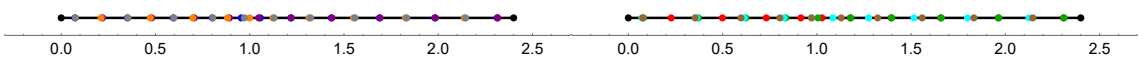

Figure A.1: Example spectra with a) $\ell = 20$ and b) $\ell = 19$ respectively and $(e_1, e_2, e_3) = (0, 1, 2.4)$.

For ellipsoidal coordinates on the $2-$sphere, consider a fixed value of the energy on (E_2), the corresponding eigenvalues λ, as well as an energy on the $3-$sphere (E_3) and eigenvalues for the Lamé system (f, g). Comparing (A.2) and (4.62a) for $k = 1, 2$, it is clear that

$$E_2 = f - E_3 \quad \lambda = g.$$

This can be geometrically interpreted as follows: each joint spectrum for the ellipsoidal S^2 system (such as those shown in Fig. A.1) corresponds to a horizontal slice of the Lamé joint spectrum (see Fig. 4.8), where the slice is specified for a given combination of (f, E_3).

A.2. Spherical Coordinates on S^2

Spherical coordinates on S^2 are defined as follows:

$$x_1^2 = s_1 \qquad x_2^2 = (1-s_1)s_2 \qquad x_3^2 = (1-s_1)(1-s_2) \tag{A.7}$$

where $0 \leq s_1 \leq s_2 \leq 1$. Separating the Hamilton-Jacobi equation gives classical integrals $(I_1, I_2) = (\ell_{12}^2 + \ell_{13}^2 + \ell_{23}^2, \ell_{12}^2)$ while doing so for the Schrödinger equation (4.5) yields the following ODEs

$$\psi_1'' + \frac{1}{2}\left(\frac{1}{s_1} + \frac{2}{s_1 - 1}\right)\psi_1' + \frac{-Es_1 + (E - m^2)}{4s_1(s_1-1)^2}\psi_1 = 0 \tag{A.8a}$$

$$\psi_2'' + \frac{1}{2}\left(\frac{1}{s_2} + \frac{1}{s_2 - 1}\right)\psi_2' + \frac{m}{4s_2(s_2-1)}\psi_2 = 0 \tag{A.8b}$$

where (E, m) are spectral parameters. The change of independent variable $s_2^2 = \cos^2\phi$ transforms (A.8b) to the trivial equation (4.32) with solution $e^{im\phi}$ and the associated boundary conditions force $m \in \mathbb{Z}$.

As with the previous degenerate systems, we have the following Lemma.

Lemma 47. *The spherical ODEs (A.8a), (A.8b) can be obtained by degenerating those arising from ellispoidal coordinates (A.4)*

For the equation in ψ_1 (A.8a), the change of independent variable $s_1 = x_1^2$ transforms (A.8a) into the form of the associated Legendre equation given in (4.83) where $E = \ell(\ell+1)$ is always even and ℓ is an integer. Polynomial solutions are this given by the Associated Legendre polynomials $P_\ell^m(x_1)$. We have the following Lemma.

Lemma 48. *For a given energy $E = \ell(\ell+1)$ the wave function of the Schrödinger equation (4.5) in spherical coordinates on S^2 is one of the following degree ℓ harmonic homogeneous polynomials*

$$\Psi_\ell = r^\ell \left(\frac{x_2 + ix_3}{\sqrt{x_2^2 + x_3^2}}\right)^m P_\ell^m\left(\frac{x_1}{r}\right), \tag{A.9}$$

where $m = -\ell, \ldots, \ell$.

Proof. The form of (A.9) is obtained by recognising $e^{im\phi} = \left(\frac{x_2+ix_3}{\sqrt{x_2^2+x_3^2}}\right)^m$. Harmonicity is clear and homogeneity follows by noting that P_ℓ^m is degree ℓ in its argument but the argument x_1/r is degree 0 in terms of the Cartesian coordinates. Moreover, $x_2^2 + x_3^2 = r^2 - x_1^2$

and so the denominator $(x_2^2+x_3^2)^{m/2}$ cancels with a factor in $r^m P_\ell^m(x_1/r)$ and the remaining polynomial in x_1/r is of degree $\ell - m$.

■

For discrete symmetries reflecting parity about the x_1 axis, we let $\mu \in \{0, 1\}$ denote the solution which is even (0) or odd (1) about the x_1 axis. The symmetry is even when $\ell - m$ is even, and odd otherwise. We note that, like for the spherical S^3 system, for a fixed ℓ and fixed symmetry class only every 2nd m is allowed so that the parity of $\ell - m$ remains fixed.

A.3. Ellipsoidal S^3 Quantised Actions

Here, we show the quantised actions for each symmetry class $\boldsymbol{\mu}$ originally presented in Fig. 4.4 a) and b). The number of eigenstates per symmetry class is given in Table 4.2. For a legend to convert between colour and symmetry class, see Table 4.3.

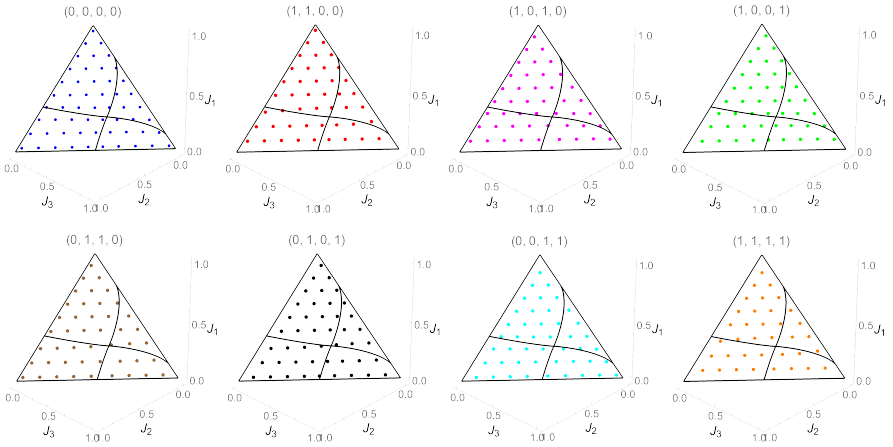

Figure A.2: Actions for each symmetry class shown in Fig. 4.2 a).

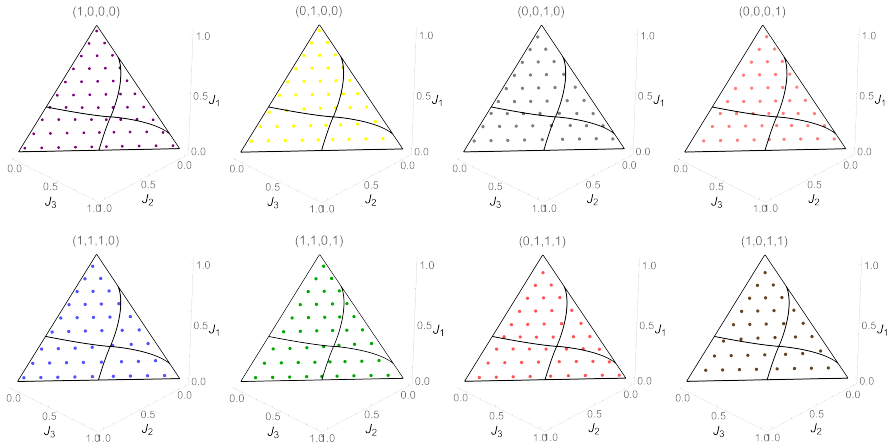

Figure A.3: Actions for each symmetry class shown in Fig. 4.2 b).

Bibliography

[ABR01] S. Axler, P. Bourdon, and W. Ramey. *Graduate Texts in Mathematics: Harmonic Function Theory*. Springer New York, 2001. 78, 86

[ADH19] J. Alonso, H. R. Dullin, and S. Hohloch. Symplectic classification of coupled angular momenta. *Nonlinearity*, 33:417–468, 2019. 75

[Ala79] M. Alam. Zeros of Stieltjes and Van Vleck polynomials. *Transactions of the American Mathematical Society*, 252(0):197–204, 1979. 20, 76

[Arn78] V. I. Arnold. *Mathematical Methods of Classical Mechanics*. Springer, Berlin, 1978. 12, 15, 54

[Ars64] F. M. Arscott. *Periodic differential equations: an introduction to Mathieu, Lamé, and allied functions*. Pergamon Press, 1964. 17, 21, 23, 30, 32, 55

[ARZ85] A. M. Al-Rashed and N. Zaheer. Zeros of Stieltjes and Van Vleck polynomials and applications. *Journal of Mathematical Analysis and Applications*, 110(2):327–339, sep 1985. 20, 76, 86

[AS92] M. Abramowitz and I. A. Stegun, editors. *Handbook of mathematical functions with formulas, graphs, and mathematical tables*. Dover Publications Inc., New York, 1992. Reprint of the 1972 edition. 23, 30, 31, 32, 106

[ASSU14] F. Arscott, I. Sneddon, M. Stark, and S. Ulam. *Periodic Differential Equations: An Introduction to Mathieu, Lamé, and Allied Functions*. International series of monographs in pure and applied mathematics. Elsevier Science, 2014. 107, 110

[Aud96] M. Audin. *Spinning Tops: A Course on Integrable Systems*, volume 51 of Cambridge Studies in Advanced Mathematics. Cambridge University Press, 1996. 54

[BCR02] S. Benenti, C. Chanu, and G. Rastelli. Remarks on the connection between the additive separation of the Hamilton–Jacobi equation and the multiplicative separation of the Schrödinger equation. I. the completeness and Robertson conditions. *Journal of Mathematical Physics*, 43(11):5183–5222, 2002. 18

[BE55] H. Bateman and A. Erdélyi. *Higher transcendental functions Vol. III*. California Institute of Technology. Bateman Manuscript project. McGraw-Hill, New York, NY, 1955. 107

[BF04] A. V. Bolsinov and A. T. Fomenko. *Integrable Hamiltonian Systems. Geometry, Topology, Classification*. Chapman & Hall/CRC, London, 2004. 12, 54

[BI22] A. V. Borisov and A. P. Ivanov. A Top on a Vibrating Base: New Integrable Problem of Nonholonomic Mechanics. *Regular and Chaotic Dynamics*, 27:2–10, 2022. 55

[BKM76] C. Boyer, E. Kalnins, and W. Miller. Symmetry and separation of variables for the Helmholtz and Laplace equations. *Nagoya Mathematical Journal*, 60:35–80, 1976. 21, 22

[BLC81] L. C. Biedenharn, J. D. Louck, and P. A. Carruthers. *Angular momentum in quantum physics: theory and application*, volume 8. Addison-Wesley Reading, MA, 1981. 71

[BM97] A. V. Borisov and I. S. Mamaev. Non-linear Poisson brackets and isomorphisms in dynamics (Russian). *Regular and Chaotic Dynamics*, 2(3):72–89, 1997. 57

[BM18] A. V. Borisov and I. S. Mamaev. *Rigid body dynamics*. de Gruyter, 2018. 54, 57

[Bog92] O. I. Bogoyavlenskii. Euler equations on finite-dimensional Lie coalgebras, arising in problems of mathematical physics. *Russ. Math. Surv.*, 47:117, 1992. 54

[Boy04] J. P. Boyd. Prolate spheroidal wavefunctions as an alternative to Chebyshev and Legendre polynomials for spectral element and pseudospectral algorithms. *Journal of Computational Physics*, 199(2):688–716, 2004. 29

[BRS20] A. V. Borisov, P. E. Ryabov, and S. V. Sokolov. On the Existence of Focus Singularities in One Model of a Lagrange Top with a Vibrating Suspension Point. In *Doklady Mathematics*, volume 3, 102, pages 468–471. Springer, 2020. 55

[BS99] A. I. Bobenko and Y. B. Suris. Discrete time Lagrangian mechanics on Lie groups, with an application to the Lagrange top. *Communications in mathematical physics*, 204(1):147–188, 1999. 54, 60

[BT92] O. Babelon and M. Talon. Separation of variables for the classical and quantum Neumann model. *Nuclear Physics B*, 379(1-2):321–339, 1992. 38

[BT05] M. Bellon and M. Talon. Spectrum of the quantum Neumann model. *Physics Letters A*, 337(4):360–368, 2005. 81

[BT06a] M. Bellon and M. Talon. The quantum Neumann model: Refined semiclassical results. *Physics Letters A*, 356(2):110–114, 2006. 81

[BT06b] M. P. Bellon and M. Talon. The Quantum Neumann model: Asymptotic analysis. *Phys. Lett. A*, 351:283–289, 2006. 81

[BZ93] L. Bates and M. Zou. Degeneration of Hamiltonian monodromy cycles. *Nonlinearity*, 6(2):313, 1993. 23, 42, 54, 69

[CAM+03] P. Cvitanovic, R. Artuso, R. Mainieri, G. Tanner, and G. Vattay. *Chaos: Classical and Quantum*. `ChaosBook.org` (Niels Bohr Institute, Copenhagen 2012), 2003. 15

[CB95] R. Cushman and L. Bates. The magnetic spherical pendulum. *Meccanica*, 30(3):271–289, 1995. 54

[CB15] R. H. Cushman and L. M. Bates. *Global aspects of classical integrable systems*. Birkhäuser Verlag, Basel, 2nd edition, 2015. 12, 54, 60

[CD88] R. H. Cushman and J. J. Duistermaat. The quantum mechanical spherical pendulum. *Bull. Amer. Math. Soc.*, 19:475–479, 1988. 22, 54, 76

[CDEW19] I. Chiscop, H. R. Dullin, K. Efstathiou, and H. Waalkens. A Lagrangian fibration of the Isotropic 3-Dimensional Harmonic Oscillator with monodromy. *Journal of Mathematical Physics*, 60(3):032103, 2019. 22, 75

[Cha03] L. Charles. Berezin-Toeplitz Operators, a Semi-Classical Approach. *Communications in Mathematical Physics*, 239(1–2):1–28, August 2003. 17

[CIAD14] C. Chen, M. Ivory, S. Aubin, and J. Delos. Dynamical monodromy. *Physical Review E*, 89(1):012919, 2014. 23, 51

[CK85] R. Cushman and H. Knörrer. The energy momentum mapping of the Lagrange top. In *Differential Geometric Methods in Mathematical Physics*, pages 12–24. Springer, 1985. 54, 68

[CKL19] Z. Chen, T.-J. Kuo, and C.-S. Lin. The geometry of generalized Lamé equation, i. *Journal de Mathématiques Pures et Appliquées*, 127:89–120, Jul 2019. 82

[CPVuN13] L. Charles, A. Pelayo, and S. Vũ Ngọc. Isospectrality for quantum toric integrable systems. *Annales scientifiques de l'École normale supérieure*, 46(5):815–849, 2013. 10

[CvdM90] R. Cushman and J.-C. van der Meer. The Hamiltonian Hopf bifurcation in the Lagrange top. In *Géométrie Symplectique et Mécanique*, pages 26–38. Springer, 1990. 54

[CVuN02] R. Cushman and S. Vũ Ngọc. Sign of the monodromy for Liouville integrable systems. *Annales Henri Poincaré*, 3(5):883–894, 2002. 42, 49

[DD24] S. Dawson and H. Dullin. Quantum Integrable Systems arising from Separation of Variables on S3, 2024. 2, 11

[DDN21] S. R. Dawson, H. R. Dullin, and D. M. H. Nguyen. Monodromy in Prolate Spheroidal harmonics. *Studies in Applied Mathematics*, 146(4):953–982, 2021. 2, 10, 11, 76, 100

[DDN22] S. R. Dawson, H. R. Dullin, and D. M. H. Nguyen. The harmonic Lagrange top and the confluent Heun equation. *Regular and Chaotic Dynamics*, 27(4):443–459, 2022. 2, 11, 76

[Del88] T. Delzant. Hamiltoniens périodiques et images convexes de l'application moment. *Bulletin de la Société Mathématique de France*, 116(3):315–339, 1988. 10

[DH12] H. R. Dullin and H. Hanßmann. The degenerate C. Neumann system I: symmetry reduction and convexity. *Central European Journal of Mathematics*, 10(5):1627–1654, 2012. 23, 38

[DLMF] *NIST Digital Library of Mathematical Functions*. http://dlmf.nist.gov/, Release 1.0.24 of 2019-09-15. F. W. J. Olver, A. B. Olde Daalhuis, D. W. Lozier, B. I. Schneider, R. F. Boisvert, C. W. Clark, B. R. Miller, B. V. Saunders, H. S. Cohl, and M. A. McClain, eds. 27, 29, 32, 55, 72, 82, 83, 94, 114

[DP16] H. R. Dullin and Á. Pelayo. Generating hyperbolic singularities in semitoric systems via Hopf bifurcations. *Journal of Nonlinear Science*, 26(3):787–811, 2016. 55

[DRVW01] H. R. Dullin, P. H. Richter, A. P. Veselov, and H. Waalkens. Actions of the Neumann systems via Picard–Fuchs equations. *Physica D: Nonlinear Phenomena*, 155:159–183, 2001. 38

[Dui80] J. J. Duistermaat. On global action-angle coordinates. *Comm. Pure Appl. Math.*, 33:687–706, 1980. 22, 51, 54, 76

[Dul04] H. R. Dullin. Poisson integrator for symmetric rigid bodies. *Regul. Chaotic Dyn.*, 9:255–264, 2004. 60

[DVuN07] H. R. Dullin and S. Vũ Ngọc. Symplectic Invariants near Hyperbolic-Hyperbolic Points. *Regul. Chaotic Dyn.*, 12:689–716, 2007. 38

[DW18] H. R. Dullin and H. Waalkens. Defect in the joint spectrum of hydrogen due to monodromy. *Phys. Rev. Lett.*, 120:020507, 2018. 22, 75, 76

[Efs05] K. Efstathiou. *Metamorphoses of Hamiltonian systems with symmetries*, volume 1864 of *Lecture Notes in Math.* Springer, 2005. 23, 42, 54

[EHM19] K. Efstathiou, H. Hanßmann, and A. Marchesiello. Bifurcations and monodromy of the axially symmetric 1: 1:- 2 resonance. *Journal of Geometry and Physics*, 146:103493, 2019. 68

[Eis34] L. P. Eisenhart. Separable Systems in Euclidean 3-Space. *Annals of Mathematics*, 35:284, 1934. 18, 74

[EMOT55] A. Erdélyi, W. Magnus, F. Oberhettinger, and F. G. Tricomi. *Higher Transcendental Functions. Vol. III*. McGraw-Hill Book Company, Inc., New York-Toronto-London, 1955. 110

[FAW03] P. E. Falloon, P. Abbott, and J. Wang. Theory and computation of spheroidal wavefunctions. *Journal of Physics A: Mathematical and General*, 36(20):5477, 2003. 29

[FC77] E. D. Fackerell and R. G. Crossman. Spin-weighted angular spheroidal functions. *Journal of Mathematical Physics*, 18(9):1849–1854, 1977. 55, 72

[Fla57] C. Flammer. *Spheroidal wave functions*. Stanford Research Institute, 1957. 21, 29

[Gol80] H. Goldstein. *Classical Mechanics*. Addison-Wesley, Reading, MA, 2nd edition, 1980. 54

[Gur95] D. Gurarie. Quantized Neumann problem, separable potentials on S^n and the Lame equation. *Journal of Mathematical Physics*, 36(10):5355–5391, 1995. 38, 80, 81, 82, 85, 89

[Gur08] D. Gurarie. *Symmetries and Laplacians: Introduction to Harmonic Analysis, Group Representations and Applications*. Springer, 2008. 81

[GZ98] L. Gavrilov and A. Zhivkov. The complex geometry of the Lagrange top. *Enseign. Math. (2)*, 44(1-2):133–170, 1998. 54

[Han97] H. Hanßmann. Quasi-periodic motions of a rigid body. I. Quadratic Hamiltonians on the sphere with a distinguished parameter. *Regular and Chaotic Dynamics*, 2(2):41–57, 1997. 54

[HBHN06] J. Hoo, H. Broer, H. Hanßmann, and V. Naudot. Nearly-integrable perturbations of the Lagrange top: applications of KAM-theory. In *Dynamics & Stochastics*, volume 48, pages 286–303. Institute of Mathematical Statistics, 2006. 54

[HO91] J. Hajnal and G. I. Opat. Stark effect for a rigid symmetric top molecule: exact solution. *Journal of Physics B: Atomic, Molecular and Optical Physics*, 24(12):2799, 1991. 54, 72

[HW95a] J. Harnad and P. Winternitz. Classical and quantum integrable systems in 263-1263-1263-1and separation of variables. *Communications in Mathematical Physics*, 172(2):263–285, 1995. 76, 85

[HW95b] J. Harnad and P. Winternitz. Harmonics on hyperspheres, separation of variables and the bethe ansatz. *Letters in Mathematical Physics*, 33(1):61–74, 1995. 76, 85

[Inc56] E. L. Ince. *Ordinary Differential Equations*. Dover, New York, 1956. 17, 19

[KKM06] E. G. Kalnins, J. M. Kress, and W. Miller. Second-order superintegrable systems in conformally flat spaces. IV. The classical 3D Stäckel transform and 3D classification theory. *Journal of mathematical physics*, 47(4):043514, 2006. 19, 75

[KKM18] E. G. Kalnins, J. M. Kress, and W. Miller. *Separation of Variables and Superintegrability*. Bristol: IOP Publishing, 2018. 18, 21, 23, 80

[KKMP02] E. G. Kalnins, J. M. Kress, W. Miller, and G. S. Pogosyan. Complete sets of invariants for dynamical systems that admit a separation of variables. *Journal of Mathematical Physics*, 43(7):3592–3609, 2002. 75

[KM86] E. G. Kalnins and W. Miller. Separation of variables on the n-dimensional Riemannian manifolds. i. the n-sphere S^n and Euclidean n-space $\mathbb{R}^n$. *Journal of Mathematical Physics*, 27(7):1721–1736, 1986. 11, 19, 75, 92, 101

[KR03] I. Kozin and R. Roberts. Monodromy in the spectrum of a rigid symmetric top molecule in an electric field. *The Journal of chemical physics*, 118(23):10523–10533, 2003. 54

[Kri10] G. Kristensson. *Second Order Differential Equations: Special Functions and Their Classification*. Springer New York, 2010. 19

[KS10] F. Klein and A. Sommerfeld. *Über die Theorie des Kreisels*. Teubner, Leipzig, 1910. 54

[KWMW76] E. G. Kalnins, J. W. Miller, and P. Winternitz. The group $O(4)$, separation of variables and the Hydrogen atom. *SIAM Journal on Applied Mathematics*, 30(4):630–664, 1976. 18

[Lea86] E. W. Leaver. Solutions to a generalized spheroidal wave equation: Teukolsky's equations in general relativity, and the two-center problem in molecular quantum mechanics. *Journal of mathematical physics*, 27(5):1238–1265, 1986. 55

[LF23] Y. Le Floch. *Berezin-Toeplitz quantization and semitoric systems*. Habilitation à diriger des recherches, Université de Strasbourg, 2023. 79

[LFP18] Y. Le Floch and A. Pelayo. Symplectic geometry and spectral properties of classical and quantum coupled angular momenta. *Journal of Nonlinear Science*, 29(2):655–708, 2018. 75, 79

[LFVuN21] Y. Le Floch and S. Vũ Ngọc. The inverse spectral problem for quantum semitoric systems. *arXiv preprint*, 2021. 54, 76

[LL77] L. D. Landau and E. M. Lifshitz. *Quantum mechanics*. Pergamon Press, Oxford, 1977. 15, 54, 60, 71

[LL84] L. D. Landau and E. M. Lifshitz. *Mechanics*. Pergamon Press, Oxford, New York, 1984. 54

[Mar09] A. P. Markeev. On the theory of motion of a rigid body with a vibrating suspension. *Doklady Physics*, 54(8):392–396, 2009. 55

[Mar12] A. P. Markeev. On the motion of a heavy dynamically symmetric rigid body with vibrating suspension point. *Mechanics of Solids*, 47(4):373–379, 2012. 55

[Mar18] N. Martynchuk. *On monodromy in integrable Hamiltonian systems*. Phd thesis, University of Groningen, 2018. 23, 40

[Mat96] V. S. Matveev. Integrable Hamiltonian systems with two degrees of freedom. Topological structure of saturated neighborhoods of saddle-saddle and focus-focus types. *Matem. Sbornik*, 187(4):29–58, 1996. 22, 42

[MDEW19] N. Martynchuk, H. R. Dullin, K. Efstathiou, and H. Waalkens. Scattering invariants in Euler's two-center problem. *Nonlinearity*, 32:1296–1326, 2019. 23

[MF53] P. Morse and H. Feshbach. *Methods of Theoretical Physics*. McGraw-Hill, New York, 1953. 30, 106

[MJ77] W. Miller Jr. *Symmetry and separation of variables*. Addison-Wesley Publishing Co., Inc., Reading, MA, 1977. 21

[Mos80a] J. Moser. Various aspects of integrable Hamiltonian systems. In S. H. J. Coates, editor, *Dynamical Systems*, C.I.M.E. Lectures, Bressanone 1978, pages 233–290. Birkhäuser, Boston, 2 edition, 1980. 38

[Mos80b] J. Moser. Geometry of quadrics and spectral theory. In W.-Y. Hsiang et al., editors, *The Chern Symposium 1979*, pages 147–188. Springer, Berlin, 1980. 38

[MPW81] W. Miller, J. Patera, and P. Winternitz. Subgroups of Lie groups and separation of variables. *Journal of Mathematical Physics*, 22(2):251–260, 1981. 27

[MR94] J. E. Marsden and T. S. Ratiu. *Introduction to Mechanics and Symmetry*. Springer, New York, 1994. 12, 54

[MRSD06] G. Mussardo, V. Riva, G. Sotkov, and G. Delfino. Kink scaling functions in 2d non-integrable quantum field theories. *Nuclear Physics B*, 736(3):259–287, feb 2006. 82

[MS54] J. Meixner and F. W. Schäfke. *Mathieusche Funktionen und Sphäroidfunktionen*. Springer-Verlag, 1954. 21, 29, 32

[Mül63] H. J. W. Müller. Asymptotic expansions of prolate spheroidal wave functions and their characteristic numbers. *J. Reine Angew. Math.*, 212:26–48, 1963. 32

[MW74] J. E. Marsden and A. Weinstein. Reduction of symplectic manifolds with symmetry. *Rep. on Math. Phys.*, 5:121–130, 1974. 10

[NDD23] D. M. H. Nguyen, S. R. Dawson, and H. R. Dullin. Integrable systems arising from separation of variables on S^3, 2023. 74, 75, 78, 79, 88, 89, 90, 91, 92, 93, 101, 102, 106, 112, 115

[Neu59] C. Neumann. De problemate quodam mechanico, quod ad primam integralium ultraellipticorum classem revocatur (Diss. Regiomonti 1856). *J. Reine Angew. Math.*, 56:46–63, 1859. 38

[OdA88] A. M. Ozorio de Almeida. *Hamiltonian Systems: Chaos and Quantization*. Cambridge University Press, Cambridge, 1988. 15

[Paw07] M. Pawellek. Quasi-doubly periodic solutions to a generalized Lamé equation. *Journal of Physics A: Mathematical and Theoretical*, 40(27):7673–7686, jun 2007. 82

[PFTV88] W. H. Press, B. P. Flannery, S. A. Teukolsky, and W. T. Vetterling. *Numerical Recipes in C. The Art of Scientific Computing*. Cambridge University Press, Cambridge, 1988. 27, 29

[PPVuN14] A. Pelayo, L. Polterovich, and S. Vũ Ngọc. Semiclassical quantization and spectral limits of $\hbar$-pseudodifferential and Berezin-Toeplitz operators. *Proceedings of the London Mathematical Society*, 109(3):676–696, 2014. 31

[PR+17] Á. Pelayo, T. S. Ratiu, et al. The affine invariant of generalized semitoric systems. *Nonlinearity*, 30(11):3993–4028, 2017. 22, 51

[PT73] W. H. Press and S. A. Teukolsky. Perturbations of a rotating black hole. II. Dynamical stability of the Kerr metric. *The Astrophysical Journal*, 185:649–674, 1973. 55

[PVuN09] A. Pelayo and S. Vũ Ngọc. Semitoric integrable systems on symplectic 4-manifolds. *Inventiones mathematicae*, 177(3):571–597, 2009. 10, 22, 54, 76

[PVuN12] A. Pelayo and S. Vũ Ngọc. First steps in symplectic and spectral theory of integrable systems. *Discrete and Continuous Dynamical Systems*, 32(10):3325–3377, May 2012. 10

[PVuN15] A. Pelayo and S. Vũ Ngọc. Spectral limits of semiclassical commuting self-adjoint operators, 2015. 17

[RA95] A. Ronveaux and F. Arscott. *Heun's differential equations*. Oxford University Press, 1995. 17, 23, 30, 55, 95

[Raţ81] T. Raţiu. The C. Neumann problem as a completely integrable system on an adjoint orbit. *Trans. Amer. Math. Soc.*, 264(2):321–329, 1981. 38

[Rei26] F. Reiche. Die Quantelung des symmetrischen Kreisels nach Schrödingers Undulationsmechanik. *Zeitschrift für Physik*, 39(5-6):444–464, 1926. 54

[Rob27] H. P. Robertson. Bemerkung über separierbare Systeme in der Wellenmechanik. *Mathematische Annalen*, 98:749, 1927. 18, 74

[RS21] P. E. Ryabov and S. V. Sokolov. Bifurcation diagram of one model of a Lagrange top with a vibrating suspension point. Slides of a presentation at IV International Conference Topological methods in dynamics and related topics, Nizhny Novgorod, 10 2021. 55

[rWR19] Wolfram Research. *Mathematica, Version 12.0*. Champaign, IL, 2019. 31

[Sak02] P. Saksida. Neumann system, spherical pendulum and magnetic fields. *Journal of Physics A: Mathematical and General*, 35(25):5237, 2002. 54

[Sch55] C. Schlier. Der Stark-effekt des symmetrischen Kreiselmoleküls bei hohen Feldstärken. *Zeitschrift für Physik*, 141(1):16–18, 1955. 54

[Sch16] K. Schöbel. Are orthogonal separable coordinates really classified? *Symmetry, Integrability and Geometry: Methods and Applications (SIGMA)*, 12:No 041, 16, 2016. 75

[Sei89] E. Seidel. A comment on the eigenvalues of spin-weighted spheroidal functions. *Classical and Quantum Gravity*, 6(7):1057, 1989. 55

[Shi63] J. H. Shirley. Stark energy levels of symmetric-top molecules. *The Journal of Chemical Physics*, 38(12):2896–2913, 1963. 54, 72

[SL00] S. Slavyanov and W. Lay. *Special functions: a unified theory based on singularities*. Oxford University Press, 2000. 17, 19, 23, 55

[Sle83] D. Slepian. Some comments on fourier analysis, uncertainty and modeling. *SIAM review*, 25(3):379–393, 1983. 29

[SMC+59] J. A. Stratton, P. Morse, L. Chu, J. Little, and F. Corbato. *Spheroidal wave functions*. MIT Press, 1959. 21, 29, 30

[Stä93] P. Stäckel. Über die Bewegung eines Punktes in einer n-fachen Mannigfaltigkeit. *Math. Ann.*, 42:537–563, 1893. 74

[SV15] K. Schöbel and A. P. Veselov. Separation coordinates, moduli spaces and Stasheff polytopes. *Communications in Mathematical Physics*, 337(3):1255–1274, 2015. 75

[SVuN17] D. Sepe and S. Vũ Ngọc. Integrable systems, symmetries, and quantization. *Letters in Mathematical Physics*, 108(3):499–571, 2017. 15

[SZ99] D. A. Sadovskií and B. I. Zhilinskií. Monodromy, diabolic points, and angular momentum coupling. *Phys. Lett. A*, 256(4):235–244, 1999. 75, 76

[SZ07a] D. Sadovskií and B. Zhilinskií. Hamiltonian systems with detuned 1:1:2 resonance: Manifestation of bidromy. *Annals of Physics*, 322:164 – 200, 2007. 68

[SZ07b] E. Sinitsyn and B. Zhilinskii. Qualitative analysis of the Classical and Quantum Manakov Top. *SIGMA. Symmetry, Integrability and Geometry: Methods and Applications*, 3:Paper 046, 23 p., 2007. 11, 75, 88

[Sze75] G. Szegő. *Orthogonal Polynomials*. American Math. Soc: Colloquium publ. American Mathematical Society, 1975. 117

[Teu73] S. A. Teukolsky. Perturbations of a rotating black hole. I. Fundamental equations for gravitational, electromagnetic, and neutrino-field perturbations. *The Astrophysical Journal*, 185:635–648, 1973. 11, 55, 72

[Tot93] J. A. Toth. The quantum C. Neumann problem. *International Mathematics Research Notices*, 1993(5):137–139, 1993. 38

[Tot94] J. A. Toth. On a class of spherical harmonics associated with rigid body motion. *Mathematical Research Letters*, 1(2):203–210, 1994. 80

[Tsi08] A. V. Tsiganov. On bi-Hamiltonian geometry of the Lagrange top. *Journal of Physics A: Mathematical and Theoretical*, 41(31):315212, 2008. 54

[Ves80] A. P. Veselov. Finite-gap potentials and integrable systems on the sphere with quadratic potentials (in Russian). *Func. Anal. Appl.*, 14(1):48–50, 1980. 38

[Viv03] O. Vivolo. The monodromy of the Lagrange top and the Picard–Lefschetz formula. *Journal of Geometry and Physics*, 46(2):99–124, 2003. 54

[Vol99] H. Volkmer. Expansions in Products of Heine-Stieltjes Polynomials. *Constructive Approximation*, 15(4):467–480, oct 1999. 76, 83, 85, 88, 95, 107, 109

[Vol03] H. Volkmer. Error estimates for Rayleigh–Ritz approximations of eigenvalues and eigenfunctions of the Mathieu and spheroidal wave equation. *Constructive approximation*, 20(1):39–54, 2003. 29

[Vuk08] M. Vuk. Algebraic integrability of the confluent Neumann system. *Journal of Physics A: Mathematical and Theoretical*, 41(39):395201, 2008. 38

[VuN99] S. Vũ Ngọc. Quantum monodromy in integrable systems. *Comm. Math. Phys.*, 203(2):465–479, 1999. 22, 37, 42, 76

[VuN07] S. Vũ Ngọc. Moment polytopes for symplectic manifolds with monodromy. *Advances in Mathematics*, 208(2):909–934, 2007. 22

[WD02] H. Waalkens and H. R. Dullin. Quantum monodromy in prolate ellipsoidal billiards. *Ann. Physics*, 295:81–112, 2002. 23

[Whi37] E. T. Whittaker. *A Treatise on the Analytical Dynamics of Particles and Rigid Bodies*. Cambridge University Press, Cambridge, 4 edition, 1937. 54, 56

[WW65] E. T. Whittaker and G. N. Watson. *A Course of Modern Analysis*. Cambridge University Press, Cambridge, 4th edition, 1965. 21

[XRY01] H. Xiao, V. Rokhlin, and N. Yarvin. Prolate spheroidal wavefunctions, quadrature and interpolation. *Inverse problems*, 17(4):805, 2001. 29

[Zha17] L. Zhao. *Spherical and Spheroidal Harmonics: Examples and Computations*. Phd thesis, The Ohio State University, 2017. 29

[Zou92] M. Zou. Kolmogorov's condition for the square potential spherical pendulum. *Physics Letters A*, 166(5-6):321–329, 1992. 54

[Zun97] N. T. Zung. A note on focus-focus singularities. *Differential Geom. Appl.*, 7(2):123–130, 1997. 22, 42